

Development of an Empirical Model to Predict the Mean Residence Time in a Tablet Press Feeder

By

Nobel Osvaldo Sierra Vega

A Thesis submitted in partial fulfillment of the requirements for the degree of

**MASTER OF SCIENCES
in
CHEMICAL ENGINEERING**

UNIVERSITY OF PUERTO RICO
MAYAGÜEZ CAMPUS
2017

Approved by:

Rafael Méndez Román, Ph.D.
President, Graduate Committee

Date

Aldo Acevedo Rullan, Ph.D.
Member, Graduate Committee

Date

Rodolfo Romañach, Ph.D.
Member, Graduate Committee

Date

Oscar Marcelo Suarez, Ph.D.
Representative of Graduate studies

Date

Aldo Acevedo Rullan, Ph.D.
Department Chair

Date

Abstract

The die filling process is a continuous operation that is crucial to comply with the specifications and quality attributes of a pharmaceutical tablet. Die filling is usually performed using a rotary tablet press that has a force-feeding device, called feed frame. The operating conditions of the feed frame can affect the properties of the tablet. The die disc speed (tableting speed), and paddle wheel speed are adjusted empirically to meet with the desired specifications.

An experimental investigation was carried out to study the pharmaceutical powder dynamic inside the feed frame and to develop an empirical model to predict the mean residence time in a tablet press feeder, having the feed frame paddle wheel speed, die disc speed and the properties of the materials as model parameters. This model is needed to optimize the die filling operation.

Pulse injection method and sampling at feed frame output was used to study the residence time distribution. Five Near Infrared calibration models were developed to determine the concentration of unknown samples. The Taylor dispersion model was used to fit the experimental data. Based on the fit, mean residence time and mean centered variance were calculated. The performance of a reproducibility study of experimental method resulted in a 3.429% of relative standard deviation.

The relationship between the experimental factors and mean residence time were examined. The results showed that paddle wheel speed, die disc speed and the properties of the materials affect significantly the mean residence time. The empirical model shows

a linear relationship between the mean residence time and the paddle wheel speed, as well as the mean residence time and the die disc speed. However, the model indicates a non-linear relationship with the cohesion parameter, the selected property of the materials.

Six independent experiments in which operating conditions and the cohesion parameter were controlled and varied were performed to validate the empirical model. Overall, the predicted mean residence time has a high correlation with the observed experimental results, finding error percentages between 0.50% and 3.12% for the validations performed.

Resumen

El proceso de llenado de dados es una operación continua que es crucial para cumplir con las especificaciones y atributos de calidad de una tableta farmacéutica. El llenado de dados es usualmente realizado usando una maquina compresora de tabletas que tiene un dispositivo de alimentación forzada, denominado dispositivo de llenado de dados. Las condiciones de operación del dispositivo de llenado de dados pueden afectar las propiedades de la tableta. Para obtener las especificaciones deseadas, la velocidad del disco de dados (velocidad de producción de tabletas), y la velocidad de las ruedas de aspas del dispositivo de llenado de dados son ajustados empíricamente.

Una investigación experimental fue realizada para estudiar la dinámica del polvo farmacéutico dentro del dispositivo de llenado de dados, y para desarrollar un modelo empírico para predecir el tiempo de residencia promedio en el alimentador de la compresora de tabletas, teniendo la velocidad de la rueda de aspas del dispositivo de llenado de dados, la velocidad del disco de dados y las propiedades del material como parámetros del modelo. Este modelo es necesario para optimizar la operación del llenado de dados.

El método de inyección de pulso y tomar muestras a la salida del dispositivo de llenado de dados fue usado para estudiar la distribución de tiempo de residencia. Cinco modelos de calibración de infrarrojo cercano fueron desarrollados para determinar la concentración de las mezclas desconocidas. El modelo de dispersión de Taylor fue usado

para ajustar los datos experimentales. Basándose en este ajuste, el tiempo de residencia promedio y la varianza fueron calculados. La ejecución de un estudio de reproducibilidad del método experimental resultó en un valor de desviación estándar relativa de 3.429%.

La relación entre los factores experimentales y el tiempo de residencia promedio fueron examinados. Los resultados muestran que la velocidad de las aspas del dispositivo de llenado de dados, la velocidad del disco de dados y la propiedad del material afectan significativamente el tiempo de residencia promedio. El modelo empírico muestra una relación lineal entre el tiempo de residencia promedio y la velocidad de la rueda de aspas, así como también del tiempo de residencia promedio y la velocidad del disco de dados. Sin embargo, el modelo muestra una relación no lineal entre el tiempo de residencia promedio y el parámetro de cohesión, la propiedad del material seleccionada.

Seis experimentos independientes en los cuales las condiciones de operación y el parámetro de cohesión fueron controlados y variados fueron realizados para validar el modelo empírico. En general, el tiempo de residencia predicho tiene una alta correlación con los resultados experimentales observados, encontrando porcentajes de error entre 0.5 y 3.12 % para las validaciones realizadas.

© Copyright 2017
Nobel Sierra-Vega
All right reserved

*To GOD,
To my wife, Diana Vargas,
To my parents, Eder and Teresa,
To my sister Nally and my niece Ana Sofia,
For their support, unconditional love and
for all the moments lived next to them.
I love them.*

Acknowledgements

*Give thanks in all circumstances; for this is God's will for you in Christ Jesus.
1 Thessalonians 5:18*

I am very grateful to God for help me meet this goal, and to bring me to this Island to discover its charm. Without Him, none of this would have been possible. I want to acknowledgements my parents Eder Sierra and Teresa Vega, to my sister Nally and my niece Ana Sofia, who from Colombia have given me the strength to keep going.

Would like to thank the University of Puerto Rico at Mayaguez Campus, the Chemical Engineering Department, InQu, for giving me the opportunity to complete my master's studies. Likewise, thank to NSF-PFI: AIR (Grant Number – 153 7197) for providing the necessary funds for this research. I also want to give thanks to Estela Sánchez and Keila Cruz from Chemical Company of PR Inc. dba Mays Ochoa for the donation of raw material made to this research work.

Thanks to my thesis advisor Dr. Rafael Mendez for his guidance and patience during my research. I will always remember with great gratitude for the support provided in my master's studies.

Thanks to Dr. Rodolfo Romañach for “adopting me” as a member of his lab group and for allowing me to use their facilities to perform the experiments. Also, would like to thank to Dr. Aldo Acevedo, for all the time dedicated to my research.

I want to give thanks to my laboratory partners Adriluz Sánchez, Carlos Ortega and Vanessa Cárdenas for all collaboration and all the useful scientific conversations on the NIR studies. I really learned a lot from each one of you. Too, to Jean and Mariana for all the help provided in doing the experiments and in properly completing this thesis.

I want to give special thanks to all my undergraduate students for their dedication and commitment to the development of the experiments: Oscar Ortiz, Nicole Febles, Christian Negron, Brian Rodriguez, Alberto Serrano, Joiris Torres, Jailyn Hernandez, Luis Torres, Luis Blanco, Kiara Santiago, Aurymarie Cerda, Adrian Colon and Giordano Concepcion. Also, I want to especially thank to my REU undergraduate student, Robert Allsopp, for the commitment with research during the summer 2016.

And I want to express my gratitude to my love, Diana, for being the angel that always accompanies me. I love you.

Table of Contents

1	INTRODUCTION	1
1.1	MOTIVATION	1
1.2	OBJECTIVES	3
1.3	SUMMARY OF FOLLOWING CHAPTERS	4
2	LITERATURE REVIEW	6
2.1	POWDER COMPACTION	6
2.2	DIE FILLING PROCESS	7
2.3	FEED FRAME.....	8
2.4	RESIDENCE TIME DISTRIBUTION (RTD)	9
2.5	NIR AND NIR CALIBRATION MODELS	12
3	MATERIALS AND METHODS.....	15
3.1	MATERIALS.....	15
3.2	CHARACTERIZATION OF MATERIALS	15
3.2.1	<i>Particle Size Distribution (PSD)</i>	15
3.2.2	<i>Powder densities</i>	16
3.2.3	<i>Powder compressibility</i>	16
3.2.4	<i>Flow factor and cohesion parameter</i>	17
3.2.5	<i>Selection of material property</i>	18
3.3	DESIGN OF THE EXPERIMENT	18
3.4	NIR CALIBRATION MODELS DEVELOPMENT	19
3.4.1	<i>Preparation of the calibration set</i>	20
3.4.2	<i>Preparation of validation set</i>	20
3.4.3	<i>Acquisition of NIR spectra</i>	20
3.4.4	<i>Multivariate data analysis and spectral preprocessing</i>	21
3.4.5	<i>NIR calibration models validation</i>	23
3.5	RESIDENCE TIME	24
3.5.1	<i>Experimental equipment</i>	24
3.5.2	<i>Preparation of the blends for RTD experiments</i>	25
3.5.3	<i>Residence time: experiments</i>	26
3.5.4	<i>Implementation of the NIR calibration models</i>	26
3.5.5	<i>Mean residence time (MRT)</i>	27
3.6	STATISTICAL ANALYSIS.....	29
3.7	VALIDATION OF THE EMPIRICAL MODEL	29
4	RESULTS AND DISCUSSION	31
4.1	CHARACTERIZATION OF MATERIALS	31
4.1.1	<i>Selection of property material</i>	34
4.2	NIR CALIBRATION MODELS	36
4.2.1	<i>Compositions of the calibrations sets</i>	36
4.2.2	<i>Compositions of the validation sets</i>	36
4.2.3	<i>Evaluation of NIR spectra</i>	36
4.2.4	<i>Development of calibration models</i>	41

4.2.5	<i>Validation of the NIR calibration models</i>	47
4.2.5.1	Linearity	48
4.2.5.2	Specificity	49
4.2.5.3	Accuracy	49
4.2.5.4	Repeatability.....	50
4.2.5.5	Intermediate precision	51
4.2.5.6	Range	52
4.3	RESIDENCE TIME	52
4.3.1	<i>RTD fitting results</i>	52
4.3.2	<i>RTD as a function of operating conditions and the property of the materials</i>	53
4.3.3	<i>Estimated mean residence time (MRT)</i>	57
4.3.4	<i>RTD experiments reproducibility</i>	60
4.3.5	<i>Effect of the paddle wheel speed on mean residence time</i>	61
4.3.6	<i>Effect of the die disc speed on mean residence time</i>	62
4.3.7	<i>Effect of the cohesion parameter on mean residence time</i>	64
4.4	STATISTICAL ANALYSIS	66
4.4.1	<i>Full model</i>	66
4.4.2	<i>Fitted Model</i>	68
4.4.3	<i>Empirical model</i>	76
4.4.4	<i>Contour plots and response surface</i>	77
4.5	VALIDATION OF THE EMPIRICAL MODEL	79
4.5.1	<i>Validation at different operating conditions</i>	80
4.5.2	<i>Validation at different cohesion parameters</i>	81
4.6	OPTIONAL EMPIRICAL MODEL.....	83
5	CONCLUSIONS AND RECOMMENDATIONS	85
5.1	GENERAL CONCLUSIONS	85
5.2	RECOMMENDATIONS AND FUTURES PERSPECTIVES	86
	REFERENCES	87
	APPENDICES	97

Table List

Table 3.1 Factors and levels for the design of experiments.....	18
Table 4.1 Physical Properties of the Powders.....	31
Table 4.2 Compositions blends (% w/w) for each level	33
Table 4.3 Physical properties of the powders blends.....	34
Table 4.4 Factors and levels for the design of experiments.....	35
Table 4.5 Figures of merit of first calibration model.....	42
Table 4.6 Figures of merit of second calibration model	43
Table 4.7 Figures of merit of third calibration model.....	44
Table 4.8. Summary selected NIR calibration models	45
Table 4.9 Linearity results obtained from calibration models validation	49
Table 4.10 Accuracy: NIR Calibration models overall evaluation.....	49
Table 4.11 Accuracy: NIR calibration models predictions RMSEP, RSEP (%) and bias per concentration level.....	50
Table 4.12 Precision: NIR calibration models, repeatability	51
Table 4.13 Mean residence time, dead time, total mean residence time, mean centered variance, and standard deviation results for different operating conditions and property of the materials	58
Table 4.14 Total MRT and MCV for the three replicas of the experiment CP=1.433 kPa; FF=20 rpm and DD=20 rpm	61
Table 4.15 ANOVA for the Mean Residence Time experiments: Full model	68

Table 4.16 ANOVA for the Mean Residence Time experiments: Fitted model	73
Table 4.17 R ² statistics for fitted model.....	73
Table 4.18 Validation experiments setup.....	80
Table 4.19 Validation experiment results at different operating conditions.....	80
Table 4.20 Compositions (%w/w) for validation blends	81
Table 4.21 Characterization of validation blends	82
Table 4.22 Validation experiments setup at different property of the materials	82
Table 4.23 Summary Selected NIR calibration models for validation blends.....	82
Table 4.24 Validation experiment results at different property of the materials.	83

Figure List

Figure 2.1 RTD measurements ⁴⁰	11
Figure 2.2 Common methods for register NIR spectra in the pharmaceutical industry (a) transmission (b) diffuse reflection	12
Figure 3.1 FT4 powder rheometer	17
Figure 3.2 Geometrical representation of the 3 ³ factorial designs.....	19
Figure 3.3 MPA FT-NIR spectrometer.....	21
Figure 3.4 A scheme depicting the feed frame from Fette 3090 tablet press and the injection of tracer	25
Figure 4.1 Change of compressibility percentage for the blends of each level	32
Figure 4.2 FT- NIR transmission spectra for caffeine anhydrate	37
Figure 4.3 NIR – Spectra for pure components	38
Figure 4.4 NIR spectra in transmission mode of 3% (w/w) caffeine blend of the level 2	39
Figure 4.5 Powder blend spectra with concentrations of 1, 2 and 3 %(w/w) caffeine	40
Figure 4.6 Transmission spectra of powder blends after second derivative with 15-points size in the spectral region of 9200 – 8800 cm ⁻¹	41
Figure 4.7 RSEP as a function of PLS factor a) First level of cohesion parameter, b) Second cohesion parameter level and c) Third cohesion parameter level	47
Figure 4.8 Linearity study built with predicted values obtained of the evaluation of validations sets into global model (a) Model 1 (b) Model 2 (c) Model 3.....	48

Figure 4.9 Fit and experimental data for experiment CP=0.733 kPa; FF=30 rpm and DD=40 rpm	53
Figure 4.10 Fitted E(t) function and ideal CSTR profile at different operating conditions and first level of cohesion parameter	54
Figure 4.11 Fitted E(t) function and ideal CSTR profile at different operating conditions and second level of cohesion parameter	55
Figure 4.12 Fitted E(t) function and ideal CSTR profile at different operating conditions and third level of cohesion parameter	56
Figure 4.13 Fit of the experimental data for the three replicas of the experiment CP=1.433 kPa; FF=20 rpm and DD=20 rpm	60
Figure 4.14 Effect of the paddle wheel speed on mean residence time at constant die disc speed (a) Cohesion parameter 0.733 kPa (b) Cohesion parameter 1.055 kPa (c) Cohesion parameter 1.433 kPa	62
Figure 4.15 Effect of the die disc speed on mean residence time at constant paddle wheel (a) Cohesion parameter 0.733 kPa (b) Cohesion parameter 1.055 kPa (c) Cohesion parameter 1.433 kPa.....	63
Figure 4.16 Effect of the material cohesion parameter on mean residence time at constant die disc speed (a) FF= 20 rpm (b) FF= 30 rpm (c) FF= 40 rpm	64
Figure 4.17 Normal probability plot of residuals.....	67
Figure 4.18 Fitted model normal probability plot.....	69
Figure 4.19 Fitted model plot of residuals versus run number	70

Figure 4.20 Plot of residuals versus predicted value for the fitted model	70
Figure 4.21 Anderson-Darling normality plot of the residual	71
Figure 4.22 Box-Cox test.....	72
Figure 4.23 Effect of paddle wheel speed on MRT from empirical model	74
Figure 4.24 Effect of die disc speed on MRT from empirical model	75
Figure 4.25 Effect of cohesion parameter on MRT from empirical model	76
Figure 4.26 Contour plots at cohesion parameter: 0.733 kPa.....	78
Figure 4.27 Response surface for mean residence time, varying the paddle wheel speed and cohesion parameter and setting the die disc speed at 30 rpm.	79

Abbreviations List

APAP	Acetaminophen
API	Active Pharmaceutical Ingredients
CP	Cohesion Parameter
CSTR	Continuous Stirred Tank Reactor
DD	Die Disc Speed
DEM	Discrete Element Method
DOE	Design of Experiment
FF	Feed Frame Paddle Wheel Speed
InGaAs	Indium Gallium Arsenide
MCV	Mean Centered Variance
MPA FT- NIR	Multi-Purpose Analyzer Fourier Transform Near Infrared
MRT	Mean Residence Time
NIR	Near-infrared
PLS	Partial Least Squares Regression
RMSEP	Root Mean Square Error of Predictions
RSD	Relative Standard Deviation
RSEP	Relative Standard Errors of Predictions
RTD	Residence Time Distribution
SNV	Standard Normal Variate

Appendices List

Appendix A.	Compositions of the Calibrations and Validation Blends for the Calibration Models	97
Appendix B.	Intermediate Precision for Model 1, Model 2 and Model 3.....	99
Appendix C.	Full Model Adequacy Checking	101
Appendix D.	NIR calibration model for Validation Experiments.....	103
Appendix E.	Contour plots.....	111
Appendix F.	Development of the optional empirical model.....	113
Appendix G.	NIR Calibration Model Adequacy Checking: Model 1	118

1 INTRODUCTION

1.1 Motivation

Pharmaceutical tablets represent more than eighty percent of the pharmaceutical market worldwide^{1,2,3}. When compared with other forms of pharmaceutical dosage, tablets offer many advantages such as physical and chemical stability, dosage reliability and low cost of production¹. Thousands of tablets are produced in one minute and while most of them are still being manufactured with traditional batch processes⁴⁻⁶ others are innovating and moving towards continuous manufacturing processes due to the efforts of pharmaceutical industries to transform the traditional manufacturing system into a continuous process^{6,7}.

Regardless of the type of production used (batch-type or continuous-type), the raw material, goes through different process units before reaching the tableting process, where the powders are transformed into a dense compact. The tableting process starts with the filling of the dies, followed by the application of the compaction force and ends with the decompression and expulsion of the tablet. Die filling is affected by the properties of the materials^{8,9,10} and operating conditions^{9,10,3} used in the tablet press. A uniform filling of dies is fundamental to ensure the final properties of the tablet. Non-uniform filling of the dies means that there is a variability in weight, which significantly affects properties such as density¹, porosity¹, hardness⁹, dissolution rate⁹, and drug content⁹ in the tablet. Non-uniform filling can also cause problems such as distortion,

cracking, low strength, shrinkage, and compromise other chemical and physical properties of the tablets⁹.

The die filling process is a continuous operation that is crucial to comply the specifications and quality attributes of a pharmaceutical tablet. The die filling is usually performed using a rotary tablet press that has a force-feeding device (feed frame), where the powder is received from the hopper and it is transported to the dies promoted by one or more paddle wheels. The feed frame has been treated as a black box¹¹, but recent studies have revealed that the dynamic nature of the feed frame can affect the quality of the tablets¹². The operating conditions of the feed frame such as die disc speed (tableting speed) and paddle wheel speed are adjusted empirically to meet specifications. Likewise, paddle wheel speed and the die disc speed are parameters used in the scale-up post-approval of the compression process^{13,14} and can be affect the dissolution rate of the pharmaceutical tablet^{1,13}. Readjusting the parameters by trial and error lead to increase costs and a delay in the production. Knowledge and understanding of the dynamics of the powder within the feed frame can help solve these types of problems.

The residence time is a parameter that allows the characterization of the dynamics of a system^{7,15}. There have been many publications focusing on this parameter in particulate processes¹⁶⁻¹⁸. The studies have demonstrated that the residence time is affected by operating conditions^{4,19}, design parameters^{4,19}, and the properties of the materials^{19,20}. Recent experimental and computational studies relate the residence time to the operating conditions^{1,11,12,10,21-23} and property of the material^{10,22} in different feed

frame types. Although these investigations have broadened the knowledge of the powder behavior within the feed frame, the powder behavior has not been fully characterized and the tools are not available to mitigate associated problems.

This study focuses on developing an empirical or statistical model to predict the mean residence time of powder inside the feed frame, based on the operating conditions and properties of the material. This model seeks to provide valuable information to determine the conditions needed to fulfil the final product specification, and provide information to develop a control strategy for the die filling process. The information extracted from the empirical model can bring a better understanding of the powder flow behavior inside the feed frame, and an estimate of the applied shear, and can result in a reduction of undesired effects such as particle attrition and powder overlubrication.

1.2 Objectives

The overall objective of this research is to develop an empirical model to predict the mean residence time in a tablet press feeder based on a property of the materials and the operating conditions. The following are the specific objectives:

- Characterize different materials properties such as tap density, true density, bulk density, compressibility, cohesion parameter (CP), flow factor and particle size distribution (PSD), to select which one can be included in the empirical model.
- To select a factorial design of experiment to develop the empirical model, based on the operating conditions and a property of the materials.

- To develop NIR calibration models using partial least square for detected the tracer at output the feed frame.
- To determine the mean residence time (MRT) based on the dataset concentrations vs time of the tracer obtained at the output of the feed frame.
- To analyze the experimental results and find the relationships between MRT, the operating conditions and a property of the materials.
- Validate the model with an independent set of experiments.

1.3 Summary of Following Chapters

The second chapter shows a literature review of the most relevant topics to this study. This is followed by seven sections describing the materials used, methodology followed and experimental setup, found within chapter three.

Chapter four contains the results for this study which are divided in five sections: characterization of materials, NIR calibration models, determination of mean residence time, statistical analysis of MRT, and validation of the empirical model. The first section shows the values of the physical properties characterized. In NIR calibration models the three calibration models are developed and their linearity, specificity, accuracy, precision and range are calculated and reported. The third section presents the results for MRT and in statistical analysis the effects of the factors on the MRT are reported, as well as a description of the developed empirical model. The validation of the empirical model

contains the data of additional experiments and the errors associated with the prediction of MRT.

Chapter five presents the conclusions for this work and recommendations.

2 LITERATURE REVIEW

2.1 Powder Compaction

Physical and mechanical properties of the pharmaceutical tablets such as hardness and density, are established during the compaction process, making it one of the most important operations in the pharmaceutical industry^{24,25}.

The specifications of the pharmaceutical tablets include: hardness, weight variation, diameter thickness, disintegration and dissolution. The die disc speed (tableting speed) and paddle wheel speed in the feed frame are adjusted empirically to meet these specifications.

Performance of the pharmaceutical tablets is significantly affected by the compaction process²⁶. This process begins with the die filling, continuous with the application of compaction force, and ending with decompression and ejection of the tablet²⁷.

There are two compression modes for pharmaceutical tablets; compression to constant thickness and compression to constant force, but usually a tablet press is designed to compress tablets at a constant thickness, where the punches stay at a constant distance. Changes in weight will generate changes in the force applied to the powders at a constant thickness and can affect the properties of the pharmaceutical tablet. When compression force increases, capping and lamination increase, density increases²⁸, porosity decrease²⁸, disintegration time increase and dissolution time might increase²⁸.

Inconsistent filling of the dies is a major source of variability in the final properties of tablets such as: weight variability, hardness, porosity, and potentially dissolution rate.

2.2 Die Filling Process

The die filling process in a continuous compression is usually performed using a forced feeder mechanical device. The die filling is comprised of three stages: powder flow from the hopper to the feed frame, powder flow in confined space promoted by a paddle wheel, and finally the transfer of the powder from the feed frame to die^{11,12}. Each of these steps can influence the final properties of the tablet²⁹ and limit their productivity³⁰. Thus, understanding the powder phenomenon during die filling can help to solve some associated problems.

The powder transfer step from feed frame to die has been studied experimental²⁹⁻³¹ and computational^{12,32-36} research by different groups. Some studies have used a shoe feed system a constant velocity over the die to determine powder flow behavior. These studies demonstrated that high shoe speed can cause incomplete filling²⁹⁻³¹ and that the uniform die filling can be controlled with the speed shoe²⁹. However, these studies were performed in systems which do not represent reality in the pharmaceutical industry.

Other researchers have realized discrete element method (DEM) simulations to study the die filling process. Mehrotra *et al*³³ used DEM models for study the effects of flow properties on tablets weight variability, and found that cohesive materials affect the die weight variability and the force required for compression. Later, Guo *et al*³⁶ used DEM to show that the difference between the densities of particle of a mixture can

promote segregation within the die during the die filling process. This study showed that the particles segregation increases as the relationship between the particles densities.

2.3 Feed Frame

During the manufacturing was found that several factors impact negatively the mechanical properties and quality attributes of the pharmaceutical tablets. Major part of this problems was reduced when the die filling process was improved, in this process the feed frame plays an important role. However, although studies show that the operating conditions and design parameter in this unit can affect the properties of the tablets; the flow powder behavior through the feed frame are not fully understood and are a field of study promising in the pharmaceutical industry.

In the feed frame, the powder is received from the hopper and it is forced to fill the dies for paddle wheels. Experimental and computational research has been conducted to study the effects of operating conditions and design parameters of the feed frame on powder properties and pharmaceutical tablets. Mendez *et al*¹⁰ used a feed frame taken from a Manesty Betapress and observed that die weight increases with increasing paddle wheel speed and decreases with increasing die disc speed at a paddle wheel speed. This study demonstrates that the cohesive materials present major mean residence time that materials with less cohesion parameter, and that the mean residence time decreases when increases the die size, the die disc speed and the paddle wheel speed.

In other research Mendez *et al*¹ demonstrated that exist relationship proportional between the applied shear in the feed frame and the lubrication of powder using the same

feed frame. Equally, they also found that by applying high shear decreases the dissolution rate and tablet hardness. Besides, Mendez *et al*²¹ analyzed the variation of particle size distribution (PSD) and powder properties by the shear applied in two different feed frames. In both cases is observed PSD variation with paddle wheel speed dependence, but a more significant effect was observed in the large feed frame (from tablet press Fette 3090).

Mateo-Ortiz *et al*¹² used DEM to simulate a feed frame from Manesty Betapress and study the segregation at die filling process. DEM simulations showed that the segregation mechanism most significant inside the feed frame is the percolation phenomenon. Likewise, that the particle size segregation inside the feed frame decrease with increment the paddle wheel speed.

Later, Ketterhagen²² used DEM to simulate a feed frame from Korsch XL100 tablet press, and demonstrated that at 10 rpm in the feed frame, the design of paddle wheel speed and the cohesion not significantly affected width of the RTD. However, the width of the RTD increases with increasing paddle wheel speed at constant turret speed.

2.4 Residence Time Distribution (RTD)

The RTD is defined as the probability distribution of time that a material spend inside one or more process units in a continuous system^{11,17}. RTD key to understand, describe and analyze the behavior of material flow systems^{15,22}. Likewise, the RTD is used to generate statistical models^{11,16}, design equipment¹¹, measure and upgrade the units performance¹⁷, and troubleshooting¹¹.

There are many studies of the effects of operating conditions and design parameters on RTD in different units with particle based operations, such as continuous blender^{4,16,18-20}, extruder³⁷, rotary drums³⁸, fluidized beds³⁹ and feed frame¹¹.

According to our literature review, few residence time studies in the feed frame have been performed. Mateo-Ortiz *et al*¹¹ demonstrated in an experimental and computational study that lower paddle wheel speeds in the feed frame from Manesty Betapress, lead higher mean residence time and RTD profiles are wider. But this study is limited to a single material and at two speeds in the paddle wheel and on the die disc.

The RTD can be measured experimentally by adding an inert material, known as tracer, at the inlet of the continuous unit being characterized^{7,40}, and measuring the concentration profile of the tracer per unit time in the output. The tracer is expected to be easily detected and has similar properties with the bulk material, to express its behavior in the analysis and introducing as few disturbances as possible on the bulk flow¹⁷.

Two commonly forms to add the tracer are pulse injection and step change. Depending on the type of addition will be the response in the output. In the pulse injection, a certain amount of the tracer is added quickly in one shot into the input of the process unit, the response will be plot of concentration versus time. The curve will have the shape of the residence time distribution function⁷. In the step change, a constant rate of tracer is added to a feed stream, and the response will have shape of a cumulative distribution function⁷. In literature the use of both methods is reported for studying RTD in solid units^{11,17}.

Figure 2.1 illustrates the two ways described for measuring residence time, the concentration curves vs time when the tracer is added, and the system response to this change are shown.

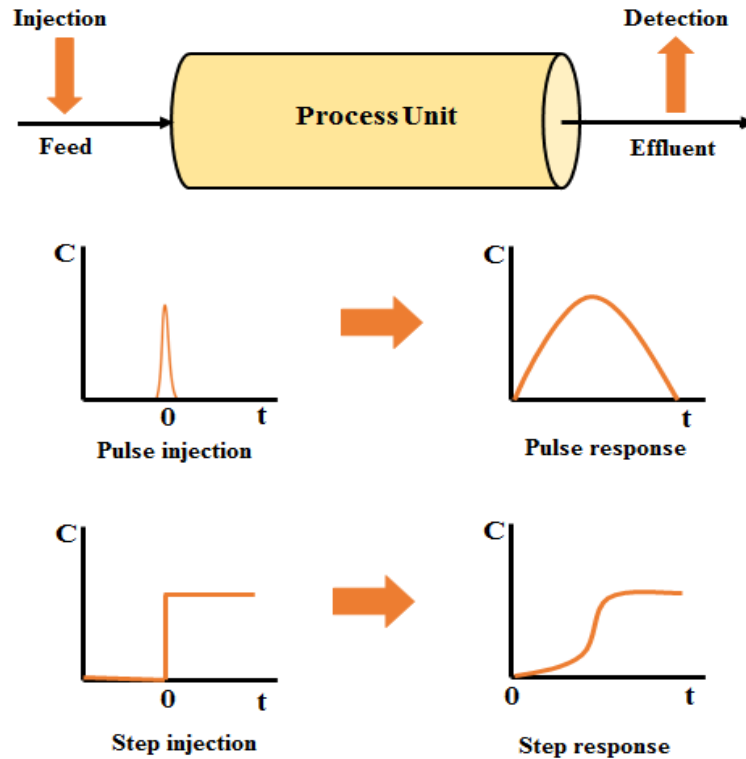


Figure 2.1 RTD measurements⁴⁰

The method of detecting the tracer to the output of the unit depends on the tracer properties¹⁷, the concentration in the blend⁴, sampling, and the analytical method to determine the concentration. Two detection methods have been reported:^{17,41} inline detection and offline detection. Although the two can be used in particle based operations, offline detection is more commonly used¹⁷. The technique analytical most

commonly used is optical detection, in which the light absorbance of the tracer is analyzed by spectroscopy. The two regions of the spectrum used by different researchers are near infrared (NIR)^{4,16,20,42,43} and ultraviolet (UV)^{11,17}.

2.5 NIR and NIR Calibration Models

Near Infrared (NIR) spectroscopy is utilized in different industries for real-time analysis. NIR spectroscopy is a nondestructive and non-invasive technique to study solids. The application of this analytical technique does not require sample preparation which leads to a reduction in analysis time and an elimination of reagents⁴⁴. Plus other physicochemical parameters that can be obtained⁴⁵.

Diffuse reflection and transmission are the two common modes to obtain NIR spectra in the pharmaceutical industry. Transmission is used for both tablets and powders, and diffuse reflection is used to analyze powder mixtures⁴⁴. The Figure 2.2 shows schemes in which differences can be observed between transmission and reflection:

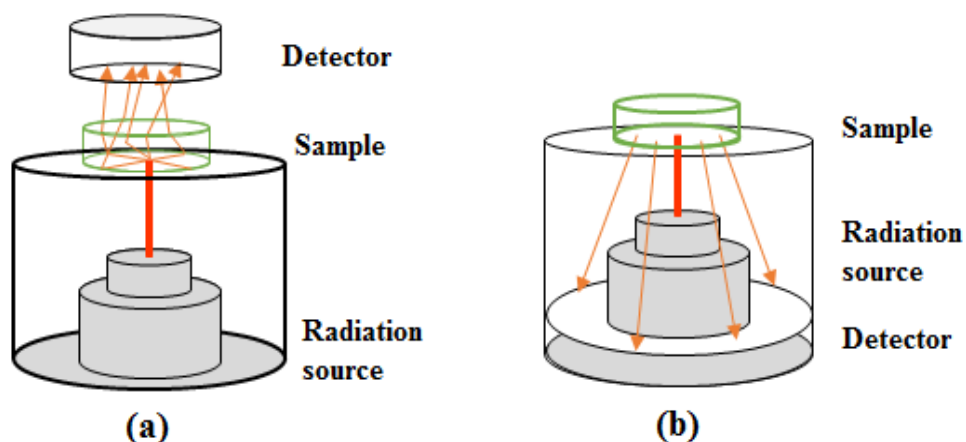


Figure 2.2 Common methods for register NIR spectra in the pharmaceutical industry (a) transmission (b) diffuse reflection

In transmission, the NIR radiation goes through the sample to the detector analyzing major quantity of the sample. Transmission is widely used in the pharmaceutical industry to determine drug content in tablets, due to large volume of the sample that is analyzed⁴⁶, but few studies have been done on powder analysis by transmission⁴⁴.

In diffuse reflection, the NIR radiation irradiates the sample on the surface, part of the radiation penetrates the sample and is absorbed⁴⁷. Another part of the radiation is scattered in all directions, and finally, a portion of the radiation is reflected back to the detector. The disadvantage in this analysis is the limited penetration of the beam in the sample, therefore a partial portion of the sample is scanned^{44,48}.

The use of NIR requires the application of chemometric techniques and statistical study for pretreatment the experimental data and generates multivariate models that help extract quantitative information from the NIR spectra⁴⁹⁻⁵¹.

Sanchez *et al*⁴⁴ innovated developing a calibration model of powder blend used NIR transmission spectra, showing a good predictive capacity with spectra of resolution 64 and 16 cm⁻¹.

NIR spectroscopy models can be used to determine drug content in pharmaceutical formulations and pharmaceutical tablets, relating the spectra changes with changes in concentration. The success of these models depends on the selection and preparation of calibration samples, the acquisition of the spectra; calculate the regression equation and the appropriate selection of calibration range^{52,53}. Many studies have reported the drug

content determination by NIR spectroscopy with a high amount of active ingredient in the tablets⁵⁴. However, in recent years it has required pharmaceutical formulations with low concentrations of drug, so that low concentrations NIR models have become important.

NIR calibration models to quantify low active pharmaceutical ingredient (API) concentrations have been recently developed⁵⁴⁻⁵⁷ confirming that this method can be used in low concentration process.

Some research has shown the importance of using NIR in the pharmaceutical industry and the role it plays in helping the challenges of the same⁵⁸, this technique has been applied in the feed frame^{41,42,43}, where Mateo-Ortiz *et al*⁴¹ demonstrated that using the NIR spectroscopy models can help to understand the powder flow behavior within the feed frame (from Fette 3090) and to monitoring of powder during die filling. Likewise, this study showed that NIR spectra changing with the feed frame paddle wheel speed as well its prediction.

Later, Sasic *et al*⁴² used NIR on the rotary tablet press feed frame (from Kilian T-100) for analyze a formulation the 3.5% the active pharmaceutical ingredient, they found NIR can be used in blends with low API concentrations and for detect small changes in API concentration in the blend.

One of the specific objectives of this research is to develop NIR calibration models to quantify the concentration of the tracer at the output of feed frame and then use the concentration to determine the MRT.

3 MATERIALS AND METHODS

3.1 Materials

Materials used in this work include: Lactose monohydrate (Lactose 70, Tablettose 70 Agglomerated, Ph.Eur./USP-NF/JP, Molkerei MEGGLE Wasserburg GmbH & Co.); lactose monohydrate (Lactose 140, Granulac 140, Ph.Eur./USP-NF/JP, Molkerei MEGGLE Wasserburg GmbH & Co.); microcrystalline cellulose (Avicel® PH-102, NF, FMC Corporation); microcrystalline cellulose (Avicel® PH-105, NF/Ph.Eur., FMC Corporation); colloidal silicon dioxide (SiO₂, specific surface area 175 to 225 m²/g from ACROS Organics) which was added as glidant; magnesium stearate (N.F. non Bovine) which was included as lubricant (MgSt), Acetaminophen USP/PH. EUR. Semi-Fine Powder (APAP, Mallinckrodt Pharmaceuticals, NJ) as API and caffeine anhydrous (MP Biomedicals, LLC) was used as tracer.

3.2 Characterization of Materials

Physical properties, bulk powder properties and external conditions can affect the powder behavior in a process unit⁵⁹. Properties such as particle size distributions, flow factor, cohesion parameter, compressibility, true density, bulk density and tap density were measured.

3.2.1 Particle Size Distribution (PSD)

Samples of approximately 15 g of powder of the raw materials or the blends were taken and analyzed using the Malvern Insitac Analyzer (Malvern Instruments Model

IDC2000) to determine the PSD. The reported result was an average of three different samples.

3.2.2 Powder densities

True density was characterized using a helium pycnometer (AccuPyc II 1340 Micromeritics Instrument, Norcross, GA), the 10 cm³ chamber and approximately 2 g of powder. Each sample was measured at 22.05 °C. Bulk density was measured with a graduated cylinder using approximately 40 g of powder. Tap density was characterized using 500 taps in the VanKel Varian Tap density. The reported densities are an average of three measurements per each powder.

3.2.3 Powder compressibility

Compressibility is a bulk property of the powders, that is defined as the capacity of a powder bed to reduction in volume under pressure⁶⁰. Compressibility percentage was determined using the compressibility tests of FT4 powder rheometer by Freeman Technology, where the powder is subject to a series of increasing normal stresses through of a vented piston from 0.5 to 15 kPa, and the change in volume is measured. Before the compressibility test, the powder is prepared by conditioning using the standard FT4 blade. The reported compressibility percentage are an average of three measurements. Detailed description of these methodologies can be found elsewhere^{59,61,62,63}.

3.2.4 Flow factor and cohesion parameter

Shear properties such as flow factor and cohesion parameter give important information on how a previously consolidated powder at rest will begin to flow. Flow factor and cohesion parameter were estimated using the shear cell tests of FT4 powder rheometer with the accessory of 48 mm of diameter, at a normal stress of 9 kPa three time per sample and using vessel with dimensions of 50 mm. Detailed description of these methodologies can be found elsewhere^{59,61,62,63}. Figure 3.1 show the FT4 powder rheometer used in this study.



Figure 3.1 FT4 powder rheometer

3.2.5 Selection of material property

After the characterization of the raw materials, an analysis of the properties of the materials was conducted to identify the properties going to be included as a factor in the empirical model.

3.3 Design of the Experiment

Factorial design of experiments with three factors, three levels and one replica was used to describe the mean residence time of the powder inside the feed frame based on a property of the materials, the feed frame paddle wheel speed and die disc speed. The experimental factors and levels are described in Table 3.1.

Table 3.1 Factors and levels for the design of experiments

Factors	Unit	Levels		
		Low	Medium	High
Paddle wheel speed	rpm	20	30	40
Die disc speed	rpm	20	30	40
Property of the material	-	Level 1	Level 2	Level 3

The experimental levels for die disc speed and the paddle wheel speed were selected based on typical operating condition of tablet press in the pharmaceutical industry. The levels for the property of the materials were selected after the characterization of raw material.

For this design of experiments, the total mean residence time is the response variable. The total number of experiments is 27, the experiment with property of the materials level 3; paddle wheel speed (FF)=20 rpm and die disc speed (DD)=20 rpm was chosen at random to perform two additional replicates and observe the reproducibility of

the experimental method used. Finally, a random order was established for the development of the experiments.

All values of the independent variables were coded, such that the high level will be symbolized by +1, the medium level by 0, and the low level by -1. Figure 3.2 show geometrical representation of the 3^3 factorial designs with all combinations of possible treatments.

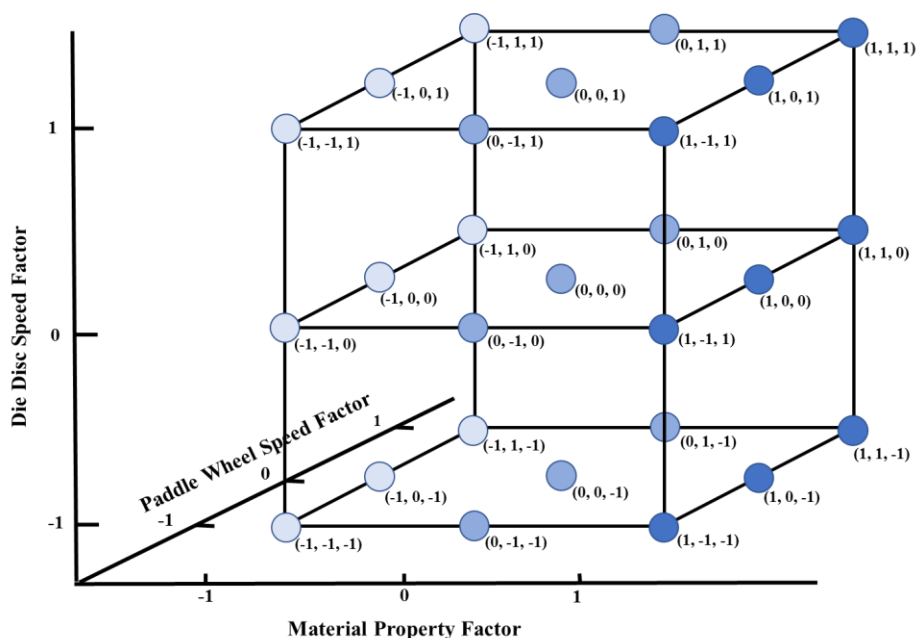


Figure 3.2 Geometrical representation of the 3^3 factorial designs

3.4 NIR Calibration Models Development

Each level of the property of the materials defined for the experiment design, contains different physical and chemical properties. Thus, it is necessary to develop three calibration models for the tracer used (caffeine), one by each level of property of the

materials. The NIR calibration models 1, 2 and 3 correspond to the NIR calibration models calculated for the levels 1, 2 and 3 of property of the materials, respectively.

3.4.1 Preparation of the calibration set

100 g of each the calibration blends were prepared in a V-blender with one liter capacity. following three mixing steps; *Step 1*: Preparation of an initial blend with the corresponding amount of lactose, microcrystalline, caffeine and silicon dioxide; and blended it for 60 minutes at 15 rpm. *Step 2*: 1% (w/w) of MgSt is added and blended for 4 minutes at 15 rpm. *Step 3*: the blend was brought to a vibration blender (Vortex) where it was mixed for an additional four minutes, with the objective of break up any possible agglomerates.

3.4.2 Preparation of validation set

Three independent validation blends were prepared, following the same procedure of the calibration set, to evaluate the performance of each one of the calibration models.

3.4.3 Acquisition of NIR spectra

Near infrared (NIR) spectra were obtained in transmission mode with a Bruker Optics (Billerica, MA) Multi-Purpose Analyzer (MPA). Detailed description of this instrument can be found in Sanchez⁴⁴. The OPUS® software (version 7.2, Build: 7, 2, Bruker Optics, Germany) was used to control the spectrometer. The spectral acquisition was performed in a glass cell (20 mm diameter x 4 mm high) was used to place the powder. The filling of the glass cell was performed using a stainless-steel laboratory

spatula, to compete a weight approximately of 0.80 g. Each spectrum was the average of 64 scans over the range of 12000 - 5800 cm^{-1} , with a resolution between 16 cm^{-1} and 64 cm^{-1} . NIR reference and background single beam spectra was obtain with an NG9 internal filter. The Figure 3.3 shows the MPA FT-NIR spectrometer that was used for NIR spectra acquisition.



Figure 3.3 MPA FT-NIR spectrometer

First, the spectra of the raw materials and the tracer were acquired. Subsequently, the spectra of 20 samples of each calibration blend and validation blend were collected, 3 replicates for each sample, for a total of 60 spectra by blend.

3.4.4 Multivariate data analysis and spectral preprocessing

For spectral preprocessing and NIR calibration model calculation was used the software SIMCA-P (Umetrics Multivariate Data Analysis Software, version 14.1). Using Partial Least Square (PLS) algorithms.

The NIR spectra are frequently disturbed by various interferences in a signal acquisition process⁶⁴, for reducing the interference in the NIR spectra, the mathematical data pretreatments or mathematical corrections in the data were used. Within the most commonly pretreatments used are found: Standard Normal Variate (SNV) and first and second derivative⁶⁴. The SNV reduce the multiplicative effect of the scattering and variation of particle size⁶⁵. A first-order derivative can eliminate variation in baseline and second-order derivative can eliminate variation in the slope of the spectra^{64,65}.

The NIR calibration models were calculated after assessment of different data pretreatments on spectral regions different, and number of PLS components different. The predictive ability of the models was assessed using the validation set, and the evaluation of the statistical errors were performed by means of Root Mean Square Errors of Prediction (RMSEP), the Relative Standard Error of Prediction (%) (RSEP) and bias. The equations of RMSEP, RSEP (%) and bias are presented below:

$$RMSEP = \sqrt{\frac{\sum_{i=1}^m (\hat{y}_i - y_i)^2}{N}} \quad 3.1$$

$$\%RSEP = \sqrt{\frac{\sum_{i=1}^m (\hat{y}_i - y_i)^2}{\sum_{i=1}^m y_i^2}} \times 100\% \quad 3.2$$

$$Bias = \frac{\sum_{i=1}^n (\hat{y} - y)}{N} \quad 3.3$$

Where; \hat{y}_i is the predicted concentration and y_i is the reference concentration for each sample and N is the number of samples.

3.4.5 NIR calibration models validation

The validation of the models provide evidence that the models can be used in analysis for new samples. The evaluation included linearity, specificity, accuracy, precision and range.

Linearity is the capacity to obtain results which are directly proportional to the amount of analyte in the sample⁶⁶. Linearity was evaluated comparing the NIR results with reference value of validation set and estimating it corresponding correlation coefficient.

Specificity is the ability to evaluate unequivocally the analyte in presence of other components⁶⁶. Specificity was validated using the linearity test.

Accuracy expresses the closeness between the measure value obtained and a reference value^{66,67}. Accuracy was validated in terms of RMSEP, RSEP (%) and bias.

Precision characterizes the closeness between the measured values obtained from multiples measurements of the same sample under the specified conditions⁶⁶. Precision was evaluated in terms of repeatability and intermediate precision studies. Repeatability study expresses the nearness of the results obtained with the same sample using the same measurement procedure, same operators, same measuring system, same operating conditions and same location over a short interval of time⁶⁶. Repeatability was determined with two concentration level from the validation set per each model, six

spectra were acquired in the same location of the blend by the same analyst and the average and standard deviation of the predictions was estimated to quantify the coefficient of variation.

The objective of the intermediate precision is to establish the effects of random elements such as different analyst and different experimental day on the precision of the method^{66,68}. In this case, the intermediate precision was performed using two analysts, and acquiring the spectral data two different days. An analysis of variance with two factors and two levels was developed.

Range is the interval for which it has been validated that the model has an appropriate level of precision, accuracy and linearity⁶⁶.

3.5 Residence Time

3.5.1 Experimental equipment

A standard feed frame taken from a Fette 3090 tablet press and tablet press hopper was the equipment used in this study. A disc of high-density polyethylene of 12.5 mm of thickness with 36 holes of 10 mm in diameter, connected to a Dayton DC gear motor (94 rpm, 90 V) was used to simulate a tablet press turret. The design of this equipment is described in detail in Mendez et al.²¹. Figure 3.4 shows a scheme depicting the feed frame used in this study. Likewise, the diagram represents the position of the pulse injection of tracer on the tablet press feed frame, where the tracer can be dispersed by three paddle wheels.

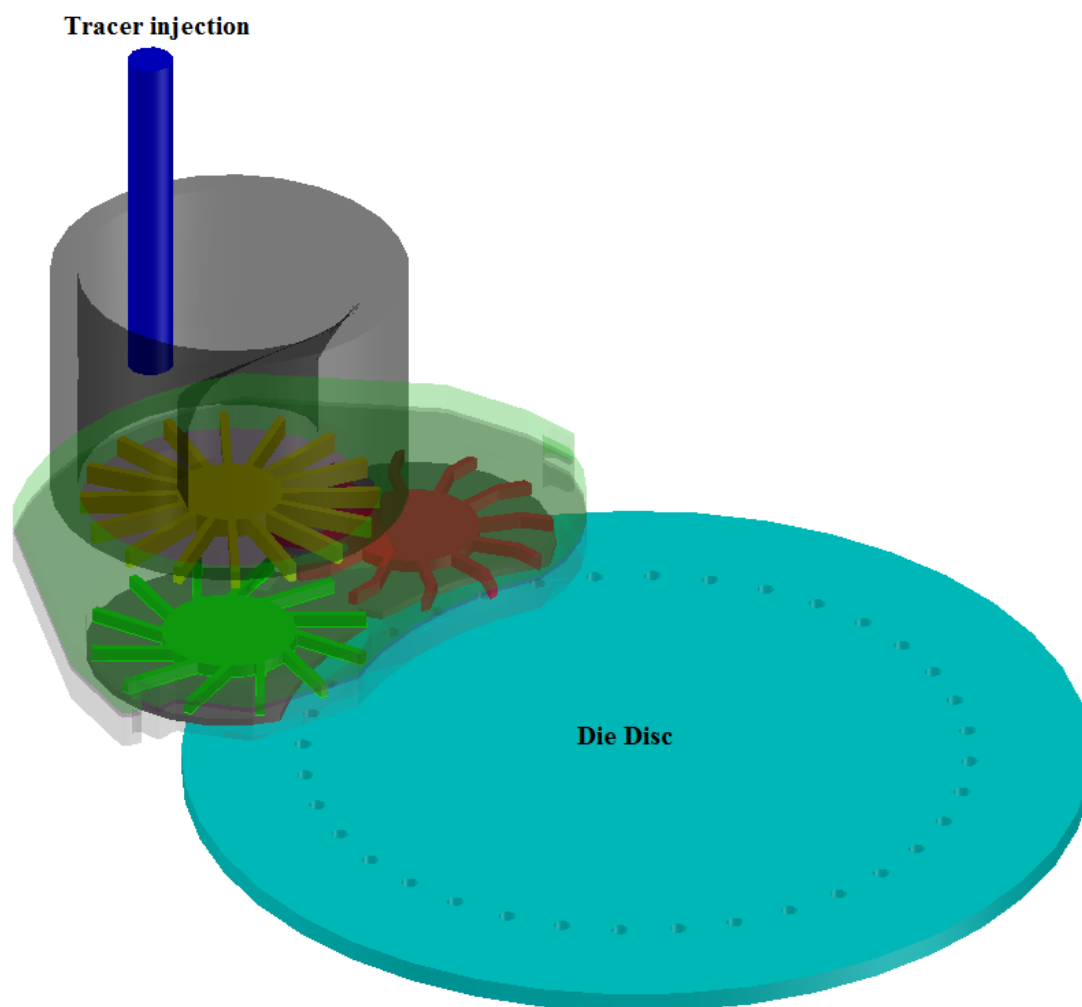


Figure 3.4 A scheme depicting the feed frame from Fette 3090 tablet press and the injection of tracer

3.5.2 Preparation of the blends for RTD experiments

Each blend was prepared with a total batch size of 7 kg. The blends were prepared in a 16-quart stainless steel V-blender that was operated at 15 rpm. Each of the blends were prepared following these steps: *Step 1*: Addition, in layers, of the corresponding amount of lactose, microcrystalline and silicon dioxide; and blended for sixty minutes. *Step 2*: 1% w/w of MgSt is added and blended for four additional minutes.

Physical properties of each of these mixtures, such as: true density, tap density, bulk density, compressibility percentage, flow factor and cohesion parameter, were characterized using the same equipment's used to characterize the raw material.

3.5.3 Residence time: experiments

To perform the residence time experiments a random order was generated with 27 total experiments including a factorial design 3^3 and the selected replicates.

RTD in the feed frame were measured by pulse response method. Initially, the paddle wheel speed and die disc speed were adjusted, and the blend was fed in the hopper before the tablet press feeder. The system is started and expected to reach steady state mass in about two minutes¹¹. Approximately 12 g of the caffeine (tracer) were added manually in the feed frame input as a pulse, and samples were collected in cups at the output of the feed frame every two second during the first two minutes of operation. The next minute, samples were collected every five seconds. At four minutes six samples were collected every 10 seconds. For the rest of the experiment samples were collected every 20 seconds.

3.5.4 Implementation of the NIR calibration models

Approximately 90 samples were collected at each experiment. Each of these samples was subjected to a vibration mixer for 3 minutes. From each one these samples, two subsamples were taken and analyzed in the NIR spectrometer and three spectra per subsample were acquired. The spectral acquisition was performed using the methodology explained in section 3.4.3. The spectral data generated by experiment was added to the

corresponding calibration model and the compositions samples were estimated. The final composition is the average of the predicted composition for each of the 6 spectra acquired by subsample.

3.5.5 Mean residence time (MRT)

From the predictions made with the calibration model a data set of concentrations vs. time is generated. The fitting of the experimental data was performed using the Taylor dispersion model. This model is commonly used for modeling RTD studies in non-ideal reactors and it has been widely used in the fitting of experimental RTD data in different solid units^{16,17,4,20}. The expression used in the fitting is:

$$E(\theta) = \frac{Pe^{0.5}}{(4\pi\theta)^{0.5}} \exp\left\{-\frac{Pe(1-\theta)^2}{4\theta}\right\} \quad 3.4$$

Where E is the residence time distribution function, $\theta = \frac{(t-t_o)}{\tau}$ is the dimensionless time, τ is the mean residence time, t_o represents the dead time and Pe denotes the Peclet dimensionless number, these parameters are estimated to reduce the error between predicted and experimental values of concentration.

Once the Taylor fit was obtained, the residence time distribution (RTD), the mean residence time (MRT), and the mean centered variance (MCV) were estimated with the following mathematical relationships⁴⁰:

Residence Time Distribution (RTD):

$$RTD = E(t) = \frac{C(t)}{\int_0^{\infty} C(t) dt} \quad 3.5$$

Where $C(t)$ is the concentration of the tracer at the output of the system.

Mean Residence Time (MRT):

$$MRT = \tau = \int_0^{\infty} tE(t) dt \quad 3.6$$

In this case, the system dynamics presents delay time (dead time), therefore the total mean residence time is determined as follows, where t_0 represents the delay time:

$$\tau_{total} = t_0 + \int_0^{\infty} tE(t) dt \quad 3.7$$

Total mean residence time was taken as the response variable for the experiment design.

Mean Centered Variance (MCV):

$$MCV = \sigma_{\tau}^2 = \int_0^{\infty} (t - \tau)^2 E(t) dt \quad 3.8$$

3.6 Statistical Analysis

A factorial design was used to examine the effect of the three-main factors (cohesion parameter, paddle wheel speed and die disc speed), as well as their interactions on mean residence time. Initially, all factors and interactions are considered. Three levels were examined for each factor in the factorial design. The methodology used for the statistical analysis in this study begins with the full quadratic model⁶⁹:

$$y_{ijk} = \mu + \alpha_i + \alpha_i^2 + \beta_j + \beta_j^2 + \gamma_k + \gamma_k^2 + \alpha\beta_{ij} + \alpha\gamma_{ik} + \beta\gamma_{jk} + \alpha\beta\gamma_{ijk} + \varepsilon_{ijk} \quad 3.9$$

In this equation, α , β and γ represent the effects of the main factors (property of the material, paddle wheel speed and die disc speed, respectively). The subscripts i, j, k refers to the number of levels of each factor, the interactions are represented for the bilinear terms, the error term is represented by ε and μ refers to the overall mean effect.

Analysis of variance was performed. The statistical model was then reduced by removing the non-significant effects. The p-value significance test was used to accept the significance of the main effects and their interactions. A p-value less than 0.05 indicates that the effect or interaction is significant. Then using an analysis of residuals, the model was verified.

Finally, a regression analysis by least square, was performed to determine the coefficient values for the empirical model.

3.7 Validation of the Empirical Model

The empirical model was validated by six additional experiments varying the conditions initially established. The mixtures used in the validation experiments were

prepared with the same protocol of the twenty-seven mixtures used in the modeling experiments.

The first three validations keep the values of the three properties of the materials levels constant, while the operating conditions were varied. The fourth validation preserves operating conditions and changed the property of the materials. The last two validations changed both, the operating condition and property of the materials.

The total mean residence time was determined experimentally following the methodology set out in section 3.5 and using the empirical model previously developed. The error percentages were estimated with the following mathematical relationship:

$$\%error = \frac{|Experimental\ MRT - Estimated\ MRT|}{Experimental\ MRT} \times 100 \quad 3.10$$

4 RESULTS AND DISCUSSION

4.1 Characterization of Materials

Table 4.1 shows the value of compressibility percentage, cohesion parameter, flow factor, true density, tap density, bulk density and mean particle size (D50) for the average of three samples of different raw materials used in this study.

Table 4.1 Physical Properties of the Powders

	Lactose 70	Lactose 140	Avicel® PH-102	Avicel® PH-105	Caffeine	APAP
Compressibility percentage (%v/v)	7.62 ±0.07	21.77±0.21	15.77±0.05	22.50±0.87	20.05±0.35	41.30±1.20
Cohesion parameter (kPa)	0.06±0.01	1.39±0.12	0.76±0.01	1.81±0.02	1.21±0.02	1.70±0.20
Flow factor	42.50±0.98	3.24±0.25	6.31±0.08	2.62±0.15	3.50±0.31	3.06±0.08
True density (g/cm ³)	1.55±0.00	1.58±0.00	1.69±0.00	1.58±0.00	1.94±0.00	1.30±0.00
Tap density (g/cm ³)	0.66±0.00	0.84±0.01	0.44±0.00	0.49±0.00	3.50±0.00	0.64±0.02
Bulk density (g/cm ³)	0.57±0.00	0.62±0.00	0.35±0.00	0.32±0.00	0.59±0.00	0.36±0.02
Particle size distribution						
<i>d</i> 10 (µm)	95.07±1.09	20.50±0.83	41.12±0.79	7.28±0.44	10.89±0.22	9.65±0.50
<i>d</i> 50 (µm)	211.46±0.85	65.35±1.50	124.76±0.21	21.69±0.60	93.27±1.05	63.90±1.02
<i>d</i> 90 (µm)	429.47±1.29	167.65±1.23	277.88±1.56	50.74±1.20	322.19±1.50	219.67±1.82

The results show that of the two-types of lactose used, the lactose 140 is the most cohesive, also shows that of the two-types of microcrystalline cellulose used, the Avicel® PH-105 present a higher compressibility. The compressibility percentage of the powder is related to particle size distribution, cohesion and flow properties^{70,71}.

Figure 4.1 show the change of compressibility percentage for the raw material, when a normal stress (kPa) is applied on powder bed. Note that the values at 15 kPa were reported values.

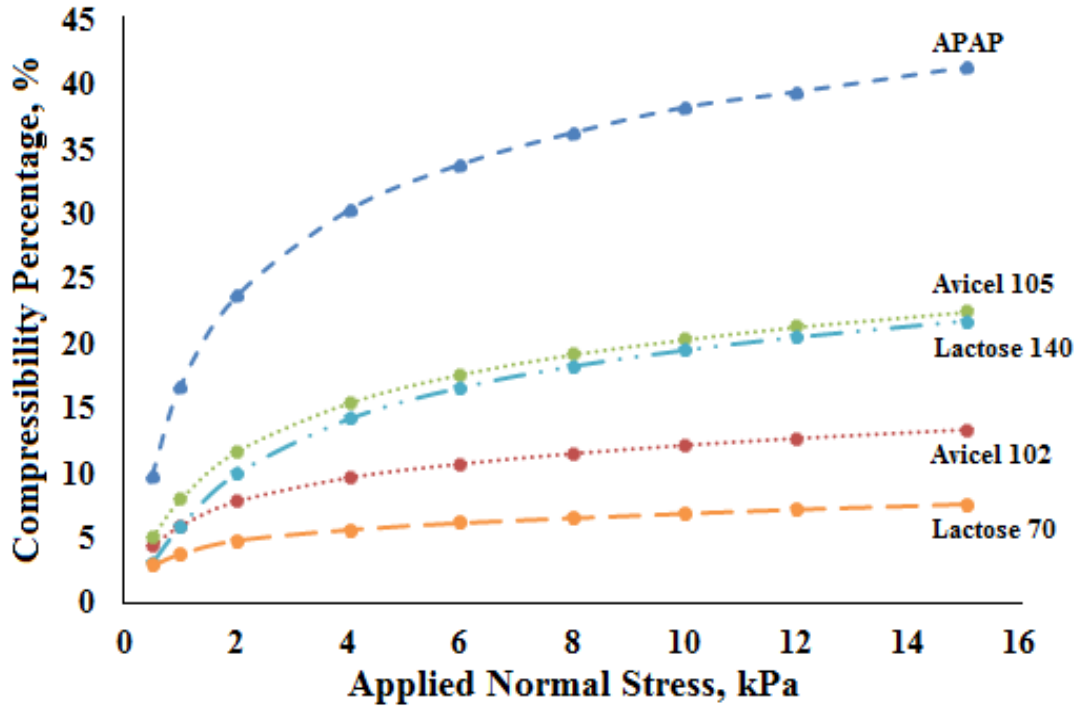


Figure 4.1 Change of compressibility percentage for the blends of each level

The results show that the material with less cohesion parameter, Lactose 70 and Avicel® PH-102, presents small changes in the compressibility, as opposed to the more cohesive material whose changes in compressibility are more significant.

Based on these characterizations, blends with different composition and materials were prepared for the experiments of residence time. The first set of blends were prepared with the less cohesive materials (lactose 70 and Avicel® PH-102), the second

set, with the combination of the less cohesive lactose with the more cohesive Avicel® and the third set with the more cohesive material (Lactose 140 and Avicel® PH-105).

In all cases, the silicon dioxide and magnesium stearate were added to the formulations, in proportion of 0.5% and 1% (w/w), respectively. Magnesium stearate is a lubricant widely used in pharmaceutical industry and, is added to avoid friction between tablet constituents and die walls. Silicon dioxide is a glidants used to improving the flow properties of the blends.

Table 4.2 shows the compositions of the defined blends (% w/w):

Table 4.2 Compositions blends (% w/w) for each level

Material	Composition (%w/w)		
	Set 1	Set 2	Set 3
Avicel® PH-102	49.25	-	-
Avicel® PH-105	-	26.00	49.25
Lactose 70	49.25	72.50	-
Lactose 140	-	-	49.25
SiO ₂	0.50	0.50	0.50
MgSt	1.00	1.00	1.00

A total of nine blends per set were prepared to perform the twenty-seven experiments required by the design of experiments. Each of these mixtures was characterized and Table 4.3 shows the physical properties of each set of the blends used in the mean residence time experiments. The reported results are the average of eighteen measurements, two for each blend in the set.

Table 4.3 Physical properties of the powders blends

	Set 1	Set 2	Set 3
Compressibility percentage (% v/v)	6.06 ±0.06	11.04±0.20	15.47±0.19
Cohesion parameter (kPa)	0.73±0.03	1.06±0.01	1.43±0.01
Flow factor	6.62±0.10	4.97±0.02	3.30±0.09
True density (g/cm ³)	1.56±0.00	1.25±0.00	1.27±0.00
Tap density (g/cm ³)	0.59±0.00	0.80±0.01	0.75±0.04
Bulk density (g/cm ³)	0.47±0.00	0.58±0.00	0.49±0.00
Particle size distribution			
<i>d</i> 10 (µm)	43.11±0.65	15.08±0.29	9.29±0.05
<i>d</i> 50 (µm)	149.4±1.59	152.55±2.27	32.62±0.57
<i>d</i> 90 (µm)	359.33±1.74	380.66±3.45	107.45±1.89

When the cohesion parameter increases the compressibility percentage increases and flow factor decreases, this is because increasing the material cohesion increases the intermolecular forces of the particles, increasing the compressibility and negatively affecting the flow properties of the material. The densities and the D50 do not show a linear tendency with an increase in compressibility percentage from 6.06 to 15.47 % (V/V).

4.1.1 Selection of property material

To reduce the number of factors in the experimental design, only one property of the materials will be used, therefore, it is necessary to define which property will be included in the empirical model. After characterizing the properties of the materials, the compressibility percentage, flow factor and cohesion parameter were the properties considered to be included in the model.

The compressibility percentage is related to the amount of material inside of the die cavity filling during the tablet compaction process^{60,62}, but previous studies⁸ have shown that compressibility is not a significant factor when using a feed frame by force feeding.

The flow properties of the material to be compacted is frequently a critical factor in the powder tableting process⁷². The determination of the flow factor in the FT4 powder rheometer depends on the relation of two parameters (Unconfined Yield Strength and Major Principal Stress) and generally this measurement is limited when the materials have a low cohesion⁶¹.

The cohesion parameter was selected as the factor for the design of experiment. The levels for the FT4 cohesion parameter factor are 0.733, 1.055 and 1.433 kPa. Once the property of the materials was selected and their levels have been defined, the information of the design of experiment for the mean residence time can be completed. Table 4.4 shows the factors and levels for this design.

Table 4.4 Factors and levels for the design of experiments

Factors	Unit	Levels		
		Low	Medium	High
Paddle wheel speed	rpm	20	30	40
Die disc speed	rpm	20	30	40
Cohesion parameter	kPa	0.733	1.055	1.433

4.2 NIR Calibration Models

This section shows the results obtained during the design, development, evaluation and validation of NIR calibration models.

4.2.1 *Compositions of the calibrations sets*

The compositions of the calibration sets are related to the blends defined for each cohesion parameter level. Appendix A shows composition of the calibration blends used in the models. The caffeine concentration increases from 0 to 3 % (w/w) in each set. The proportion of colloidal silicon dioxide and magnesium stearate remains constant in 0.5% and 1% (w/w), respectively.

4.2.2 *Compositions of the validation sets*

The validation sets are blends independent to the calibration sets. Appendix A shows the composition for the validation blends by NIR calibration model.

4.2.3 *Evaluation of NIR spectra*

An evaluation of the NIR spectra is necessary to know the characteristic bands or peaks of the caffeine and the potential regions to develop the calibration models.

Figure 4.2 shows the caffeine FT-NIR transmission spectra which has the main absorption bands (wavenumber) at 8580, 7294 and 6959 cm^{-1} . Previous studies have reported similar bands for caffeine^{68,73}.

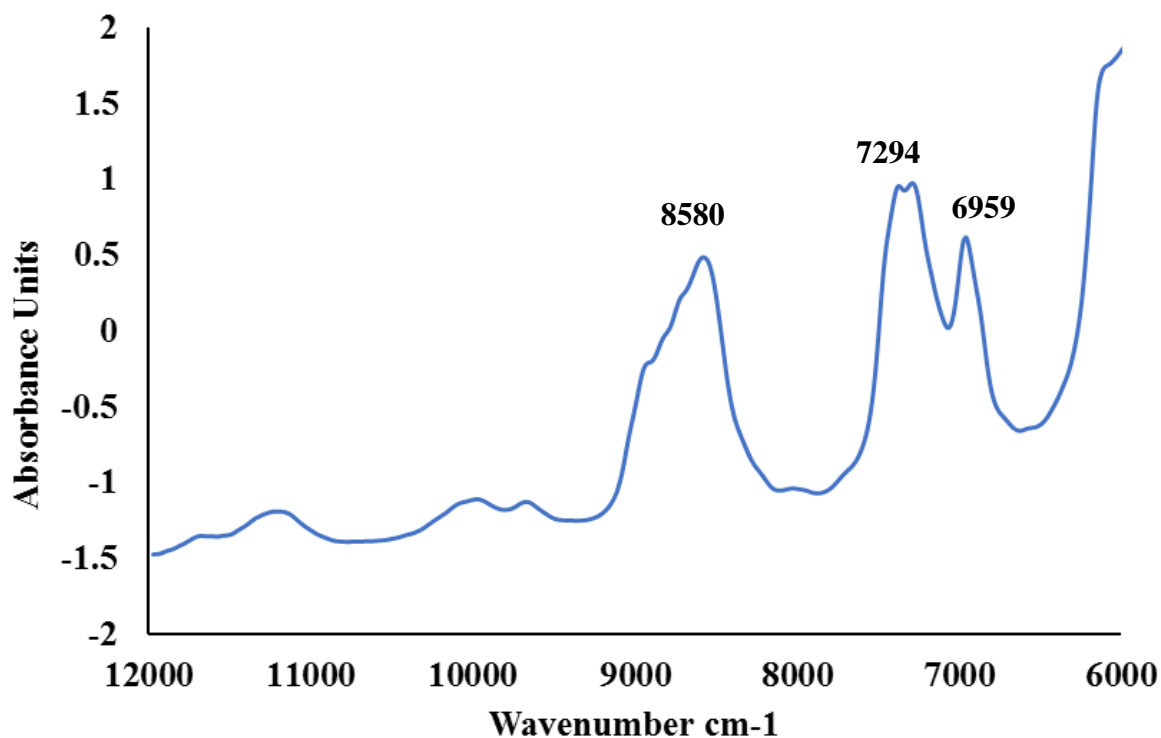


Figure 4.2 FT- NIR transmission spectra for caffeine anhydrate

Major bands at wavenumber 8580 cm^{-1} may be due to the second overtone vibration of C – H stretching⁶⁸. Bands at 7294 cm^{-1} may be due to combination bands: stretching (2C-H) and deformation (C – H)⁶⁸. Peaks at 6959 cm^{-1} were reported by Downey and Boussion⁷³ but were not assigned a vibrational mode.

Smaller bands were observed in the caffeine anhydrate spectrum from 11500 to 9500 cm^{-1} , similar to a previous study by Masatomo *et al.*⁷⁴ that reported some bands at 890 and 990 nm in their study.

Figure 4.3 shows the NIR transmission spectra for caffeine anhydrate and the placebos for the three cohesion parameter levels. Caffeine has somewhat narrow bands in the range of 7000 to 9000 cm^{-1} while the placebos have wide bands.

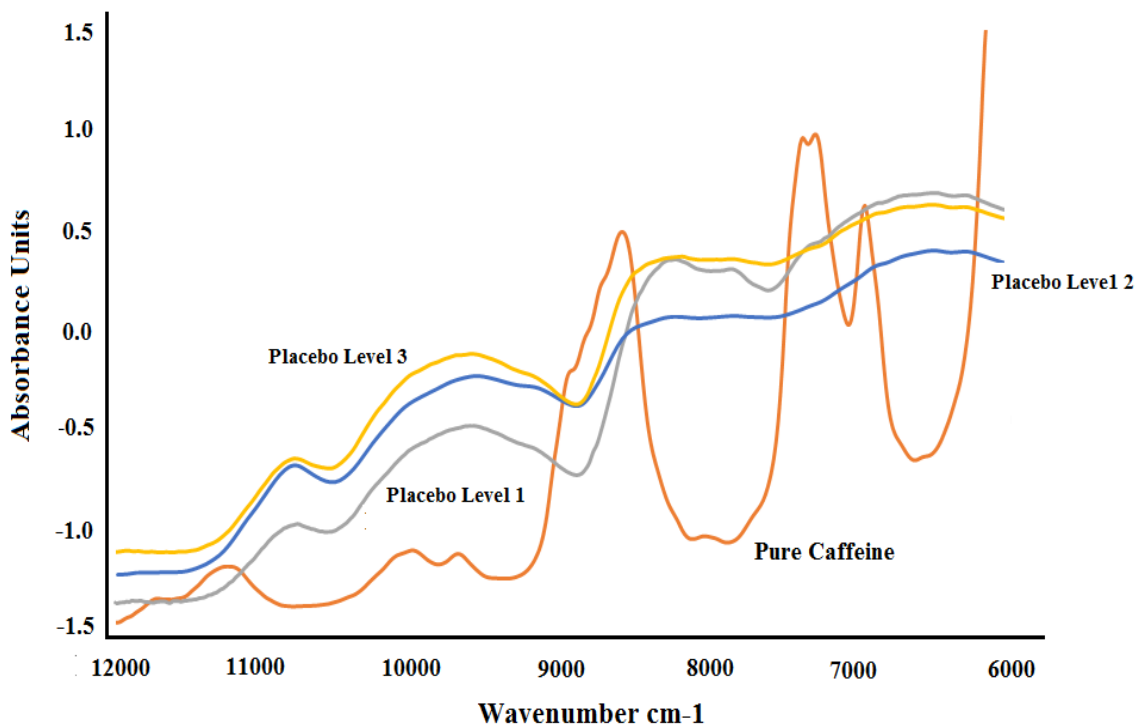


Figure 4.3 NIR – Spectra for pure components

Figure 4.4 shows the near infrared spectra in transmission mode for the concentration level of 3% (w/w) of caffeine blend of the third cohesion parameter level. The spectra show differences in baseline related to particle size and the sample heterogeneity.

The transmission spectra present variations in their baseline around of an absorbance of -0.7. This condition is attributed to the intensity of the radiation that reaches the detector. An absorbance value (A) of -0.7 indicates that the intensity of

radiation received by the detector (I) is approximately 5 times higher than the reference (I_0), which can be explain by the following equation:

$$A = \log\left(\frac{1}{T}\right) = -\log\left(\frac{I}{I_0}\right) \quad 4.1$$

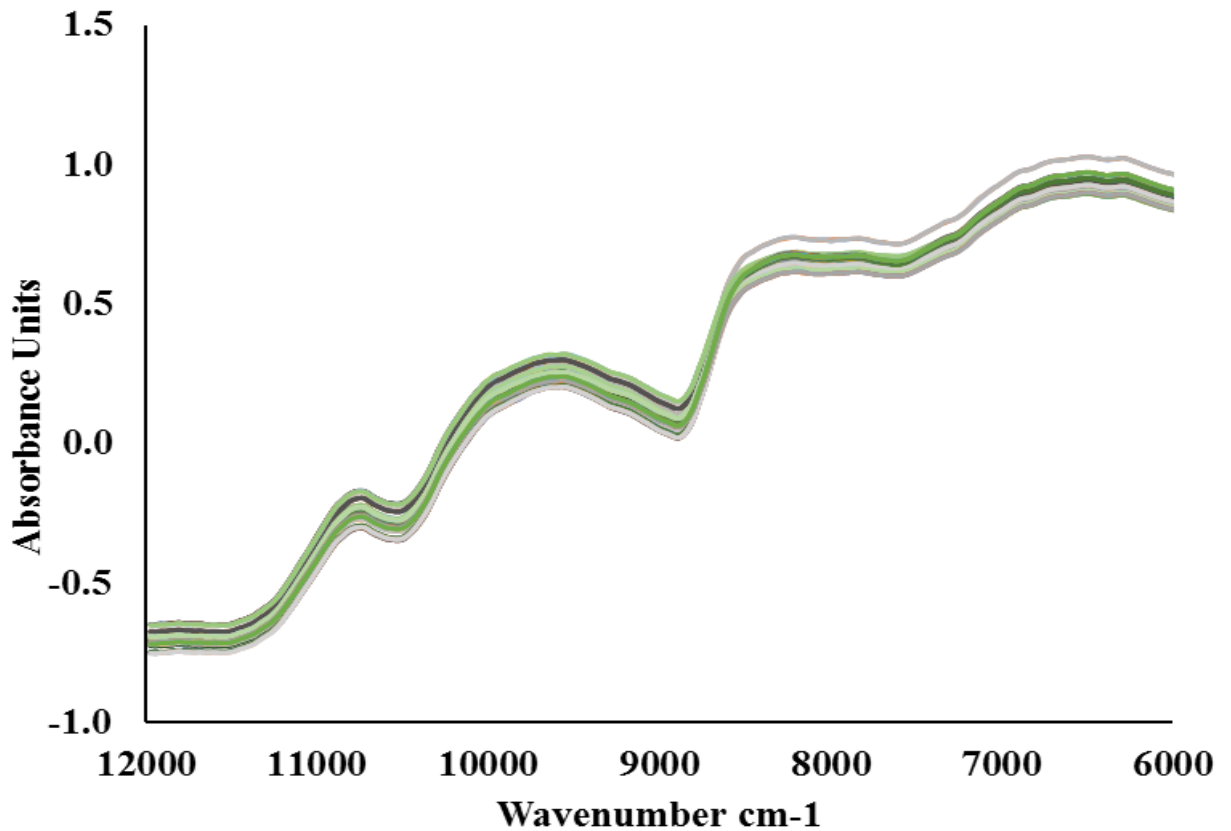


Figure 4.4 NIR spectra in transmission mode of 3% (w/w) caffeine blend of the level 2

Figure 4.5 present the powder blend spectra, for to first level of cohesion parameter, with concentrations of 1, 2 and 3 % (w/w) caffeine in the spectral region from 12000 to 6000 cm^{-1} .

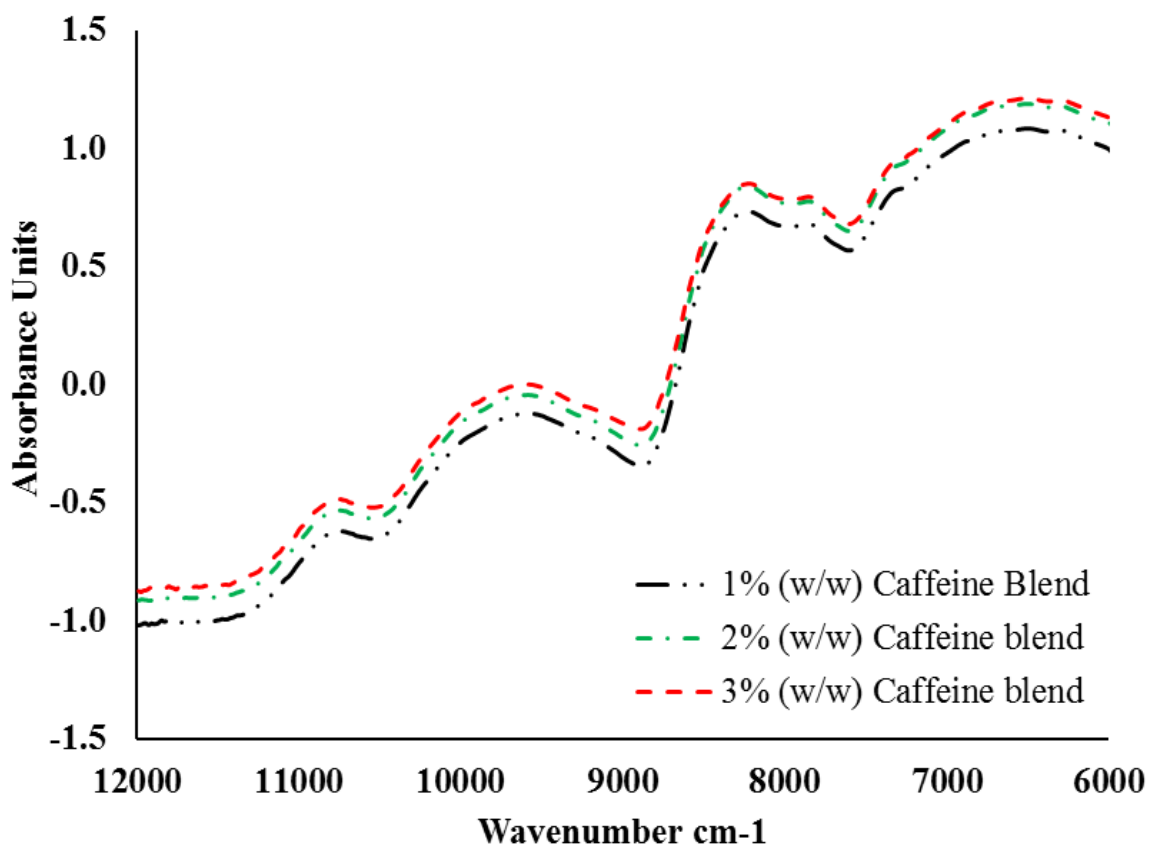


Figure 4.5 Powder blend spectra with concentrations of 1, 2 and 3 % (w/w) caffeine

Figure 4.6 shows the transmission spectra of powder blends for the first cohesion parameter level, with concentrations of 1, 2 and 3% (w/w) caffeine in the spectral region from 9200 to 8700 cm^{-1} . Second derivative with 15-point segment size was applied as spectral preprocessing. In this case, transmission spectra of powder blends with 20 and 50% (w/w) caffeine were added to identify characteristic bands of the caffeine in different blends. When the concentration of caffeine increase in the blends, the absorption bands increases.

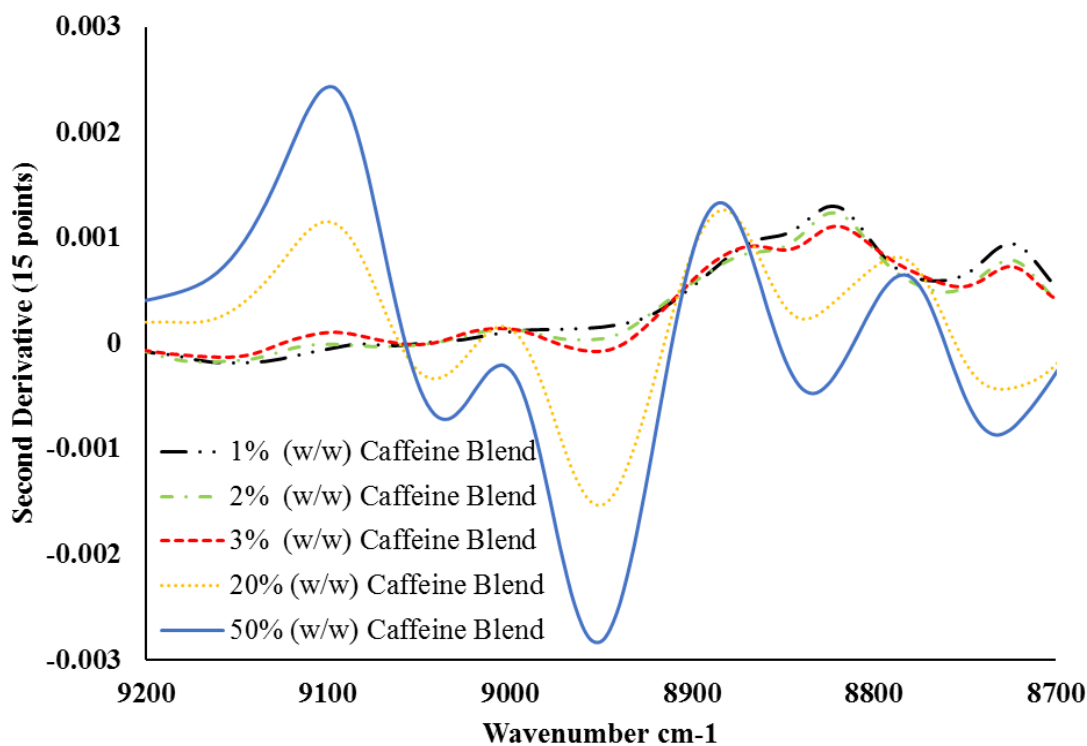


Figure 4.6 Transmission spectra of powder blends after second derivative.

4.2.4 Development of calibration models

For the calculation of the calibration models a calibration set of eight levels of concentration was used, a total of sixty spectra per level were acquired for a total number of four hundred and eighty spectra per calibration model. Different PLS calibration models were calculated to determine caffeine concentration in validation sets.

Different spectral regions, pretreatments and validation sets were analyzed to choose the appropriate model by level of the cohesion parameter. Table 4.5 shows the five best models developed for the first level of cohesion parameter. The selected model was the simplest one and the one with the best performance in terms of RMSEP, RSEP

(%) and bias. The error was calculated from the predictions of the validation set for the level 1.

Table 4.5 Figures of merit of first calibration model

Data Pretreatment	Spectral Range (cm⁻¹)	PLS Factors	R²Y(cum)	RMSEP (%w/w)	RSEP (%)	Bias (%w/w)
SNV	9496.5 - 8809.91	1	0.976	0.152	7.706	0.0047
		2	0.987	0.125	6.407	-0.0502
		3	0.992	0.091	4.652	-0.0082
		4	0.994	0.111	5.678	0.0522
SNV + 1st Derivative (15 points)	9442.5 - 8863.91	1	0.976	0.150	7.682	0.0239
		2	0.987	0.123	6.310	-0.0446
		3	0.988	0.121	6.175	-0.0438
		4	0.989	0.114	5.826	0.0141
1st Derivative (15 points) +SNV	10939.1 - 8663.33	1	0.981	0.106	5.405	-0.0385
		2	0.990	0.089	4.556	0.0104
		3	0.992	0.092	4.723	0.0389
		4	0.992	0.093	4.752	0.0459
SNV	10939.1- 8663.33	1	0.979	0.162	8.264	-0.1233
		2	0.984	0.153	7.803	-0.0999
		3	0.992	0.085	4.364	-0.0055
		4	0.993	0.085	4.336	0.0208
SNV	11494.5 - 8509.05	1	0.909	0.266	13.603	-0.0544
		2	0.981	0.157	8.032	-0.1230
		3	0.986	0.141	7.200	-0.0868
		4	0.993	0.082	4.173	0.0178

The calibration model with lower value of RSEP (%) and RMSEP (%w/w) was selected for the first cohesion parameter level, using the spectral region from 11494.5 – 8509.05 cm⁻¹, the pretreatment SNV and four PLS factors.

Appendix G show the verification of the assumptions of normality, equality of variance and independence for the residuals of the first NIR calibration model. The assumptions of the analysis of variance are fulfilled.

Table 4.6 show the five best models built for the second level of cohesion parameter. The errors were estimated from the predictions value of validation set for the second cohesion parameter level.

Table 4.6 Figures of merit of second calibration model

Data Pretreatment	Spectral Range (cm⁻¹)	PLS Factors	R²Y(cum)	RMSEP (%w/w)	RSEP (%)	Bias (%w/w)
SNV	10954.5 - 8023.04	1	0.634	0.539	29.133	0.155
		2	0.985	0.162	8.751	-0.032
		3	0.994	0.087	4.691	-0.033
		4	0.994	0.082	4.450	-0.022
1st Derivative (15 points) + SNV	10738.5 - 8239.04	1	0.510	0.543	29.344	0.166
		2	0.994	0.127	6.890	-0.027
		3	0.995	0.083	4.478	-0.030
		4	0.995	0.080	4.297	-0.018
SNV+1st Derivative (15 points)	10738.5- 8239.04	1	0.655	0.653	35.259	0.153
		2	0.989	0.078	4.232	-0.006
		3	0.994	0.074	3.985	-0.0005
		4	0.995	0.072	3.910	0.0105
SNV+1st Derivative (15 points)	10738.5 - 7745.31	1	0.690	0.518	27.998	0.172
		2	0.986	0.154	8.336	-0.0207
		3	0.994	0.080	4.348	-0.0301
		4	0.995	0.079	4.246	-0.0219
1st Derivative (15 points) + SNV	10738.5 - 7745.31	1	0.528	0.643	34.754	0.155
		2	0.994	0.085	4.604	-0.0157
		3	0.995	0.072	3.913	0.0100
		4	0.995	0.075	4.065	0.0130

The calibration model with a value of RSEP (%) of 3.913 was selected, using the spectral region from 10738.5 - 7745.31 cm^{-1} , three PLS factors and, the pretreatment first derivative with fifteen points segment size followed by SNV.

Table 4.7 shows the best models developed for the third level of cohesion parameter. The errors were estimated from the predictions value of the validation set for the highest level of cohesion parameter.

Table 4.7 Figures of merit of third calibration model

Data Pretreatment	Spectral Range (cm^{-1})	PLS Factors	R²Y(cum)	RMSEP (%w/w)	RSEP (%)	Bias (%w/w)
SNV+1st Derivative (15 points)	10877.4 - 7020.16	1	0.854	0.611	34.183	0.395
		2	0.942	0.620	34.685	0.546
		3	0.991	0.095	5.320	0.067
		4	0.995	0.074	4.137	-0.0034
SNV + 1st Derivative (11 points)	10908.2 - 6989.3	1	0.855	0.610	34.147	0.395
		2	0.943	0.619	34.628	0.546
		3	0.992	0.113	6.332	0.086
		4	0.995	0.083	4.641	0.0342
SNV+1st Derivative (17 points)	10862 - 7035.58	1	0.853	0.612	34.229	0.395
		2	0.941	0.622	34.782	0.548
		3	0.991	0.090	5.023	0.059
		4	0.995	0.078	4.336	-0.0184
SNV+1st Derivative (15 points)	10887.4 - 7637.31	1	0.840	0.554	30.977	0.306
		2	0.948	0.527	29.497	0.463
		3	0.990	0.127	7.082	0.108
		4	0.996	0.068	3.819	0.0013
SNV	11078 - 7930.46	1	0.810	0.670	37.410	0.169
		2	0.951	0.535	29.917	0.467
		3	0.990	0.276	15.456	0.254
		4	0.996	0.072	4.017	0.0248

The calibration model with four PLS factors, in the spectral region from 10887.4 – 7637.31 cm^{-1} and pretreatment SNV followed by first derivative with fifteen points segment size was selected, because this model presents the lower error.

The following table is a short description of the calibration models developed for the caffeine concentration determination in each one of the three cohesion parameter levels, the concentration range in each model is from 0 to 3%(w/w) of caffeine. The models 1, 2 and 3 correspond to the NIR calibration models developed for the levels 1, 2 and 3 of cohesion parameter factor, respectively.

Table 4.8. Summary selected NIR calibration models

Model	Pretreatment	Spectral range (cm^{-1})	PLS factors	RMSEP (%w/w)	RSEP (%)	Bias
1	SNV	11494.5 – 8509.05	4	0.082	4.173	0.0178
2	1st Derivative (15 points) + SNV	10738.5 - 7745.31	3	0.072	3.913	0.0100
3	SNV+1st Derivative (15 points)	10887.4 – 7637.31	4	0.068	3.819	0.0013

Table 4.8 shows that the selected NIR calibration models have three to four components. The number of PLS factors is a critical parameter when calculating a calibration model. Previous studies that have developed NIR calibration models at low concentrations have considered models with more than three factors^{54,57}.

In this case, the number of factors was selected by the lowest RSEP (%) and RMSEP (%w/w) values. The Figure 4.7 show the plot of the RSEP (%) values versus PLS factor number for the selected pretreatment in each model by cohesion parameter level. As can be seen in the figure, RSEP (%) values begin to decrease until they reach a minimum and increase again as function of PLS factor number. That minimum value of RSEP (%) represents the optimal PLS factor number for the model.

Figure 4.7a and Figure 4.7b show that the PLS factors number selected to first and second cohesion parameter level are those with the lowest RSEP values. However, for the third calibration model, in Figure 4.7c is observed that a model with 4 PLS factor (RSEP = 3.819) and not with 5 PLS factor containing the lowest RSEP value (3.812) has been selected. This is justified because the inclusion of a fifth factor does not significantly improve the predictions of the model but increases its complexity.

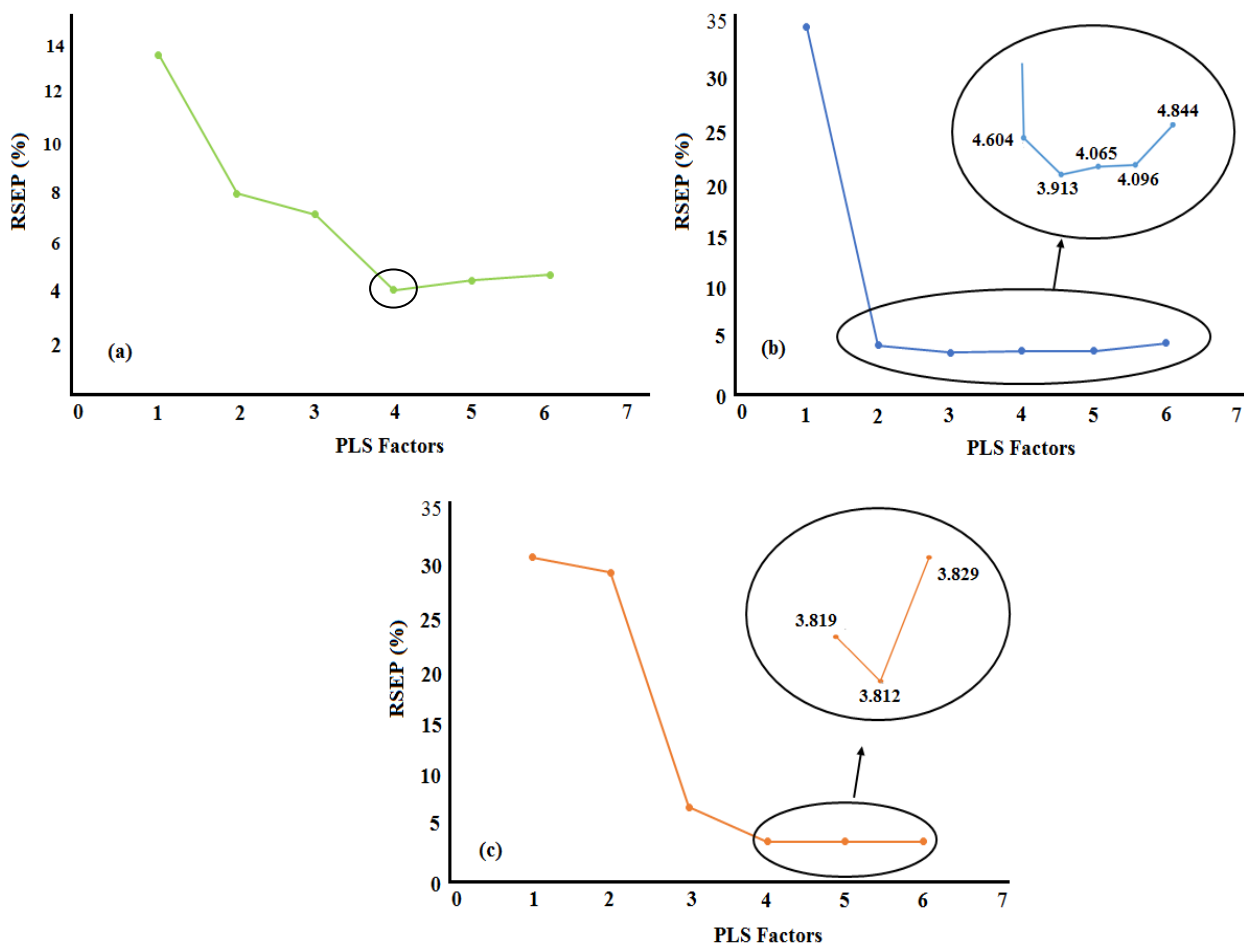


Figure 4.7 RSEP as a function of PLS factor **a)** First level of cohesion parameter, **b)** Second cohesion parameter level and **c)** Third cohesion parameter level

4.2.5 Validation of the NIR calibration models

The validation of the models provide evidence that the models can be used in analysis for unknown samples. The three NIR calibration models were evaluated in terms of linearity, specificity, accuracy, range, and precision.

4.2.5.1 Linearity

The linearity plots were built using the predicted concentrations versus the reference values (gravimetric values) of the validation blends. Figure 4.8 shows a plot of the reference values vs predicted values for each one of the models developed. A good fit between references and predicted values is observed in each case, as evidenced by the correlation coefficients (R^2).

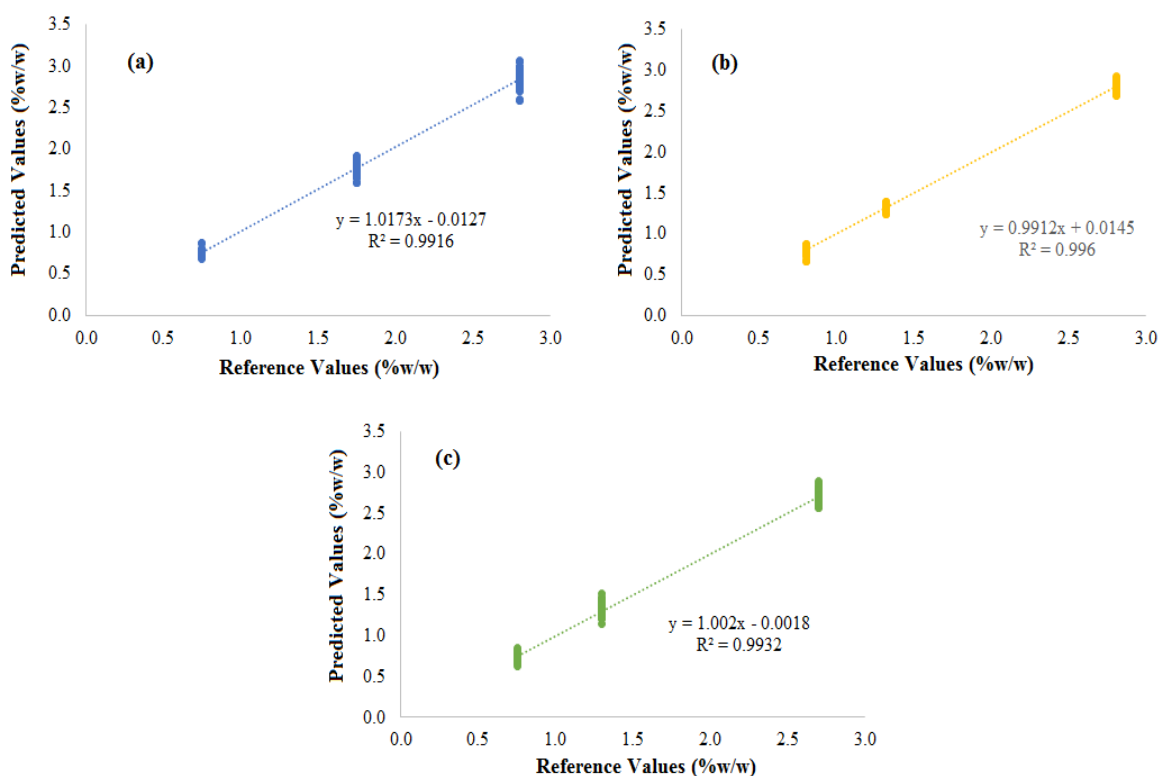


Figure 4.8 Linearity study built with predicted values obtained of the evaluation of validations sets into global model (a) Model 1 (b) Model 2 (c) Model 3

Table 4.9 shows the parameters considered in the assessment of linearity, the intercept and slope are shown with their corresponding 95% confidence interval. In all cases, the confidence interval for the intercept includes the zero.

Table 4.9 Linearity results obtained from calibration models validation

Parameter	Model 1	Model 2	Model 3
<i>n</i>	60	60	60
Concentration range (%m/m)	0.751 – 2.802	0.802 – 2.810	0.756 – 2.705
Intercept	-0.0127 ± 0.0271	0.0145 ± 0.0184	-0.0018 ± 0.022
Slope	1.017 ± 0.0138	0.991 ± 0.0099	1.002 ± 0.0123
R ²	0.992	0.996	0.993

The *n* value corresponds to the number of spectra predicted by level of concentration.

4.2.5.2 Specificity

The linearity studies show that when the caffeine concentration increases or decreases in the blends, the calibration model responds to a change in such variation.

4.2.5.3 Accuracy

Three validation blends were evaluated for accuracy analysis. Accuracy was evaluated in terms of RMSEP, RSEP (%) and bias. A total of one hundred and eighty spectra were predicted. Table 4.10 shows the results of the evaluation of validation sets into the developed global models.

Table 4.10 Accuracy: NIR Calibration models overall evaluation

Model	RMSEP (%w/w)	RSEP (%)	Bias (w/w)
1	0.0817	4.173	0.0178
2	0.0724	3.913	0.0100
3	0.0683	3.819	0.0013

The RMSEP (%w/w) and RSEP (%) indicate how the individual predictions differ from the concentration reference level values. The proposed models show good

predictive ability and accuracy according with the results in Table 4.10 which shows low RMSEP values (%w/w) and an acceptable RSEP (%) values. The models show a good performance base on the obtained results of bias.

Table 4.11 shows the results corresponding to accuracy analysis developed in each validation set with sixty spectra each one. When the concentration blends validation decreases the value of RSEP (%) and RMSEP calculated increases.

Table 4.11 Accuracy: NIR calibration models predictions RMSEP, RSEP (%) and bias per concentration level.

Reference value	RMSEP (%w/w)	RSEP (%)	Bias (%w/w)
0.751	0.0406	5.282	0.00396
1.752	0.0790	4.510	0.0104
2.802	0.1104	3.940	0.0392
Reference value	RMSEP (%w/w)	RSEP (%)	Bias (%w/w)
0.8017	0.0603	7.520	0.0112
1.3205	0.0758	5.736	0.0441
2.8097	0.0798	2.840	-0.0253
Reference value	RMSEP (%w/w)	RSEP (%)	Bias (%w/w)
0.757	0.0455	6.012	-0.0108
1.301	0.0764	5.872	0.0153
2.705	0.0779	2.879	-0.00053

4.2.5.4 Repeatability

Repeatability studies were designed to evaluate short term instrument precision. Repeatability was demonstrated using the two blends of the validation sets. NIR spectra were collected in static mode; six consecutive spectra were obtained for a powder blends.

The average, the standard deviations and relative standard deviations (RSD) or the coefficient of variation (CV) were calculated.

Table 4.12 show the predicted values, the mean, standard deviations and relative standard deviations for the repeatability study for the NIR calibration models calculated.

Table 4.12 Precision: NIR calibration models, repeatability

NIR Spectra number	Model 1		Model 2		Model 3	
	Validation Blend					
	2	3	2	3	2	3
1	1.746	2.817	1.184	2.620	1.335	2.762
2	1.743	2.803	1.182	2.611	1.340	2.720
3	1.756	2.818	1.181	2.619	1.329	2.745
4	1.754	2.817	1.192	2.616	1.330	2.801
5	1.755	2.816	1.172	2.608	1.314	2.748
6	1.756	2.820	1.159	2.680	1.347	2.744
Average (%w/w)	1.752	2.815	1.178	2.626	1.333	2.753
SD	0.006	0.006	0.011	0.027	0.011	0.027
RSDs (%)	0.342	0.213	0.934	1.028	0.825	0.981

The RSD gives an immediate idea of the precision of the models. RSD less than 1%^{68,75} is considered very good, while a RSD values less than 5% are considered good⁷⁵. Repeatability for the three models was validated due to RSD values that were within the commonly acceptable criteria.

4.2.5.5 Intermediate precision

Intermediate precision was determined by collecting NIR spectra of one blend from the validation set, acquired by two analysts on two days. An analysis of variance with two factors and two levels was developed. On Appendix B the tables of experimental

data and ANOVA corresponding to the evaluation of intermediate precision of the three NIR calibration models can be found. The analysis of variance with a level of significance of 95%, shows that the factors (analysts and days) does not have any effect on the precision of the models, because the p-values in all cases are greater than 0.05.

4.2.5.6 Range

The range was validated in each one of the calibration models, because the linearity, accuracy and precision were validated.

4.3 Residence Time

4.3.1 RTD fitting results

The Taylor dispersion method was used to fit the experimental data. This fit is required to eliminate the added noise in the experimental data, which helps filter the prediction errors of the NIR calibration models for concentrations closer to 0%.

Figure 4.9 shows the curve that corresponds to the Taylor dispersion model fit and experimental data for experiment with cohesion parameter (CP) of 0.733 kPa, feed frame paddle wheel speed (FF) of 30 rpm and die disc speed (DD) of 40 rpm, which demonstrates precision of the axial dispersion model in this process. Negative values in the concentration of caffeine predicted were observed. This is due to the low concentrations obtained at these points. However, these values are corrected by the fit of the experimental data.

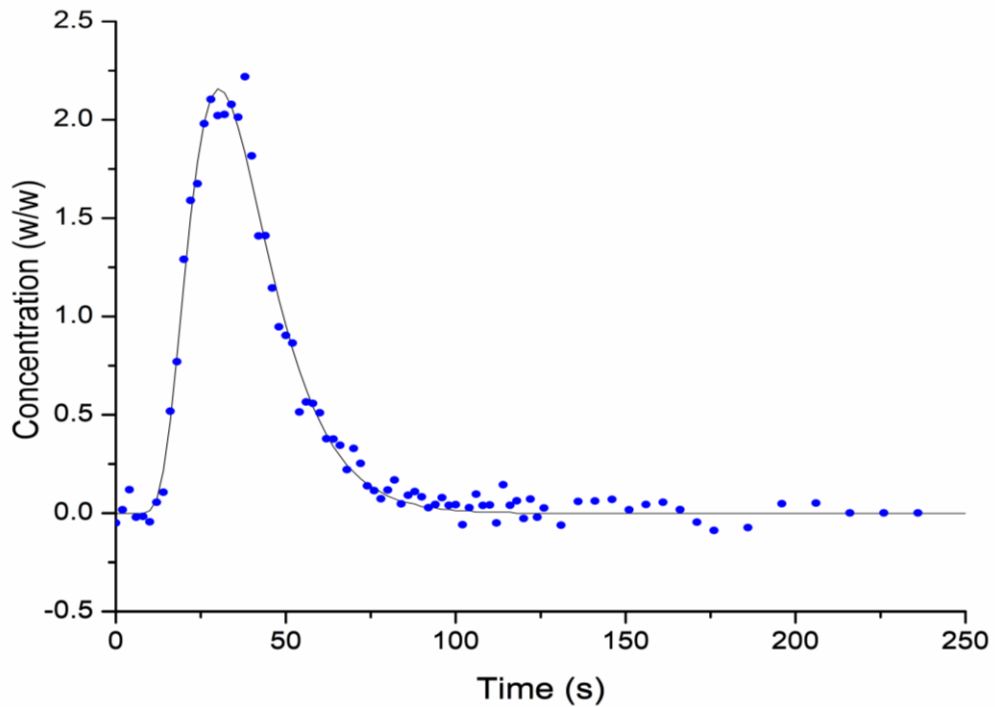


Figure 4.9 Fit and experimental data for experiment CP=0.733 kPa; FF=30 rpm and DD=40 rpm

4.3.2 *RTD as a function of operating conditions and the property of the materials*

The objective to characterize the RTD is to illustrate the powder dynamic in the feed frame include the powder flowability, the tracer dispersion, and the mixing effect.

Figure 4.10, Figure 4.11, and Figure 4.12 shows the experimental RTD profiles and ideal continuous stirred tank reactor (CSTR) profile (with dead time) at different operating conditions, for the first, second and third level of the cohesion parameter.

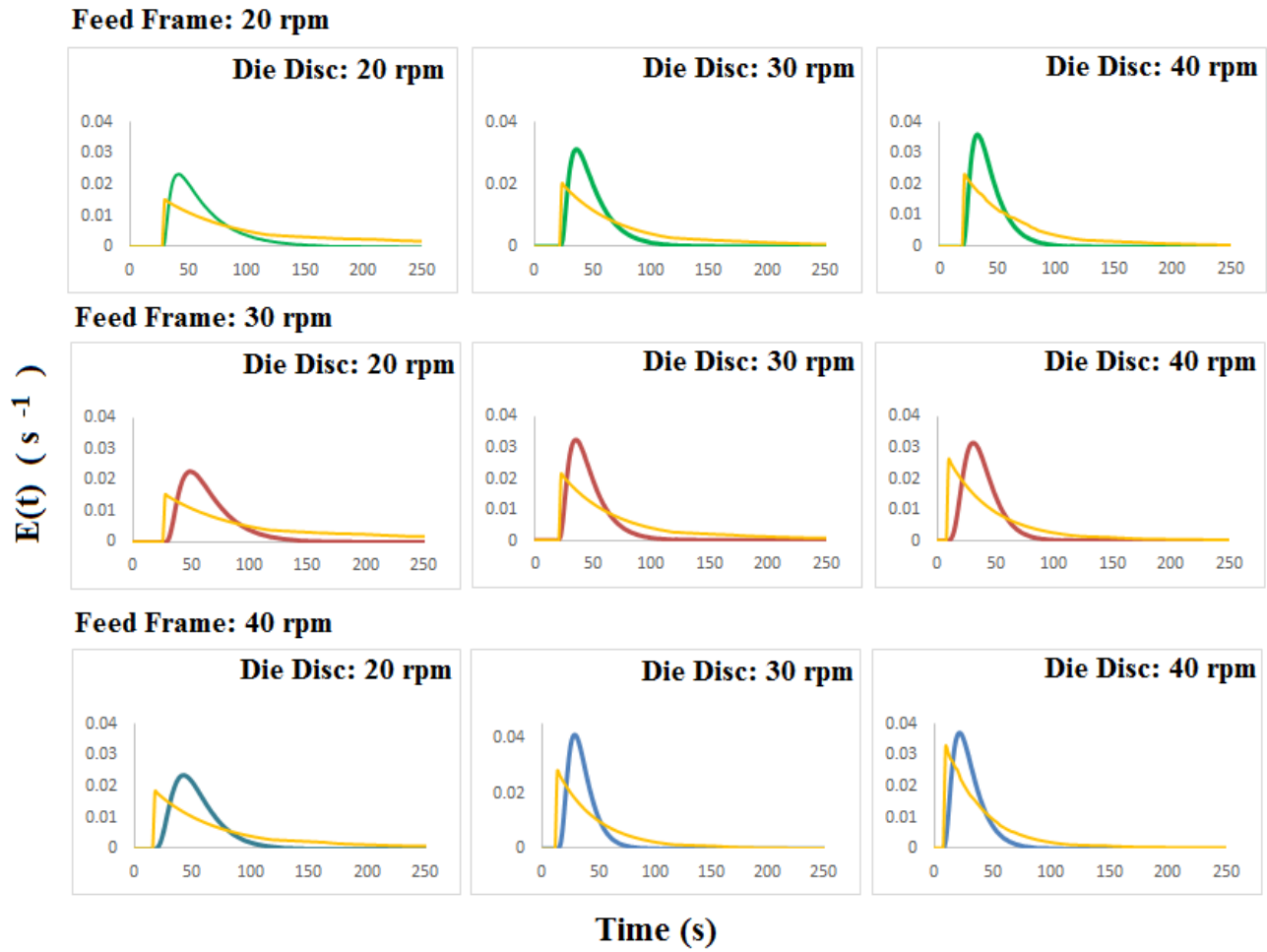


Figure 4.10 Fitted $E(t)$ function and ideal CSTR profile at different operating conditions and first level of cohesion parameter

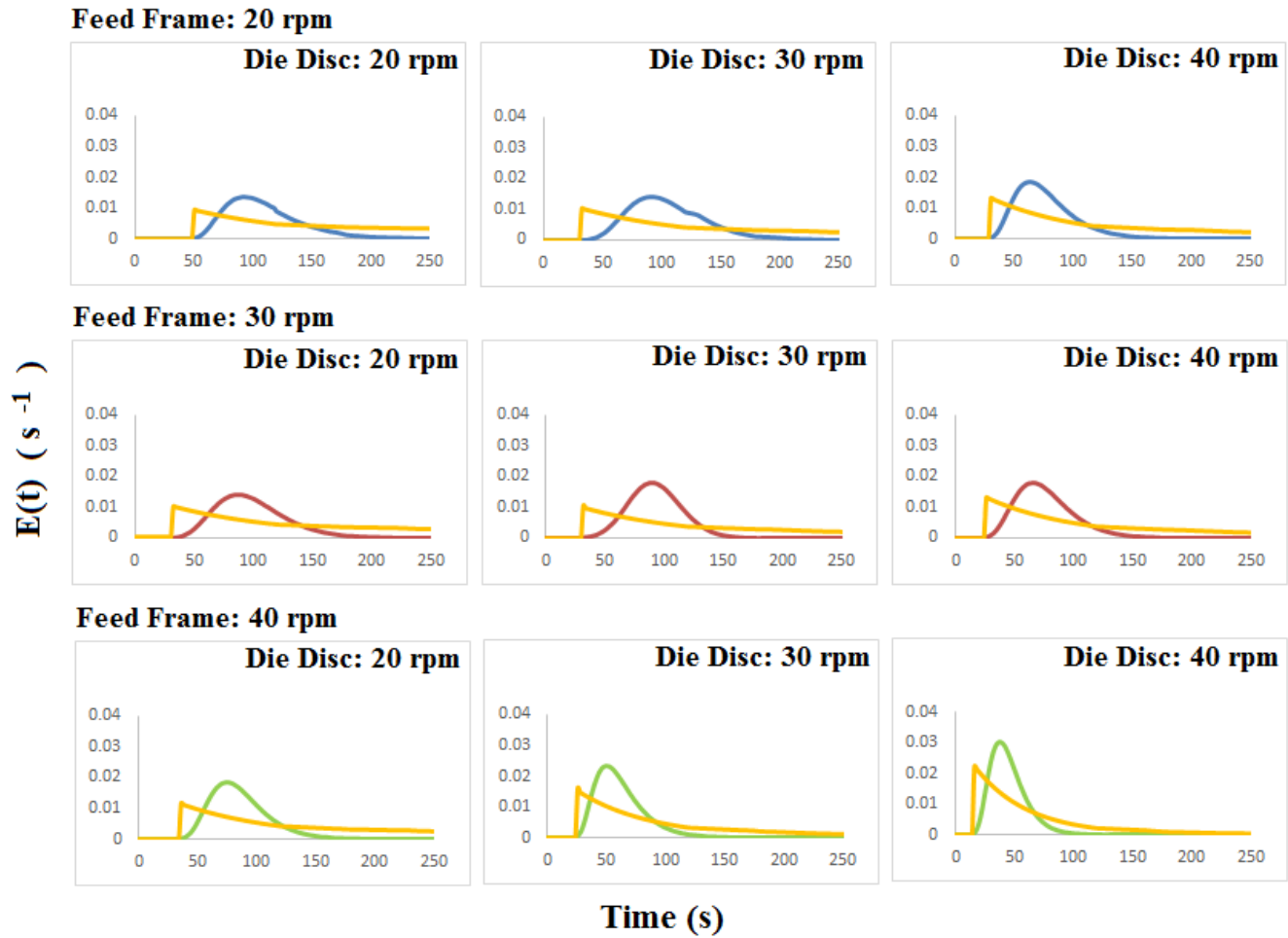


Figure 4.11 Fitted $E(t)$ function and ideal CSTR profile at different operating conditions and second level of cohesion parameter

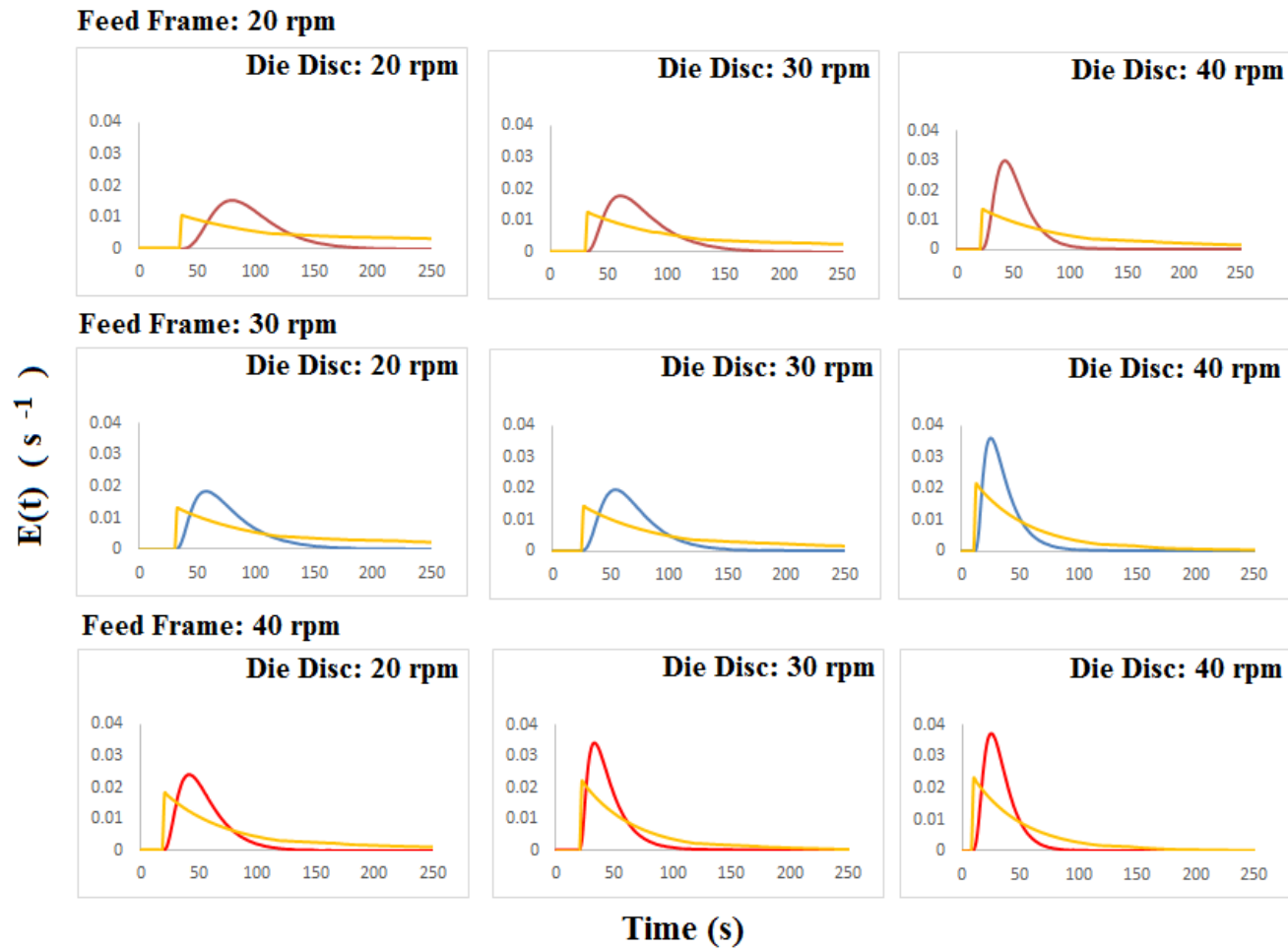


Figure 4.12 Fitted E(t) function and ideal CSTR profile at different operating conditions and third level of cohesion parameter

The width of the RTD decreases and the experimental RTD shape tends to ideal CSTR profile, consistent with previous computational¹¹ studies when increasing the paddle wheel speed, using the same die disc speed value. These trends demonstrate that at low paddle wheel speed the powder dispersion inside the feed frame is high. However, the change in the width of the RTD is more significant when the paddle wheel speed of the feed frame changes from 30 to 40 rpm. Major peaks of the residence time distribution are found at high paddle wheel and die disc speeds.

Dead time is the time that the first particle of tracer takes to exit of the feed frame. Regardless of the cohesion parameter level in study, a dead time was observed in tracer concentration at the exit of the feed frame. This dead time decreases when increasing the die disc speed, due to this the die disc speed controlled the outlet flowrate. At higher die disc speeds, more material is removed from the feed frame, allowing that the particle of tracer to be detected quickly at the output of the feed frame.

4.3.3 *Estimated mean residence time (MRT)*

The MRT and the mean centered variance (MCV) were used to quantify the flow behavior in the feed frame. The equations presented in section 3.5.5 were used to determine the RTD parameters. Table 4.13 shows the mean residence time (τ), delay time (t_0), total mean residence time (τ_{total}), mean centered variance (MCV) and standard deviation (SD) results for different operating conditions and cohesion parameter levels.

The highest mean residence time found is 152.734 s and the lowest is 38.306 s, at operating conditions and cohesion parameter of FF= 20 rpm, DD= 20 rpm, CP=1.055 kPa and FF = 40 rpm, DD = 40 rpm, CP=0.733 kPa, respectively.

Table 4.13 Mean residence time, dead time, total mean residence time, mean centered variance, and standard deviation results for different operating conditions and property of the materials

Cohesion Parameter kPa	Paddle wheel speed (rpm)	Die Disc speed (rpm)	τ (s)	t_o (s)	τ_{total} (s)	MCV (s ²)	SD (s)
0.733	20	20	65.240	30	95.240	885.829	29.763
0.733	30	20	64.854	28	92.854	556.836	23.597
0.733	40	20	54.340	16	70.340	433.266	20.815
0.733	20	30	48.798	24	72.798	335.033	18.304
0.733	30	30	46.291	22	68.291	271.701	16.483
0.733	40	30	35.562	14	49.562	141.555	11.898
0.733	20	40	43.023	21	64.023	228.728	15.124
0.733	30	40	38.125	10	48.125	216.852	14.726
0.733	40	40	30.306	8	38.306	196.769	14.027
1.055	20	20	104.734	48	152.734	985.588	31.394
1.055	30	20	98.811	30	128.811	921.621	30.358
1.055	40	20	85.650	34	119.650	587.538	24.239
1.055	20	30	102.939	34	136.939	939.931	30.658
1.055	30	30	92.884	26	118.884	491.803	22.177
1.055	40	30	61.927	24	85.927	424.430	20.602
1.055	20	40	76.081	28	104.081	622.532	24.951
1.055	30	40	76.347	24	100.347	616.751	24.834
1.055	40	40	44.716	14	58.716	223.998	14.967
1.433	20	20	94.435	36	130.435	899.549	29.992
1.433	30	20	76.492	32	108.492	849.711	29.150
1.433	40	20	54.184	20	74.184	441.821	21.020
1.433	20	30	78.962	32	110.962	851.767	29.185
1.433	30	30	68.459	26	94.459	631.253	25.125
1.433	40	30	44.657	22	66.657	288.123	16.974
1.433	20	40	51.179	22	73.179	265.113	16.282
1.433	30	40	34.864	12	46.864	232.203	15.238
1.433	40	40	32.922	10	42.922	178.548	13.362

The mean centered variance is an estimate of the degree of dispersion of powder inside the feed frame. The highest values of MCV were found when the operating conditions were FF =20 rpm and DD = 20 rpm. When the paddle wheel speed increases at a constant die disc speed and constant cohesion parameter, the mean centered variance decreases. Lower paddle wheel speed and lower die disc speed lead to larger mean residence time and a less narrow RTD. This phenomenon is associated with dispersion and the degree of confinement particles occurred in the feed frame. A computational study (DEM)^{12,23} demonstrated that when the paddle wheel speed is low, the powder has lower degree of confinement and some freedom to be rearranged, that promotes higher particle dispersion, which is consistent with a broad band in the E(t) function, and high mean centered variance value.

In this case, when the tracer is added in the frame feed and the paddle wheel speed is low, the tracer can be dispersed easily inside the feed frame, spending more time for be detected at the output and to leave the system completely. However, when the paddle wheel speed increases, the degree of confinement particles increases. This condition minimizes the powder rearrangement and when the tracer is added, it cannot disperse so easily inside the feed frame. This allows the tracer to be detected quickly at the output and reducing the time to completely exit the system.

4.3.4 RTD experiments reproducibility

An experiment was selected at random and two additional replicates were made, with the objective of studying the reproducibility of the experimental method used. Figure 4.13 shows the fit of the experimental data for the three replicates made to the experiment with the conditions: CP = 1.433 kPa, FF = 20 rpm, DD = 20 rpm.

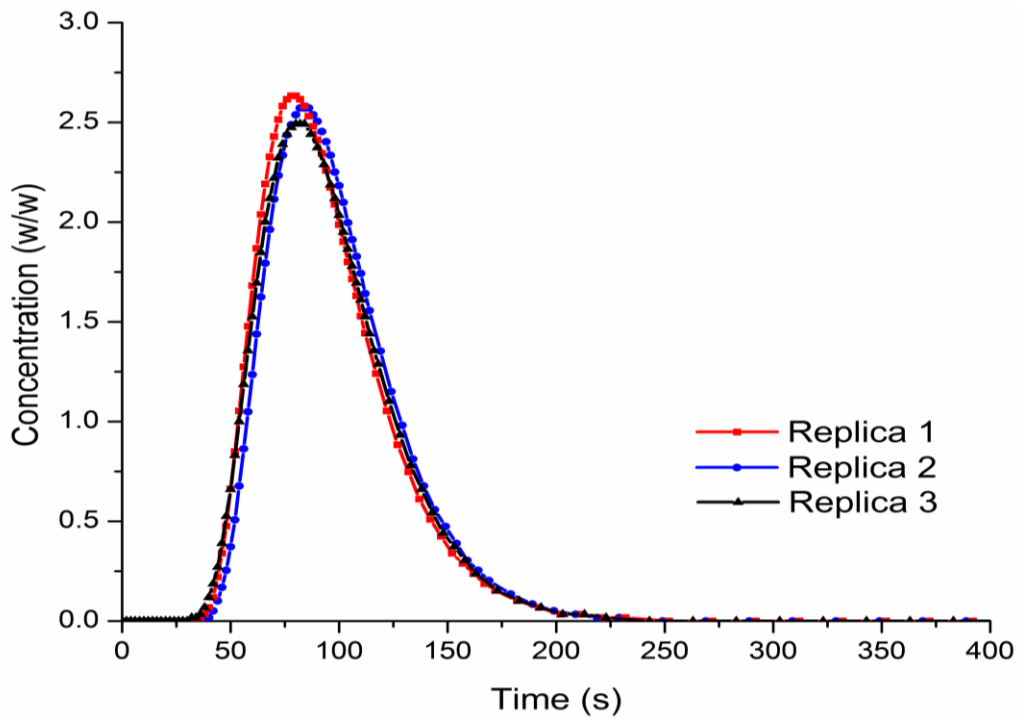


Figure 4.13 Fit of the experimental data for the three replicates of the experiment CP=1.433 kPa; FF=20 rpm and DD=20 rpm

Table 4.14 shows the total mean residence time and the mean centered variance estimates for each of the replicates, the average, standard deviation (SD) and relative standard deviation (RSD) of the measurements.

Table 4.14 Total MRT and MCV for the three replicas of the experiment CP=1.433 kPa;
FF=20 rpm and DD=20 rpm

Replica	τ (s)	t_o (s)	τ_{total} (s)	MCV
1	94.435	36	130.435	899.549
2	98.338	38	136.338	878.538
3	95.487	32	127.487	911.742
Average	96.087	35.333	131.420	896.610
SD	2.0196	3.055	4.507	16.796
RSDs			3.429	1.873

The difference between MRT values may be associated with sampling errors and non-ideal pulse injection, among others. However, the value of 4.507 s for the standard deviation and of 3.429% for the coefficient of variation (CV) demonstrated that the experimental method has a good RTD reproducibility.

4.3.5 *Effect of the paddle wheel speed on mean residence time*

The feed frame from Fette 3090 tablet press has two levels and three-paddle wheels at the same speed, the dispersion in this feed frame is a contribution of the dispersion in its two levels and promoted by each of the paddle wheel.

Figure 4.14 shows the effect of the paddle wheel speed on the mean residence time, as paddle wheel speed increases, the mean residence time decreases. This is because the paddle wheel is forcing material to exit in less time from the feed frame. Also, when increases the paddle wheel speed the mean centered variance decrease. This behavior is directly associated with the degree of confinement and the dispersion phenomenon of the powder within the feed frame.

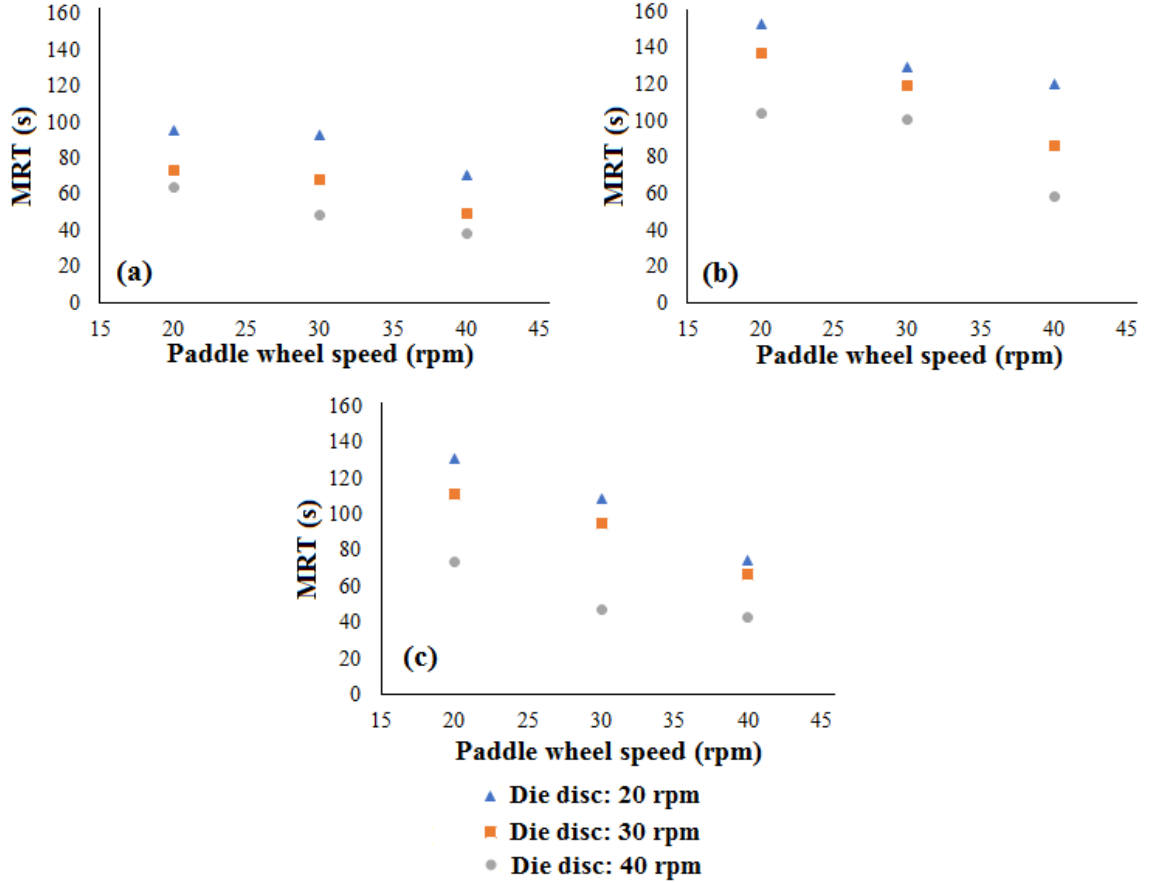


Figure 4.14 Effect of the paddle wheel speed on mean residence time at constant die disc speed (a) Cohesion parameter 0.733 kPa (b) Cohesion parameter 1.055 kPa (c) Cohesion parameter 1.433 kPa

4.3.6 Effect of the die disc speed on mean residence time

The die disc speed is one important process variable that is related to the capacity of the manufacturing and is established by the production rate. Figure 4.15 demonstrates the effect of the die disc speed on the total MRT. When the die disc speed values increase from 20 to 40 rpm, the total mean residence time decreases, mostly due to the increase in the mass of powder removed by the die disc by time unit from the feed frame. Moreover, when the cohesion parameter is 0.733 kPa and the operating conditions are FF=20 rpm,

DD=20 rpm and FF=30 rpm, DD=20 rpm, the mean residence times are similar. This is mainly due because at 20 rpm in the die disc, the die filling is greater²⁹ than 30 rpm due to the higher feeding force.

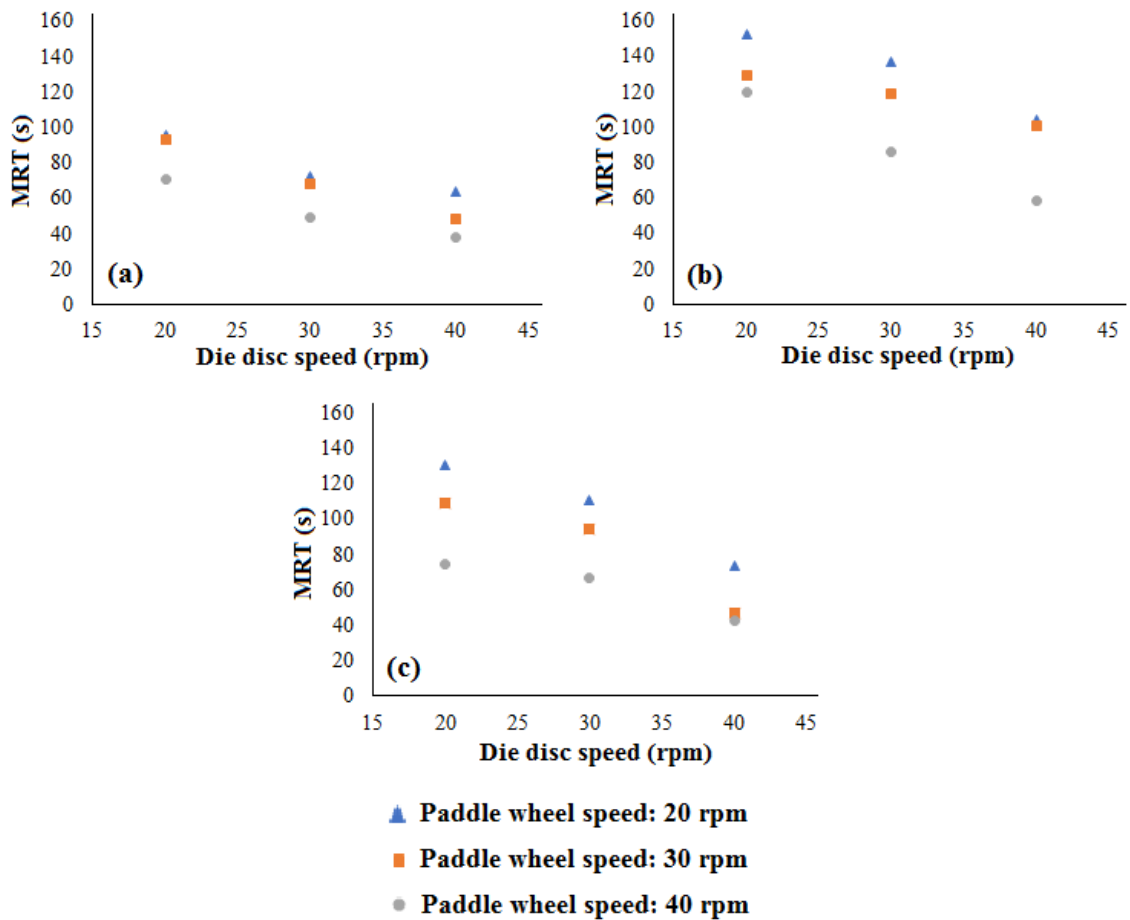


Figure 4.15 Effect of the die disc speed on mean residence time at constant paddle wheel (a) Cohesion parameter 0.733 kPa (b) Cohesion parameter 1.055 kPa (c) Cohesion parameter 1.433 kPa

When comparing the Figure 4.14 and the Figure 4.15 it is noticed that the mean residence time is more sensitive to changes in the die disc speed than changes in the paddle wheel speed.

4.3.7 Effect of the cohesion parameter on mean residence time

In addition to the operating conditions of the feed frame, the properties of the materials represent another source of variation for the MRT of the powder inside the feed frame. To the best of our knowledge, there have been no publications with experimental studies, dedicated to the effect of the cohesion parameter on powder behavior inside the feed frame. Figure 4.16 shows the effect of the cohesion parameter on the mean residence time.

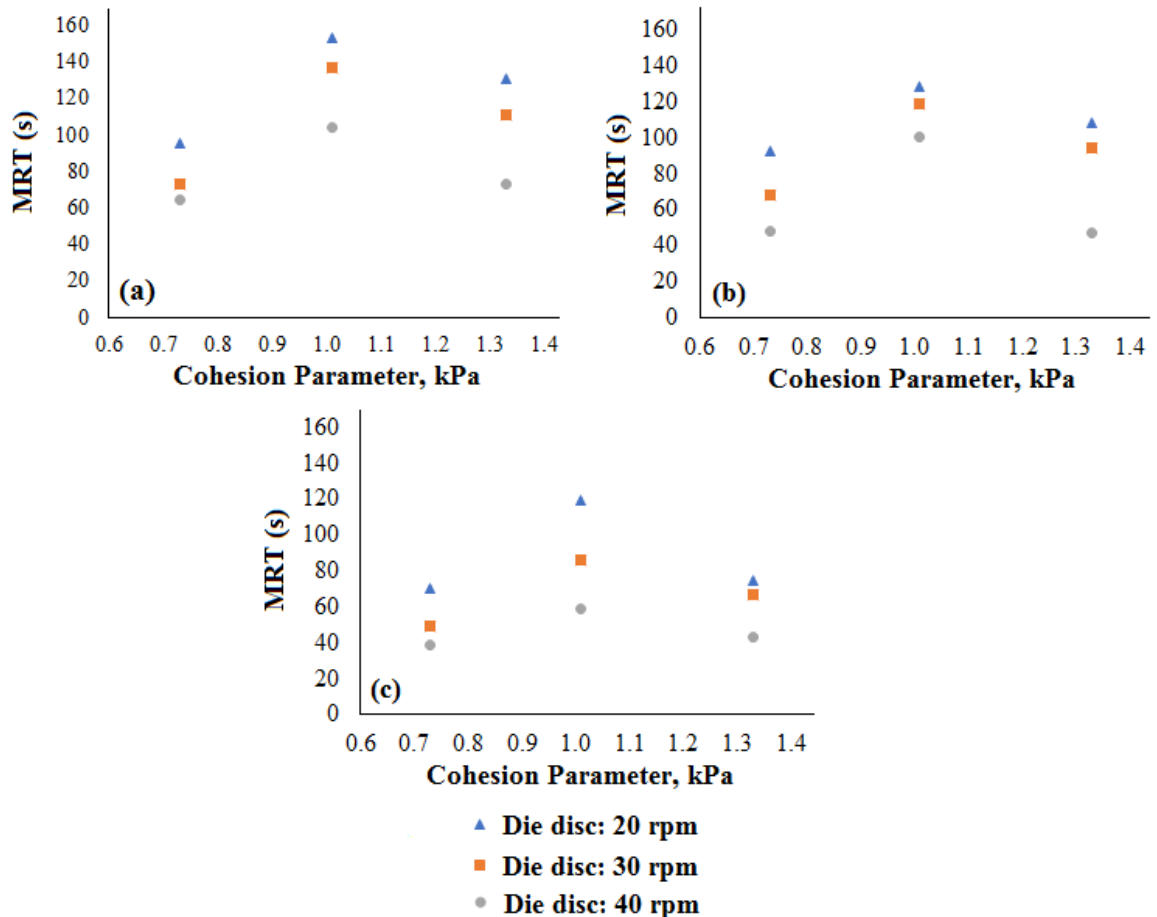


Figure 4.16 Effect of the material cohesion parameter on mean residence time at constant die disc speed (a) FF= 20 rpm (b) FF= 30 rpm (c) FF= 40 rpm

Figure 4.16 shows that when the cohesion parameter increases, a non-linear behavior is observed in the mean residence time. This behavior is mainly due to the percolation phenomenon that occurred inside the feed frame. Table 4.1 shows the averages values of the D50 for raw materials. It may be noted that the lactose 70 has a D50 of about 10 times higher than the D50 of the Avicel® PH-105. These are the main constituents of the mixtures of the second level of the cohesion parameter, while the D50 differences of the principal components of the mixtures of the level 1 and 3 are 1.7 and 3 times, respectively.

Previous studies^{76,77} have shown that percolation segregation phenomenon in granular pharmaceutical mixtures is principally a function of the difference of densities, size and geometrical form between the particles. Recently, Mateo et al¹² showed that the phenomenon of percolation can occur within the feed frame, placing the largest particles at the top and smaller at the bottom.

In this case, the particles of Avicel® PH-105 would be placed at the bottom and those of lactose 70 at the top of the feed frame. Then, when the tracer is added, it finds a space between the particles of lactose 70 and the percolation phenomenon occurs, which leads to a greater dispersion of the tracer within the feed frame and therefore a longer residence time.

4.4 Statistical Analysis

To develop the statistical model, the effects of the main factors or model parameters (α : cohesion parameter, kPa, β : paddle wheel speed, rpm; γ : die disc speed, rpm) and their interactions were determined, based on the significance to the mean residence time, an analysis of variance (ANOVA) was performed to analyze the data.

4.4.1 Full model

Initially, the statistical model used is:

$$y_{ijk} = \mu + \alpha_i + \alpha_i^2 + \beta_j + \beta_j^2 + \gamma_k + \gamma_k^2 + \alpha\beta_{ij} + \alpha\gamma_{ik} + \beta\gamma_{jk} + \alpha\beta\gamma_{ijk} + \varepsilon_{ijk} \quad 4.2$$

This model is not completely solvable when the replicate number is one, because the error has no degrees of freedom. One approach to the analysis is to assume that the high-order interactions are not significant and use the degrees of freedom to form an error term. Eliminating the high-order interactions, the following model appears:

$$y_{ijk} = \mu + \alpha_i + \alpha_i^2 + \beta_j + \beta_j^2 + \gamma_k + \gamma_k^2 + \alpha\beta_{ij} + \alpha\gamma_{ik} + \beta\gamma_{jk} + \varepsilon_{ijk} \quad 4.3$$

The residuals (difference between the predicted and experimental MRT) were analyzed under the typical assumptions of normality, independence and equality of variance. Figure 4.17 show the normal probability plot of the residuals for this experiment, although small deviations are observed to the line of normality, the general impression is that the distribution of the residuals is approximately normal.

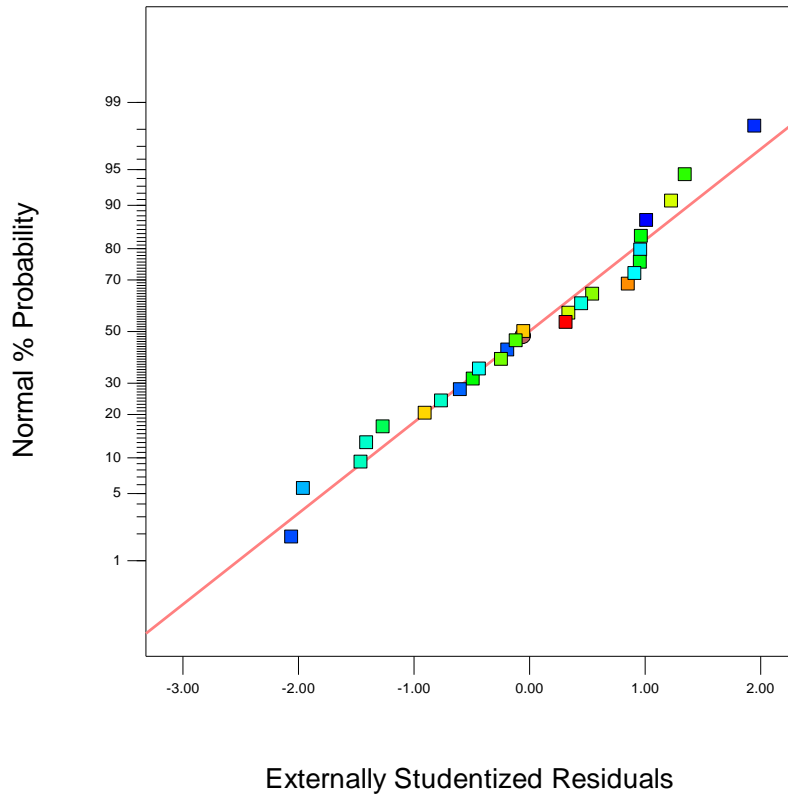


Figure 4.17 Normal probability plot of residuals

Appendix C shows the verification of the assumptions of equality of variance and independence for the residuals of the full model. It is concluded that the variances are constant and that there is no correlation between the residuals.

The analysis of variance for this model was performed as shown on Table 4.15, The model is significant with a p-value lower than 0.0001. Also, it can be concluded that the main factors: cohesion parameter, paddle wheel speed and die disc speed are significant, likewise the quadratic term of the cohesion parameter, with a confidence level of 95%.

All interactions and the quadratic terms of the paddle wheel speed and the die disc speed, are enough insignificant with p-values greater than 0.05.

Table 4.15 ANOVA for the Mean Residence Time experiments: Full model

Source	Sum of Squares	df	Mean Square	F Value	p-value Prob > F
Model	24890.95	9	2765.66	43.96	< 0.0001
<i>A-Cohesion parameter</i>	1236.49	1	1236.49	19.65	0.0004
<i>B-Paddle wheel speed</i>	6276.95	1	6276.95	99.78	< 0.0001
<i>C-Die disc speed</i>	8782.90	1	8782.90	139.61	< 0.0001
<i>AB</i>	256.28	1	256.28	4.07	0.0596
<i>AC</i>	144.51	1	144.51	2.30	0.1480
<i>BC</i>	13.86	1	13.86	0.22	0.6448
<i>A²</i>	8453.67	1	8453.67	134.38	< 0.0001
<i>B²</i>	84.62	1	84.62	1.35	0.2622
<i>C²</i>	65.91	1	65.91	1.05	0.3204
Residual	1069.48	17	62.91		
Cor Total	25960.44	26			

For this model, the $R^2=0.9588$ and the prediction R^2 is **0.8914**. Only the significant terms of this model will be included in the fitted model, this is expected to improve the model.

4.4.2 Fitted Model

The nonsignificant interaction terms were removed of the full quadratic model. The fitted model now contains only the main effects cohesion parameter, paddle wheel speed, die disc speed and the quadratic term of cohesion parameter.

The equation for this model is:

$$y_{ijk} = \mu + \alpha_i + \alpha_i^2 + \beta_j + \gamma_k + \varepsilon_{ijk} \quad 4.4$$

The assumptions of normality, independence, and uniformity of variance of the residuals for the fitted model are verified. Figure 4.18 show the normal probability plot, once again the error distribution is approximately normal. A plot of residuals versus run number is shown in Figure 4.19 and a plot of residuals versus predicted value is shown in the Figure 4.20. There is no reason to suspect any violation of the independence or constant variance assumptions, namely, the assumptions are satisfied.

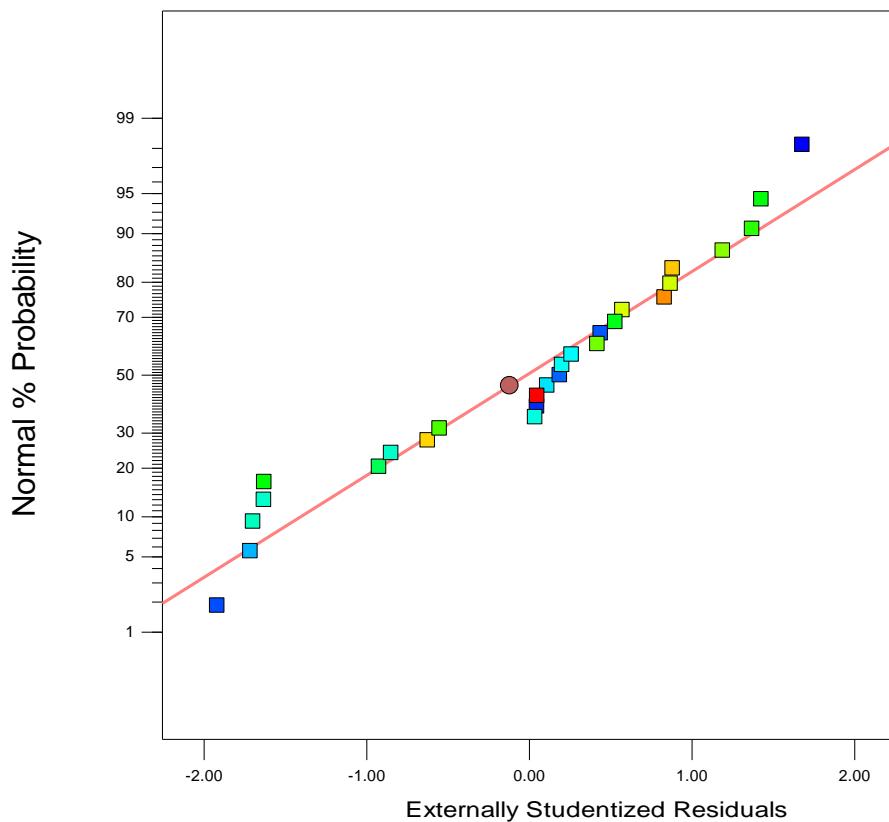


Figure 4.18 Fitted model normal probability plot

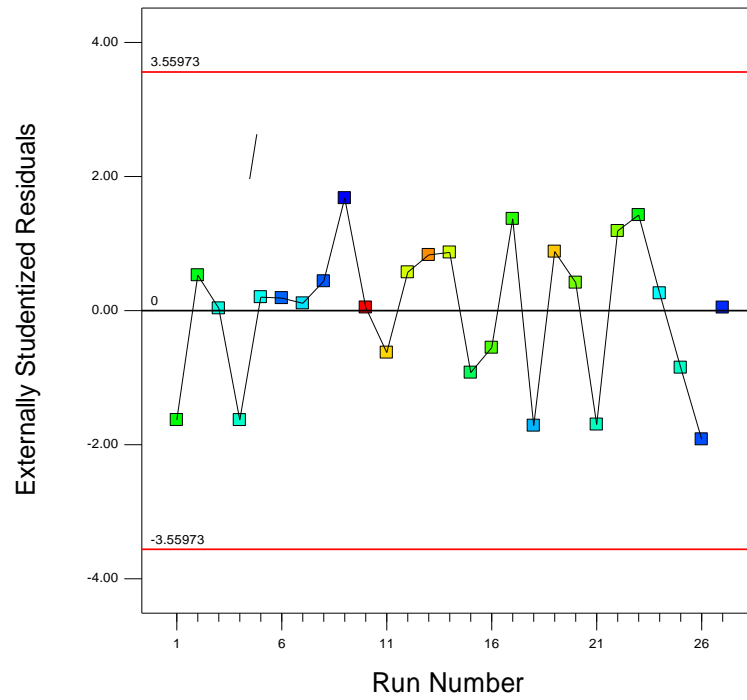


Figure 4.19 Fitted model plot of residuals versus run number

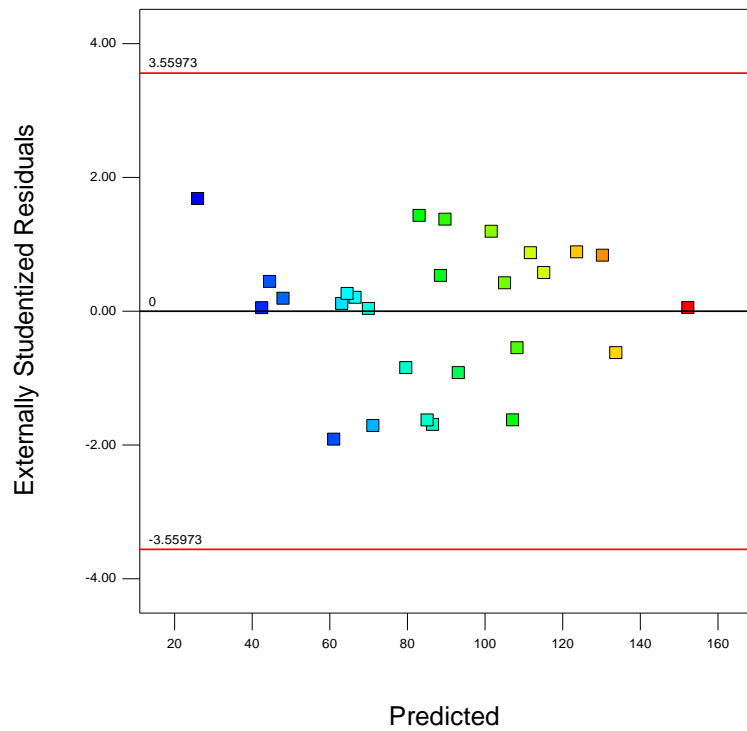


Figure 4.20 Plot of residuals versus predicted value for the fitted model

However, the Figure 4.18 displays small deviations to the line of normality, for this reason the Anderson-Darling normality test was performed. The Anderson-Darling is a statistic tool that measures how well the data from a population follow a specific distribution. Figure 4.21 present the results of this analytical test. The Anderson-Darling (AD) statistic (0.611) has a value less that the critical value of the statistic (0.751) for a sample size of 27 and at a 95% level of significance^{78,79}. The p-value is greater than the chosen significance level (0.05), the residuals follow a normal distribution.

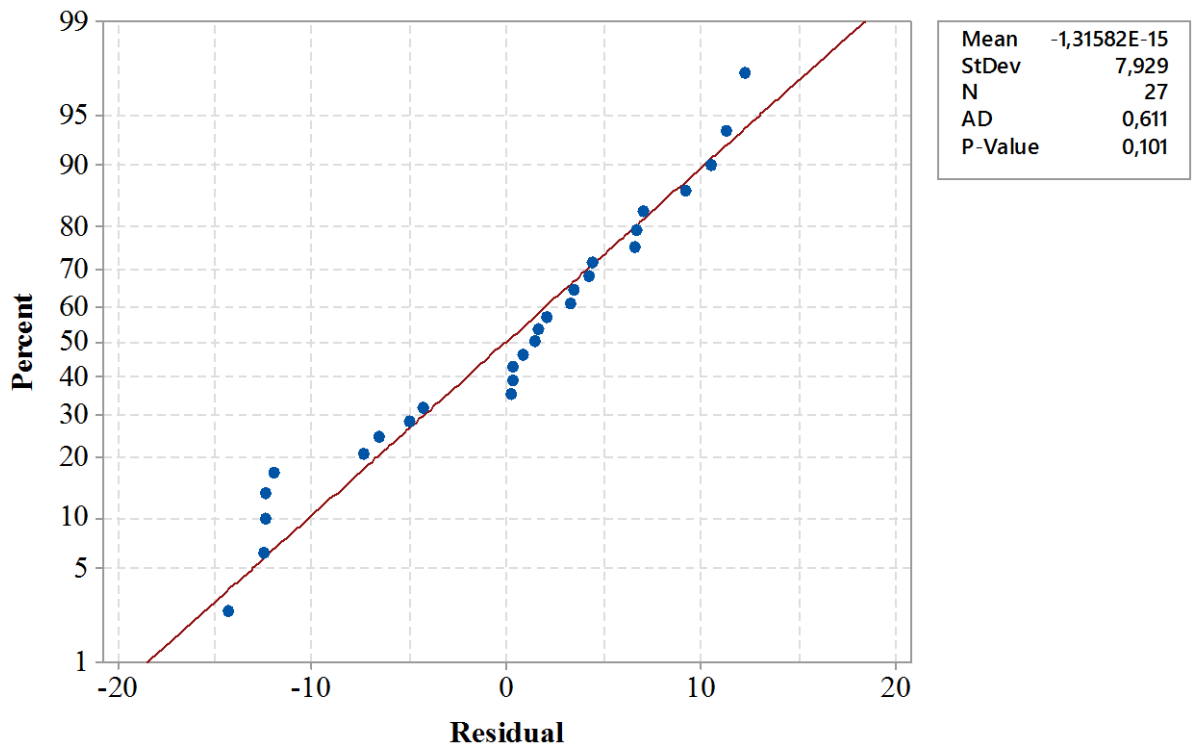


Figure 4.21 Anderson-Darling normality plot of the residual

Figure 4.22 show the Box-Cox test; this test was done with the objective of verifying if a transformation of the data was necessary to stabilize the variance or to

approximate more the variable response to the normal distribution^{69,80}. Thus, it is shown that a transformation of the data is not necessary, due to confidence limits include the value 1.

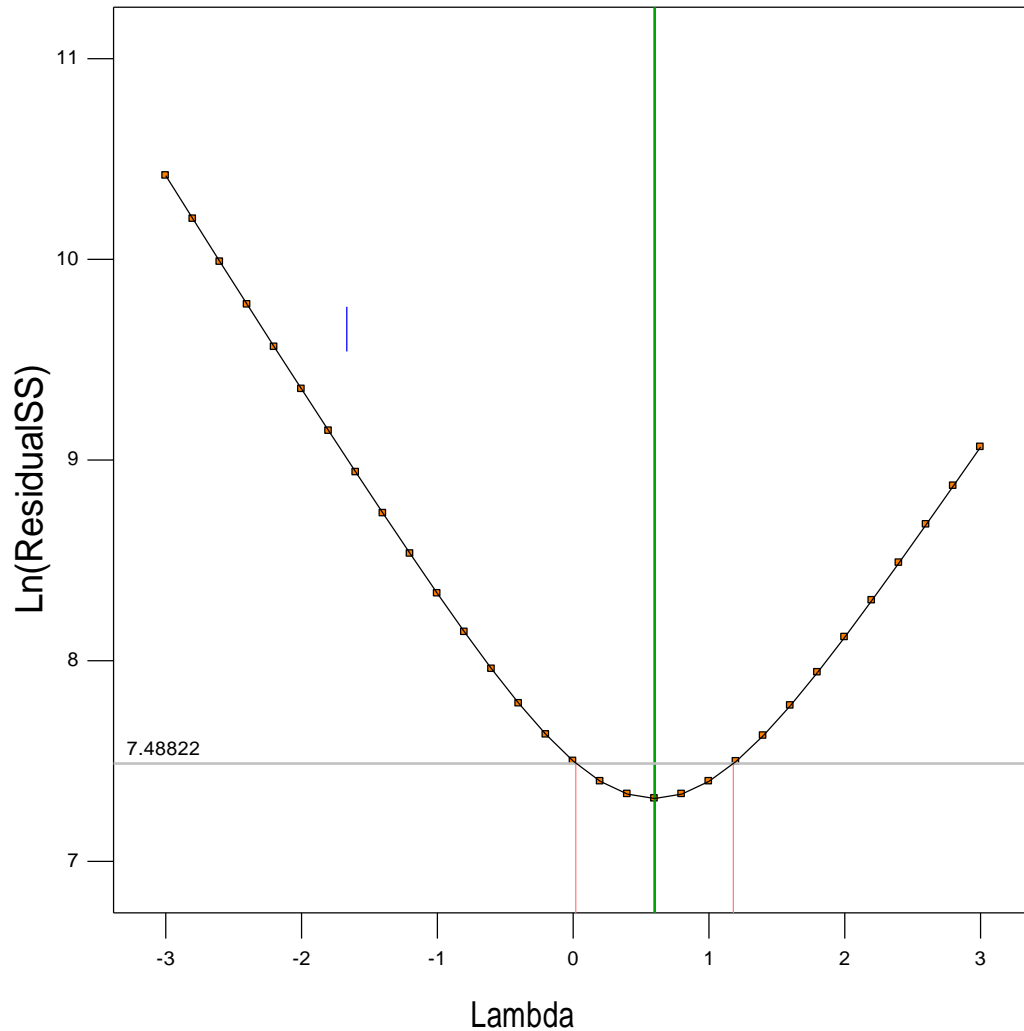


Figure 4.22 Box-Cox test

Table 4.16 show the analysis of variance (ANOVA) for this model. Clearly, the model and all terms included are significant, presenting very small value of p .

Table 4.16 ANOVA for the Mean Residence Time experiments: Fitted model

Source	Sum of Squares	Df	Mean Square	F Value	p-value Prob > F
Model	24325.78	4	6081.44	81.85	< 0.0001
<i>A-Cohesion parameter</i>	1236.49	1	1236.49	16.64	0.0005
<i>B-Paddle wheel speed</i>	6202.27	1	6202.27	83.47	< 0.0001
<i>C-Die disc speed</i>	8719.78	1	8719.78	117.35	< 0.0001
A^2	8453.67	1	8453.67	113.77	< 0.0001
Residual	1634.66	22	74.30		
Cor Total	25960.44	26			

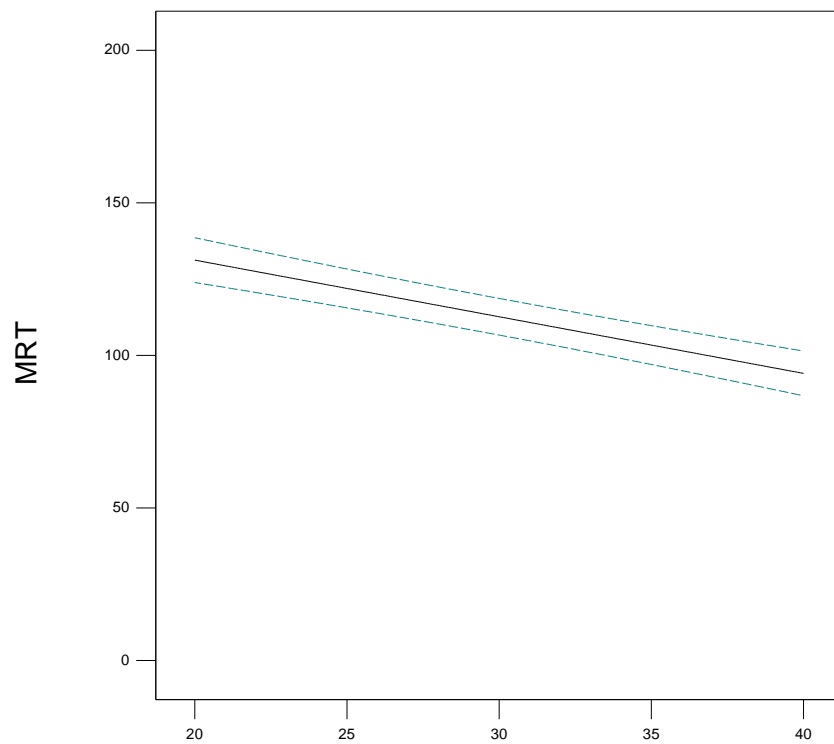
Table 4.17 presents the R^2 statistical for the fitted model. The proportion of total variability in mean residence time that is explained by this model is $R^2=0.9370$, which is smaller than the R^2 for the full model ($R^2=0.9588$). It is usual for this statistic to increase with the number of factors in the model⁶⁹. However, the *Prediction R^2* of the fitted model is higher than *Prediction R^2* of the full model. This indicates that the fitted model would be expected to explain about **90.46** percent of the variability in new data. Finally, the *Adeq Precision* measures the signal-to-noise ratio. A high value is desirable, the ratio obtained is 34.053, which indicates an adequate signal and that this model can be used to navigate the design space.

Table 4.17 R^2 statistics for fitted model

Statistic	Value
R^2	0.9370
Adjusted R^2	0.9256
Prediction R^2	0.9046
Adeq Precision	34.053

Clearly, when the nonsignificant terms are removed from the full model has produced a final model that is probable to function more effectively as a predictor of new data.

The effect of each of the factors on MRT is shown below, with 95% confidence interval bands. Figure 4.23 show the effect of paddle wheel speed on the mean residence time, when cohesion parameter is setup in 0.733 kPa and die disc speed in 30 rpm. The relationship between mean residence time and paddle wheel speed is linear in the space design.



B: Paddle wheel speed (rpm)

Figure 4.23 Effect of paddle wheel speed on MRT from empirical model

Figure 4.24 show the effect of die disc speed on the mean residence time, when the cohesion parameter is 0.733 kPa and paddle wheel speed is 30 rpm. It can be observed that, when die disc speed increases the MRT increases linearly.

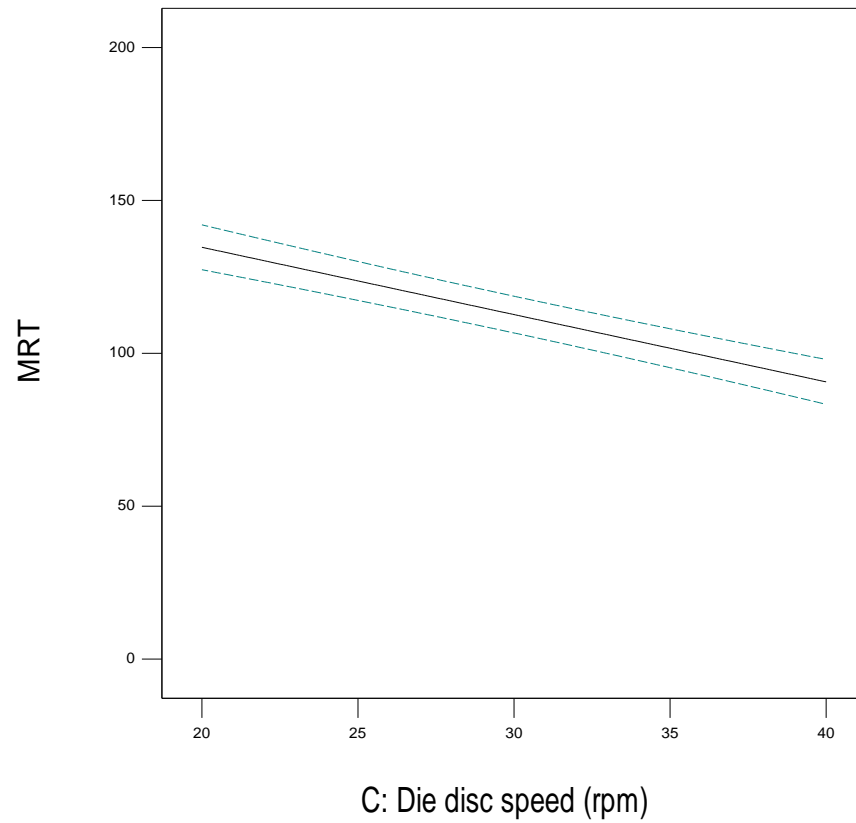
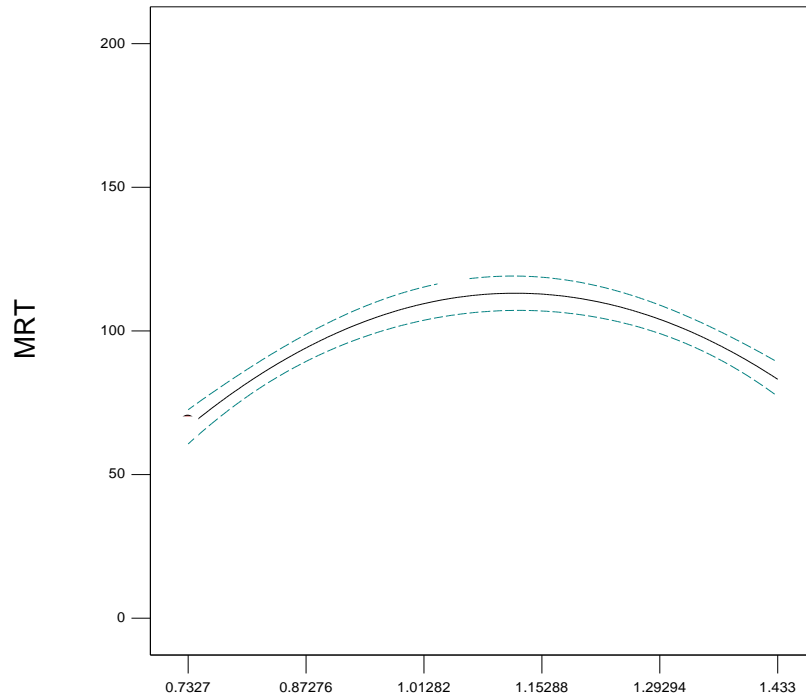


Figure 4.24 Effect of die disc speed on MRT from empirical model

Figure 4.25 show the effect of cohesion parameter in kPa, on the mean residence time at paddle wheel speed 30 rpm and die disc speed 20 rpm. It may be noted that unlike the other two factors, cohesion and MRT do not have a linear relationship within the design space.



A: Cohesion Parameter (kPa)

Figure 4.25 Effect of cohesion parameter on MRT from empirical model

4.4.3 Empirical model

The statistical model will be presented in terms of coded variables and natural variables. Equation 4.5 is in terms of the coded factors, and can be used to make predictions corresponding the response variable for the levels of each factor, where +1, -1 and 0 represent the high, low and medium level, respectively. Equally, the equation in terms of coded factors allows to identify the relative impact of factors by comparing the factor coefficients.

$$MRT (s) = 112.69 + 8.29*A - 18.56*B - 22.01*C - 37.79*A^2 \tag{4.5}$$

Here A , represent the coded cohesion parameter, B is the coded paddle wheel speed and C represent the coded die disc speed.

This equation can be used to predict mean residence times with different conditions to the levels defined by factor, in this case, the conversion of the natural variable to the codified one must be done.

Finally, the *empirical model* in terms of natural variables to predict the mean residence time based on the cohesion parameter (kPa), wheel speed (rpm), and die disc speed (rpm), is:

$$\begin{aligned}
 MRT (s) = & -152.587 + 691.099 * (\text{Cohesion parameter}) \\
 & -1.856 * (\text{Paddle wheel speed}) \\
 & -2.201 * (\text{Die disc speed}) \\
 & -308.186 * (\text{Cohesion parameter})^2
 \end{aligned}
 \tag{4.6}$$

The equation in terms of natural factors can be used to make predictions within space design using the levels specified in the original units for each factor.

4.4.4 Contour plots and response surface

The contour plots and response surface allows to make a graphical estimate of the response variable, in this case the mean residence time. Figure 4.26 highlights the contour plot when the paddle wheel speed and the die disc speed variates at cohesion parameter of 0.733 kPa. The contour plots when the cohesion parameter is 1.055 kPa and 1.433 kPa, can be found in the Appendix E.

These plots take importance when the properties of the material are known and the interest is to determine the mean residence time based on the operating conditions of the feed frame.

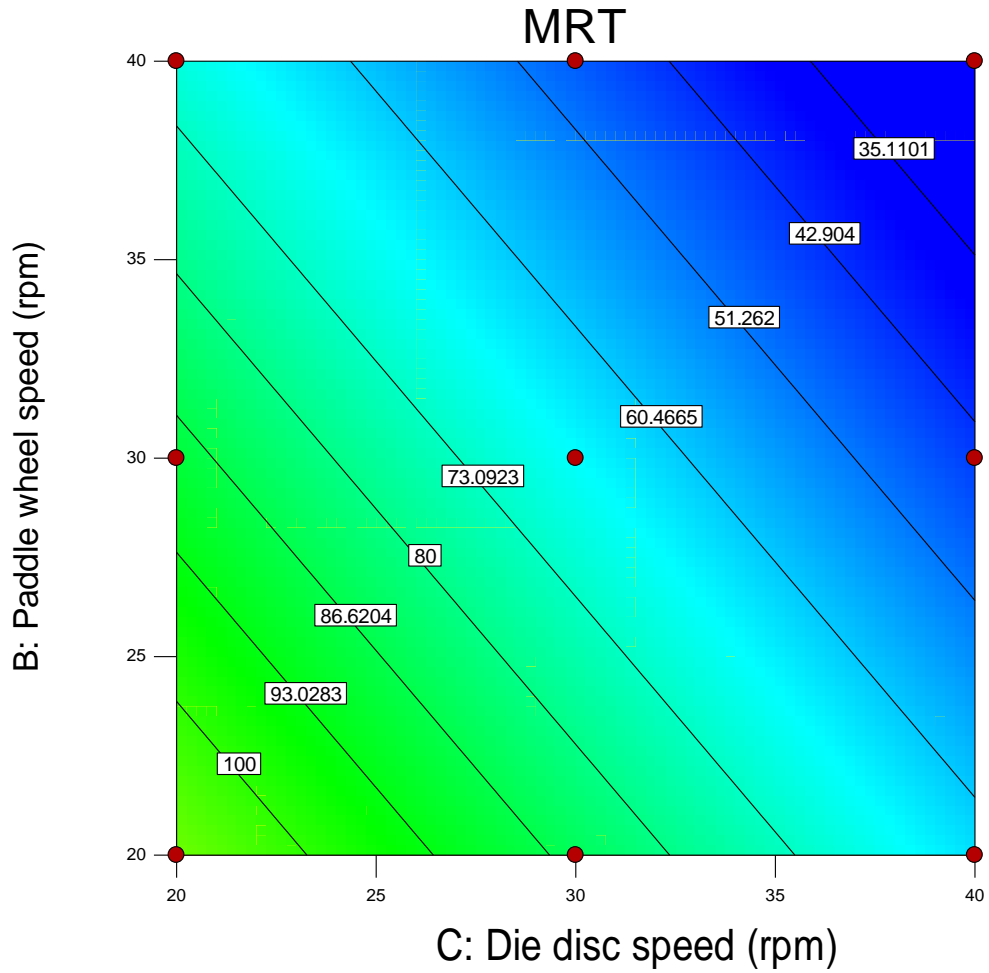


Figure 4.26 Contour plots at cohesion parameter: 0.733 kPa.

Figure 4.27 present the three-dimensional plot for the mean residence time obtained from the regression model o fitted model. In the response surface the paddle wheel speed versus cohesion parameter is plotted. The die disc speed factor is set at 30 rpm.

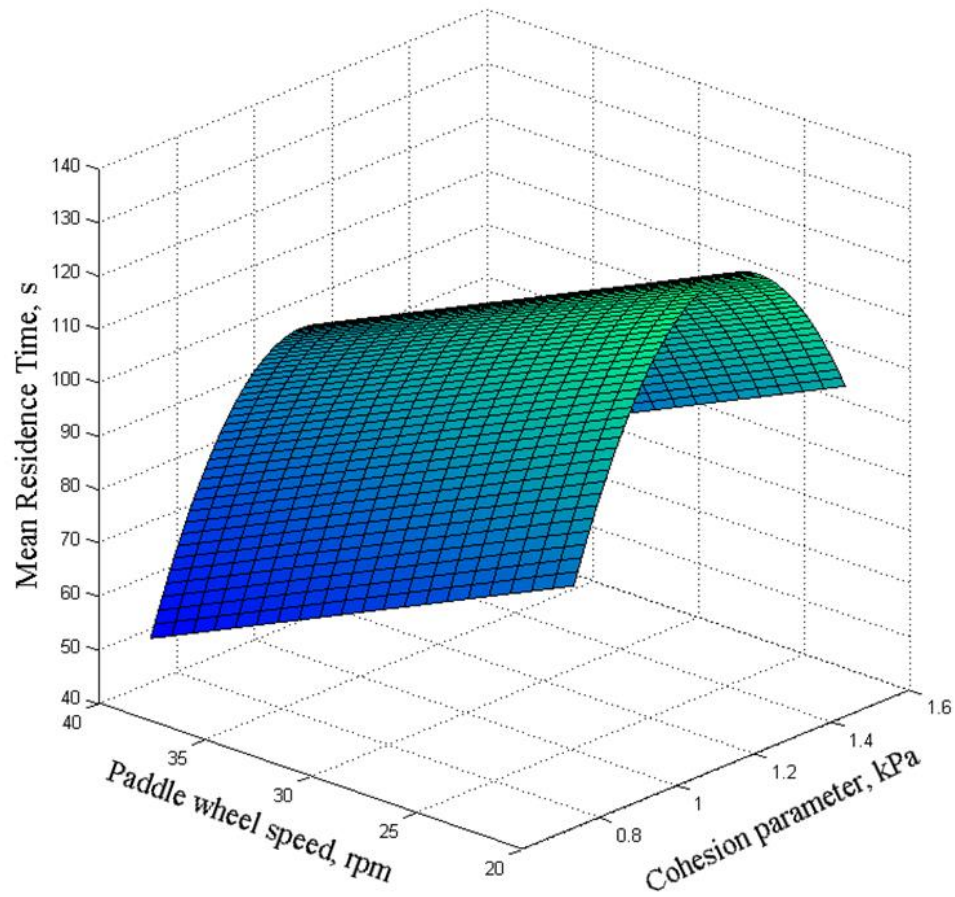


Figure 4.27 Response surface for mean residence time, varying the paddle wheel speed and cohesion parameter and setting the die disc speed at 30 rpm.

4.5 Validation of the Empirical Model

Two strategies were used to validate the empirical model; the first strategy used blends with the same cohesion parameters included in the empirical model and varying the operating conditions, and the second strategy with a new formulation, meaning a new cohesion parameter.

4.5.1 Validation at different operating conditions

Table 4.18 shows the validation experiment setup when the cohesion parameters included in the empirical model remain constant and, the operating conditions are being modified. These validations are needed to determine the capability of the model to predict the MRT when the tablet production speed and paddle wheel speed are changed before starting the compression process.

Table 4.18 Validation experiments setup

Validation	Cohesion parameter, kPa	Paddle wheel speed (rpm)	Die disc speed (rpm)
1	0.733	34.1	25.8
2	1.433	20	35
3	1.055	23.8	40

Table 4.19 shows the experimental and estimated total mean residence time (τ_{total}), the mean centered variance (MCV) and the estimated error percentage for these validations:

Table 4.19 Validation experiment results at different operating conditions

Validation	τ_{total} (s) Experimental	MCV	τ_{total} (s) Estimated	% Error
1	66.253	256.067	68.321	3.12
2	90.295	569.451	90.743	0.50
3	104.242	623.801	101.287	2.84

Table 4.19 show that the highest error percentage is 3.12% and the lowest 0.50%, which shows that the empirical model developed is effective in predicting the mean residence time when variations are made in the operating conditions of the feed frame between 20 and 40 rpm and the cohesion parameters remain unchanged.

4.5.2 Validation at different cohesion parameters

The validation of the empirical model at different cohesion parameters was performed with three additional experiments: one that keeps operating conditions, included in the empirical model, unchanged, while the other two did not.

Validations at different cohesion parameters are necessary to determine if the model can predict the MRT for any formulations between the lowest and highest cohesion parameter, in the range of operating conditions included in the model.

Table 4.20 show the compositions of the blends used for these validations.

Table 4.20 Compositions (% w/w) for validation blends

Material	Composition (%w/w)	
	Blend 1	Blend 2
APAP	10.00	-
Avicel® PH-105	38.50	45.00
Lactose 70	50.00	55.00
SiO ₂	0.50	-
MgSt	1.00	-

Table 4.21 presents the compressibility percentage, cohesion parameter, flow factor, particle size (D50) and densities for the blends used for these experiments. The reported results are the average of three different samples.

Table 4.21 Characterization of validation blends

	Blend 1	Blend 2
Compressibility percentage (% v/v)	12.52 ±0.16	18.23±0.50
Cohesion parameter (kPa)	0.92±0.02	1.21±0.04
Flow factor	5.06±0.02	3.61±0.12
True density (g/cm ³)	1.59±0.00	1.59±0.00
Tap density (g/cm ³)	0.63±0.00	0.71±0.01
Bulk density (g/cm ³)	0.48±0.00	0.44±0.00
Particle size distribution		
<i>d</i> 10 (μm)	11.22±0.15	11.65±0.10
<i>d</i> 50 (μm)	84.06±1.71	67.42±0.76
<i>d</i> 90 (μm)	336.14±2.5	307.13±1.98

For these validations, the selected operating conditions are summarized in Table 4.22.

Table 4.22 Validation experiments setup at different property of the materials

Validation	Cohesion parameter, kPa	Paddle wheel speed (rpm)	Die disc speed (rpm)
4	0.924	30.0	30.0
5	0.924	22.9	37.5
6	1.213	38.1	22.4

Two additional NIR calibration models were developed for these validations. The development and evaluation of these models can be found in Appendix D. Table 4.23 shows RMSEP, RSEP (%) and Bias for the selected NIR calibration models.

Table 4.23 Summary Selected NIR calibration models for validation blends

Cohesion parameter, kPa	PLS factors	RMSEP (%w/w)	RSEP (%)	Bias (%w/w)
0.924	4	0.086	4.927	-0.010
1.213	2	0.0839	5.055	-0.00354

Table 4.24 shows the experimental and estimated total mean residence time (τ_{total}), the mean centered variance (MCV) and the estimated error percentage for the validations with cohesion parameter equal to 0.924 and 1.213 kPa:

Table 4.24 Validation experiment results at different property of the materials.

Validation	τ_{total} (s)	MCV	τ_{total} (s)	%
	Experimental		Estimated	Error
4	102.383	592.421	101.150	1.204
5	96.804	507.880	97.823	1.052
6	114.977	730.114	112.237	2.384

When changes are made in the properties of the material and, both operating conditions were at 30 rpm, an error of 1.204% was obtained, and when all factors were changed the errors were 1.052 and 2.384%.

A two-sample t-test was performed to assess the statistical significance of the difference between the experimental MRT and predicted MRT by model. The result shows a $t_{estimated}$ value (0.060) less than $t_{tabulated}$ value (1.812), demonstrating that there is non-significant difference between the results.

In general, the predicted mean residence time correlated equally well with the observed experimental results. This confirms the validity of the developed empirical model over the entire design space under evaluation.

4.6 Optional Empirical Model

To measure the cohesion parameter and the flow function is requiring a powder rheometer with a shear cell device which is not necessarily available in all areas of

pharmaceutical manufacture sites. Therefore, a new empirical model was developed using the compressibility percentage as property of the materials. The development of this empirical model is found in the Appendix F.

When performing a series of validations with this model, it was found a higher prediction errors relative to the model developed with the cohesion parameter. This prediction errors were between 2.72 and 10.85%.

5 CONCLUSIONS AND RECOMMENDATIONS

5.1 General Conclusions

The focus of this study was to develop a model based on experimental data to predict the mean residence time in a tablet press feeder. The paddle wheel speed in the feed frame, the die disc speed and the cohesion parameter were the three-experimental factor under consideration.

Five NIR calibration models by transmission mode were developed to obtain the tracer (caffeine) concentration in the samples collected at the output of the feed frame, the relative standard errors of prediction values were less than 5%, which demonstrates a high accuracy of the models.

The experimental results indicate that as the paddle wheel speed increases, the width of the RTD decreases, and the experimental RTD shape tends to ideal CSTR profile. Likewise, the mean residence time decreases as increases the paddle wheel speed in the feed frame, and the degree of dispersion of powder decrease. Similarly, when the die disc speed increase, the mean residence time decrease and the dispersion of the powder within of the feed frame tends to decrease.

The empirical model developed shows a linear relationship between the mean residence time and the paddle wheel speed and the die disc speed, it also indicates that the change in the mean residence time with the cohesion parameter is non-linear and that

the interactions between factors are not significant. The accuracy of the model was verified by an analysis of residuals.

In general, the predicted mean residence time correlated well with the observed experimental results, finding errors percentage between 0.50% and 3.12% for the different validations performed. The empirical model is valid over the design space under evaluation.

5.2 Recommendations and Futures Perspectives

Based on this study, some recommendations can be made with the aim of improving and optimizing the die filling process such as additional experimental studies to generalize the empirical model to other types of tablet press feeder.

Perform simulations in EDEM with different particles, which have different particle size distribution and different cohesion model, to study the behavior of powder inside the feed frame.

This study opens the door to find a relationship between the mean residence time of the pharmaceutical powder in the feed frame and the tablet weight variability.

REFERENCES

- (1) Mendez, R.; Muzzio, F. J.; Velazquez, C. Powder Hydrophobicity and Flow Properties: Effect of Feed Frame Design and Operating Parameters. *AIChE J.* **2012**, *7*, 697–706. DOI: 10.1002/aic.
- (2) Donoso, M.; Ghaly, E. S. Prediction of drug dissolution from tablets using near-infrared diffuse reflectance spectroscopy as a nondestructive method. *Pharm. Dev. Technol.* **2004**, *9* (3), 247–263 DOI: 10.1081/PDT-200031423.
- (3) Peeters, E.; De Beer, T.; Vervaet, C.; Remon, J.-P. Reduction of tablet weight variability by optimizing paddle speed in the forced feeder of a high-speed rotary tablet press. *Drug Dev. Ind. Pharm.* **2015**, *41* (4), 530–539 DOI: 10.3109/03639045.2014.884121.
- (4) Vanarase, A. U.; Muzzio, F. J. Effect of operating conditions and design parameters in a continuous powder mixer. *Powder Technol.* **2011**, *208* (1), 26–36 DOI: 10.1016/j.powtec.2010.11.038.
- (5) Teżyk, M.; Milanowski, B.; Ernst, A.; Lulek, J. Recent progress in continuous and semi-continuous processing of solid oral dosage forms: a review. *Drug Dev. Ind. Pharm.* **2015**, *9045* (January 2016), 1–20 DOI: 10.3109/03639045.2015.1122607.
- (6) Rantanen, J.; Khinast, J. The Future of Pharmaceutical Manufacturing Sciences. *J. Pharm. Sci.* **2015**, *104* (11), 3612–3638 DOI: 10.1002/jps.24594.
- (7) Engisch, W.; Muzzio, F. Using Residence Time Distributions (RTDs) to Address the Traceability of Raw Materials in Continuous Pharmaceutical Manufacturing. *J. Pharm. Innov.* **2016**, *11* (1), 64–81 DOI: 10.1007/s12247-015-9238-1.
- (8) Yaginuma, Y.; Ozeki, Y.; Kakizawa, M.; Gomi, S. I.; Watanabe, Y. Effects of powder flowability on die-fill properties in rotary compression. *J. Drug Deliv. Sci. Technol.* **2007**, *17* (3), 205–210 DOI: 10.1016/S1773-2247(07)50037-7.

- (9) Xie, X.; Puri, V. M. Uniformity of Powder Die Filling Using a Feed Shoe: A Review. *Part. Sci. Technol.* **2006**, *24* (4), 411–426 DOI: 10.1080/02726350600934663.
- (10) Mendez, R.; Muzzio, F.; Velazquez, C. Study of the effects of feed frames on powder blend properties during the filling of tablet press dies. *Powder Technol.* **2010**, *200* (3), 105–116 DOI: 10.1016/j.powtec.2010.02.010.
- (11) Mateo-Ortiz, D.; Méndez, R. Relationship between residence time distribution and forces applied by paddles on powder attrition during the die filling process. *Powder Technol.* **2015**, *278*, 111–117 DOI: 10.1016/j.powtec.2015.03.015.
- (12) Mateo-Ortiz, D.; Muzzio, F. J.; Méndez, R. Particle size segregation promoted by powder flow in confined space: The die filling process case. *Powder Technol.* **2014**, *262*, 215–222 DOI: 10.1016/j.powtec.2014.04.023.
- (13) Gad, S. C.; Chowdhury, D. F.; Gad, S. C. *Pharmaceutical Manufacturing Handbook: Production and Processes*; 2008.
- (14) Natoli, D.; Levin, M.; Tsygan, L.; Liu, L. Development, Optimization, and Scale-up of Process Parameters: Tablet Compression. In *Developing Solid Oral Dosage Forms*; 2009.
- (15) Nauman, E. B. Residence Time Theory. *Ind. Eng. Chem. Res.* **2008**, *47* (10), 3752–3766.
- (16) Gao, Y.; Vanarase, A.; Muzzio, F.; Ierapetritou, M. Characterizing continuous powder mixing using residence time distribution. *Chem. Eng. Sci.* **2011**, *66* (3), 417–425 DOI: 10.1016/j.ces.2010.10.045.
- (17) Gao, Y.; Muzzio, F. J.; Ierapetritou, M. G. A review of the Residence Time Distribution (RTD) applications in solid unit operations. *Powder Technol.* **2012**, *228*, 416–423 DOI: 10.1016/j.powtec.2012.05.060.
- (18) Portillo, P. M.; Ierapetritou, M. G.; Muzzio, F. J. Effects of rotation rate, mixing

- angle, and cohesion in two continuous powder mixers-A statistical approach. *Powder Technol.* **2009**, *194* (3), 217–227 DOI: 10.1016/j.powtec.2009.04.010.
- (19) Portillo, P. M.; Vanarase, A. U.; Ingram, A.; Seville, J. K.; Ierapetritou, M. G.; Muzzio, F. J. Investigation of the effect of impeller rotation rate, powder flow rate, and cohesion on powder flow behavior in a continuous blender using PEPT. *Chem. Eng. Sci.* **2010**, *65* (21), 5658–5668 DOI: 10.1016/j.ces.2010.06.036.
- (20) Vanarase, A. U.; Osorio, J. G.; Muzzio, F. J. Effects of powder flow properties and shear environment on the performance of continuous mixing of pharmaceutical powders. *Powder Technol.* **2013**, *246*, 63–72 DOI: 10.1016/j.powtec.2013.05.002.
- (21) Mendez, R.; Velazquez, C.; Muzzio, F. J. Effect of feed frame design and operating parameters on powder attrition, particle breakage, and powder properties. *Powder Technol.* **2012**, *229*, 253–260 DOI: 10.1016/j.powtec.2012.06.045.
- (22) Ketterhagen, W. R. Simulation of powder flow in a lab-scale tablet press feed frame: Effects of design and operating parameters on measures of tablet quality. *Powder Technol.* **2015**, *275*, 361–374 DOI: 10.1016/j.powtec.2015.01.073.
- (23) Mateo-Ortiz, D.; Méndez, R. Microdynamic analysis of particle flow in a confined space using DEM: The feed frame case. *Adv. Powder Technol.* **2016** DOI: 10.1016/j.appt.2016.05.023.
- (24) Mohan, S. Compression Physics of Pharmaceutical Powders: A Review. *Int. J. Pharm. Sci. Res.* **2012**.
- (25) Patel, S.; Kaushal, A. M.; Bansal, A. K. Compression physics in the formulation development of tablets. *Crit. Rev. Ther. Drug Carrier Syst.* **2006** DOI: 10.1615/CritRevTherDrugCarrierSyst.v23.i1.10.
- (26) Elkhider, N.; Chan, K. L. A.; Kazarian, S. G. Effect of Moisture and Pressure on Tablet Compaction Studied With FTIR Spectroscopic Imaging. *Pharm. Sci.* **2006**,

96, 351–360 DOI: 10.1002/jps.20805.

- (27) Mohammed, H.; Briscoe, B. J.; Pitt, K. G. The interrelationship between the compaction behaviour and the mechanical strength of pure pharmaceutical tablets. *Chem. Eng. Sci.* **2005**, *60* (14), 3941–3947 DOI: 10.1016/j.ces.2005.02.027.
- (28) HIGUCHI, T.; RAO, A. N.; BUSSE, W.; SWINTOSKY, J. V. The Influence of Degree of Compression on Properties of Tablets. **1952**, 194–200.
- (29) Wu, C.-Y.; Cocks, a. C. F. Flow behaviour of powders during die filling. *Powder Metall.* **2004**, *47* (2), 127–136 DOI: 10.1179/003258904225015617.
- (30) Mills, L. A.; Sinka, I. C. Effect of particle size and density on the die fill of powders. *Eur. J. Pharm. Biopharm.* **2013**, *84* (3), 642–652 DOI: 10.1016/j.ejpb.2013.01.012.
- (31) Sinka, I. C.; Schneider, L. C. R.; Cocks, A. C. F. Measurement of the flow properties of powders with special reference to die fill. *Int. J. Pharm.* **2004**, *280* (1–2), 27–38 DOI: 10.1016/j.ijpharm.2004.04.021.
- (32) Guo, Y.; Wu, C. Y.; Kafui, K. D.; Thornton, C. 3D DEM/CFD analysis of size-induced segregation during die filling. *Powder Technol.* **2011**, *206* (1–2), 177–188 DOI: 10.1016/j.powtec.2010.05.029.
- (33) Mehrotra, A.; Chaudhuri, B.; Faqih, A.; Tomassone, M. S.; Muzzio, F. J. A modeling approach for understanding effects of powder flow properties on tablet weight variability. *Powder Technol.* **2009**, *188* (3), 295–300 DOI: 10.1016/j.powtec.2008.05.016.
- (34) Bierwisch, C.; Kraft, T.; Riedel, H.; Moseler, M. Die filling optimization using three-dimensional discrete element modeling. *Powder Technol.* **2009**, *196* (2), 169–179 DOI: 10.1016/j.powtec.2009.07.018.
- (35) Wu, C. Y.; Cocks, A. C. F.; Gillia, O. T.; Thompson, D. A. Experimental and numerical investigations of powder transfer. *Powder Technol.* **2003**, *138* (2–3),

216–228 DOI: 10.1016/j.powtec.2003.09.011.

- (36) Guo, Y.; Wu, C. Y.; Thornton, C. The effects of air and particle density difference on segregation of powder mixtures during die filling. *Chem. Eng. Sci.* **2011**, *66* (4), 661–673 DOI: 10.1016/j.ces.2010.11.017.
- (37) Bi, C.; Jiang, B. Study of residence time distribution in a reciprocating single-screw pin-barrel extruder. *J. Mater. Process. Technol.* **2009**, *209* (8), 4147–4153 DOI: 10.1016/j.jmatprotec.2008.10.006.
- (38) Sheritt, R. G.; Chaouki, J.; Mehrotra, A. K.; Behie, L. A. Axial dispersion in the three-dimensional mixing of particles in a rotating drum reactor. *Chem. Eng. Sci.* **2003**, *58* (2), 401–415 DOI: 10.1016/S0009-2509(02)00551-1.
- (39) Harris, A. T.; Davidson, J. F.; Thorpe, R. B. Particle residence time distributions in circulating fluidised beds. *Chem. Eng. Sci.* **2003**, *58* (11), 2181–2202 DOI: 10.1016/S0009-2509(03)00082-4.
- (40) Fogler, H. S. *Element of Chemical Reaction Engineering*, 4rd ed.; Prentice Hall, 2005.
- (41) Mateo-Ortiz, D.; Colon, Y.; Romañach, R. J.; Méndez, R. Analysis of powder phenomena inside a Fette 3090 feed frame using in-line NIR spectroscopy. *J. Pharm. Biomed. Anal.* **2014**, *100*, 40–49 DOI: 10.1016/j.jpba.2014.07.014.
- (42) Sasic, S.; Blackwood, D.; Liu, A.; Ward, H. W.; Clarke, H. Detailed analysis of the online near-infrared spectra of pharmaceutical blend in a rotary tablet press feed frame. *J. Pharm. Biomed. Anal.* **2015**, *103*, 73–79 DOI: 10.1016/j.jpba.2014.11.008.
- (43) Ward, H. W.; Blackwood, D. O.; Polizzi, M.; Clarke, H. Monitoring blend potency in a tablet press feed frame using near infrared spectroscopy. *J. Pharm. Biomed. Anal.* **2013**, *80*, 18–23 DOI: 10.1016/j.jpba.2013.02.008.
- (44) Sánchez-Paternina, A.; Román-Ospino, A. D.; Martínez, M.; Mercado, J.; Alonso,

- C.; Romañach, R. J. Near infrared spectroscopic transmittance measurements for pharmaceutical powder mixtures. *J. Pharm. Biomed. Anal.* **2016**, *123*, 120–127 DOI: 10.1016/j.jpba.2016.02.006.
- (45) Blanco, M.; Coello, J.; Iturriaga, H.; Maspoch, S.; de la Pezuela, C. Near-infrared spectroscopy in the pharmaceutical industry. *Analyst* **1998**, *123* (8), 135R–150R DOI: 10.1039/a802531b.
- (46) Andersson-engels, S.; Svanberg, S. Time-Resolved NIR / Vis Spectroscopy for Analysis of Solids : Pharmaceutical Tablets. **2002**, *56* (6), 725–731.
- (47) Dahm, D. J.; Dahm, K. D. *Interpreting Diffuse Reflectance and Transmittance—A Theoretical Introduction to Absorption Spectroscopy of Scattering Materials*, 1st ed.; 2007.
- (48) Berntsson, O.; Burger, T.; Folestad, S.; Danielsson, L. G.; Kuhn, J.; Fricke, J. Effective sample size in diffuse reflectance near-IR spectrometry. *Anal. Chem.* **1999**, *71* (3), 617–623 DOI: 10.1021/ac980652u.
- (49) Amigo, J. M.; Cruz, J.; Bautista, M.; Maspoch, S.; Coello, J.; Blanco, M. Study of pharmaceutical samples by NIR chemical-image and multivariate analysis. *TrAC - Trends Anal. Chem.* **2008**, *27* (8), 696–713 DOI: 10.1016/j.trac.2008.05.010.
- (50) Blanco, M.; Peguero, A. An expeditious method for determining particle size distribution by near infrared spectroscopy: Comparison of PLS2 and ANN models. *Talanta* **2008**, *77* (2), 647–651 DOI: 10.1016/j.talanta.2008.07.015.
- (51) Blanco, M.; Peguero, A. Analysis of pharmaceuticals by NIR spectroscopy without a reference method. *TrAC - Trends Anal. Chem.* **2010**, *29* (10), 1127–1136 DOI: 10.1016/j.trac.2010.07.007.
- (52) Alcalá, M.; León, J.; Ropero, J.; Blanco, M.; Romañach, R. J. Analysis of Low Content Drug Tablets by Transmission Near Infrared Spectroscopy: Selection of Calibration Ranges According to Multivariate Detection and Quantitation Limits

- of PLS Models. *J. Pharm. Sci.* **2008**, *97* (10), 5318–5327 DOI: 10.1002/jps.21373.
- (53) Blanco, M.; Bautista, M.; Alcalá, M. Preparing Calibration Sets for Use in Pharmaceutical Analysis by NIR Spectroscopy. *J. Pharm. Sci.* **207AD**, *97* (10), 1236–1245 DOI: 10.1002/jps.21105.
- (54) Meza, C. P.; Santos, M. a; Romañach, R. J. Quantitation of drug content in a low dosage formulation by transmission near infrared spectroscopy. *AAPS PharmSciTech* **2006**, *7* (1), E29 DOI: 10.1208/pt070129.
- (55) Alvarenga, L.; Ferreira, D.; Altekruise, D.; Menezes, J. C.; Lochmann, D. Tablet identification using near-infrared spectroscopy (NIRS) for pharmaceutical quality control. *J. Pharm. Biomed. Anal.* **2008**, *48* (1), 62–69 DOI: 10.1016/j.jpba.2008.05.007.
- (56) Blanco, M.; Cueva-Mestanza, R.; Peguero, A. Controlling individual steps in the production process of paracetamol tablets by use of NIR spectroscopy. *J. Pharm. Biomed. Anal.* **2010**, *51* (4), 797–804 DOI: 10.1016/j.jpba.2009.09.038.
- (57) Càrdenas, V.; Blanco, M.; Alcalà, M. Strategies for Selecting the Calibration Set in Pharmaceutical Near Infrared Spectroscopy Analysis. A Comparative Study. *J. Pharm. Innov.* **2014**, *9* (4), 272–281 DOI: 10.1007/s12247-014-9192-3.
- (58) Blanco, M.; Peguero, A. Influence of physical factors on the accuracy of calibration models for NIR spectroscopy. *J. Pharm. Biomed. Anal.* **2010**, *52* (1), 59–65 DOI: 10.1016/j.jpba.2009.12.009.
- (59) Leturia, M.; Benali, M.; Lagarde, S.; Ronga, I.; Saleh, K. Characterization of flow properties of cohesive powders: A comparative study of traditional and new testing methods. *Powder Technol.* **2014**, *253*, 406–423 DOI: 10.1016/j.powtec.2013.11.045.
- (60) Grossmann, L.; Tomas, J.; Csöke, B. Compressibility and flow properties of a cohesive limestone powder in a medium pressure range. *Granul. Matter* **2004**, *6*

(2–3), 103–109 DOI: 10.1007/s10035-004-0164-z.

- (61) Freeman, R. Measuring the flow properties of consolidated, conditioned and aerated powders - A comparative study using a powder rheometer and a rotational shear cell. *Powder Technol.* **2007**, *174* (1–2), 25–33 DOI: 10.1016/j.powtec.2006.10.016.
- (62) Llusà, M.; Faulhammer, E.; Biserni, S.; Calzolari, V.; Lawrence, S.; Bresciani, M.; Khinast, J. The effects of powder compressibility, speed of capsule filling and pre-compression on plug densification. *Int. J. Pharm.* **2014**, *471* (1–2), 182–188 DOI: 10.1016/j.ijpharm.2014.04.073.
- (63) Freeman, R.; Fu, X. Characterisation of powder bulk, dynamic flow and shear properties in relation to die filling. *Powder Metall.* **2008**, *51* (3), 196–201 DOI: 10.1179/174329008X324115.
- (64) Bi, Y.; Yuan, K.; Xiao, W.; Wu, J.; Shi, C.; Xia, J.; Chu, G.; Zhang, G.; Zhou, G. A local pre-processing method for near-infrared spectra, combined with spectral segmentation and standard normal variate transformation. *Anal. Chim. Acta* **2016**, *909*, 30–40 DOI: 10.1016/j.aca.2016.01.010.
- (65) Zeaiter, M.; Roger, J. M.; Bellon-Maurel, V. Robustness of models developed by multivariate calibration. Part II: The influence of pre-processing methods. *TrAC - Trends Anal. Chem.* **2005**, *24* (5), 437–445 DOI: 10.1016/j.trac.2004.11.023.
- (66) Ich. ICH Topic Q2 (R1) Validation of Analytical Procedures: Text and Methodology. *Int. Conf. Harmon.* **2005**, *1994* (November 1996), 17 DOI: http://www.ich.org/fileadmin/Public_Web_Site/ICH_Products/Guidelines/Quality/Q2_R1/Step4/Q2_R1__Guideline.pdf.
- (67) Sileoni, V.; Marconi, O.; Perretti, G.; Fantozzi, P. Evaluation of different validation strategies and long term effects in NIR calibration models. *Food Chem.* **2013**, *141* (3), 2639–2648 DOI: 10.1016/j.foodchem.2013.04.110.

- (68) Laasonen, M.; Harmia-Pulkkinen, T.; Simard, C.; Räsänen, M.; Vuorela, H. Development and validation of a near-infrared method for the quantitation of caffeine in intact single tablets. *Anal. Chem.* **2003**, *75* (4), 754–760 DOI: 10.1021/ac026262w.
- (69) Montgomery, D. C. *Design and Analysis of Experiments*, Eighth.; 2013.
- (70) Villanova, J. C. O.; Ayres, E.; Oréface, R. L. Design of prolonged release tablets using new solid acrylic excipients for direct compression. *Eur. J. Pharm. Biopharm.* **2011**, *79* (3), 664–673 DOI: 10.1016/j.ejpb.2011.07.011.
- (71) Florian, M.; Velázquez, C.; Méndez, R. New continuous tumble mixer characterization. *Powder Technol.* **2014**, *256*, 188–195 DOI: 10.1016/j.powtec.2014.02.023.
- (72) Augsburger, L. L.; Shangraw, R. F. Effect of glidants in tableting. *J. Pharm. Sci.* **1966**, *55 IS 4*, 418.
- (73) Downey, G. Authentication of Coffee Bean Variety by Near-infrared Reflectance Spectroscopy of Dried Extract. **1996**, *0*, 41–49.
- (74) Ito, M.; Suzuki, T.; Yada, S.; Kusai, A.; Nakagami, H.; Yonemochi, E.; Terada, K. Development of a method for the determination of caffeine anhydrate in various designed intact tables by near-infrared spectroscopy: A comparison between reflectance and transmittance technique. *J. Pharm. Biomed. Anal.* **2008**, *47* (4–5), 819–827 DOI: 10.1016/j.jpba.2008.03.033.
- (75) Hibbert, D. B.; Gooding, J. J. *Data analysis for chemistry: an introductory guide for students and laboratory scientists*; 2006.
- (76) Abatzoglou, N.; Simard, J.-S. Prediction of segregation tendency occurrence in dry particulate.pdf. 2005.
- (77) Tüzün, U.; Arteaga, P. A microstructural model of flowing ternary mixtures of equal-density granules in hoppers. *Chem. Eng. Sci.* **1992**, *47* (7), 1619–1634 DOI:

10.1016/0009-2509(92)85010-9.

- (78) Pettitt, A. N. Testing the Normality of Several Independent Samples Using the Anderson-Darling Statistic. *J. R. Stat. Soc. Ser. C (Applied Stat.* **1977**, 26 (2), 156–161 DOI: 10.2307/2347023.
- (79) Stephens, M. a. EDF Statistics for Goodness of Fit and Some Comparisons. *J. Am. Stat. Assoc.* **1974**, 69 (347), 730–737 DOI: 10.1080/01621459.1974.10480196.
- (80) G. E. P. Box and D. R. Cox. An Analysis of Transformations. *R. Stat. Soc.* **1964**, 26, 211–252.

APPENDICES

Appendix A. Compositions of the Calibrations and Validation Blends for the Calibration Models

Calibration Set: Model 1 (Cohesion parameter 0.733 kPa)					
Blend	Avicel® PH-102 (%)	Lactose 70 (%)	SiO ₂ (%)	MgSt (%)	Caffeine (%)
Cal 1	49.250	49.250	0.50	1.00	0.00
Cal 2	49.125	49.125	0.50	1.00	0.25
Cal 3	49.000	49.000	0.50	1.00	0.50
Cal 4	48.750	48.750	0.50	1.00	1.00
Cal 5	48.500	48.500	0.50	1.00	1.50
Cal 6	48.250	48.250	0.50	1.00	2.00
Cal 7	48.000	48.000	0.50	1.00	2.50
Cal 8	47.750	47.750	0.50	1.00	3.00

Calibration Set: Model 2 (Cohesion parameter 1.055 kPa)					
Blend	Avicel® PH-105 (%)	Lactose 70 (%)	SiO ₂ (%)	MgSt (%)	Caffeine (%)
Cal 1	26.000	72.500	0.50	1.00	0.00
Cal 2	25.875	72.375	0.50	1.00	0.25
Cal 3	25.750	72.250	0.50	1.00	0.50
Cal 4	25.500	72.000	0.50	1.00	1.00
Cal 5	25.250	71.750	0.50	1.00	1.50
Cal 6	25.000	71.500	0.50	1.00	2.00
Cal 7	24.750	71.250	0.50	1.00	2.50
Cal 8	24.500	71.000	0.50	1.00	3.00

Calibration Set: Model 3 (Cohesion parameter 1.433 kPa)					
Blend	Avicel® PH-105 (%)	Lactose 140 (%)	SiO ₂ (%)	MgSt (%)	Caffeine (%)
Cal 1	49.250	49.250	0.50	1.00	0.00
Cal 2	49.125	49.125	0.50	1.00	0.25
Cal 3	49.000	49.000	0.50	1.00	0.50
Cal 4	48.750	48.750	0.50	1.00	1.00
Cal 5	48.500	48.500	0.50	1.00	1.50
Cal 6	48.250	48.250	0.50	1.00	2.00
Cal 7	48.000	48.000	0.50	1.00	2.50
Cal 8	47.750	47.750	0.50	1.00	3.00

Compositions of the validation set by calibration models

Validation set: Model 1 (Cohesion parameter 0.733 kPa)					
Blend	Avicel® PH- 102 (%)	Lactose 70 (%)	SiO₂ (%)	MgSt (%)	Caffeine (%)
Val 1	48.885	48.862	0.502	1.000	0.751
Val 2	48.378	48.363	0.501	1.000	1.752
Val 3	47.856	47.834	0.504	1.005	2.802

Validation set: Model 2 (Cohesion parameter 1.055 kPa)					
Blend	Avicel® PH- 105 (%)	Lactose 70 (%)	SiO₂ (%)	MgSt (%)	Caffeine (%)
Val 1	25.614	71.970	0.516	1.097	0.802
Val 2	25.354	71.729	0.505	1.091	1.320
Val 3	24.609	71.052	0.508	1.022	2.810

Validation set: Model 3 (Cohesion parameter 1.433 kPa)					
Blend	Avicel® PH- 105 (%)	Lactose 140 (%)	SiO₂ (%)	MgSt (%)	Caffeine (%)
Val 1	48.876	48.854	0.506	1.007	0.756
Val 2	48.600	48.594	0.501	1.004	1.301
Val 3	47.900	47.884	0.505	1.005	2.705

Appendix B. Intermediate Precision for Model 1, Model 2 and Model 3

1. NIR calibration model: Cohesion parameter 0.733 kPa

Experimental Data:

Day	Analyst	[Caffeine]
1	1	1.811
1	2	1.855
2	1	1.853
2	2	1.856

ANOVA:

ANOVA for selected factorial model						
Analysis of variance table [Partial sum of squares - Type III]						
Source	Sum of Squares	df	Mean Square	F Value	p-value Prob > F	
Model	0.00103	2	0.000513	1.27765	0.5303	not significant
A-Day	0.00047	1	0.000473	1.17791	0.4740	
B-Analyst	0.00055	1	0.000553	1.37739	0.4493	
Residual	0.0004	1	0.000402			
Cor Total	0.00143	3				

2. NIR calibration model: Cohesion parameter 1.055 kPa

Experimental Data:

Day	Analyst	[Caffeine]
1	1	2.660
1	2	2.611
2	1	2.641
2	2	2.749

ANOVA:

ANOVA for selected factorial model						
Analysis of variance table [Partial sum of squares - Type III]						
Source	Sum of Squares	df	Mean Square	F Value	p-value Prob > F	
Model	0.004369	2	0.002184	0.357106	0.7638	not significant
A-Day	0.00352	1	0.00352	0.575464	0.5868	
B-Analyst	0.000849	1	0.000849	0.138747	0.7730	
Residual	0.006117	1	0.006117			
Cor Total	0.010485	3				

3. NIR calibration model: Cohesion parameter 1.433 kPa

Experimental Data:

Day	Analyst	[Caffeine]
1	1	1.101
1	2	1.242
2	1	1.227
2	2	1.177

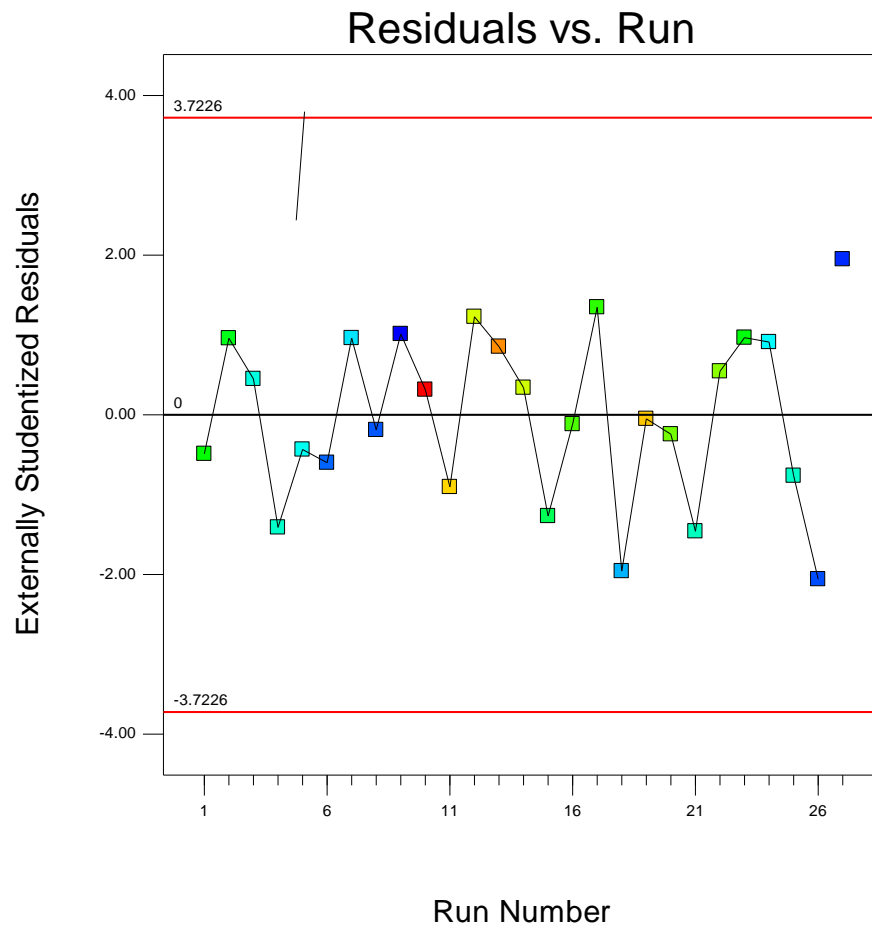
ANOVA

ANOVA for selected factorial model						
Analysis of variance table [Partial sum of squares - Type III]						
Source	Sum of Squares	df	Mean Square	F Value	p-value Prob > F	
Model	0.003007	2	0.00150	0.17	0.8670	not significant
A-Day	0.000932	1	0.00093	0.10	0.8029	
B-Analyst	0.002075	1	0.00208	0.23	0.7165	
Residual	0.009106	1	0.00911			
Cor Total	0.012000	3				

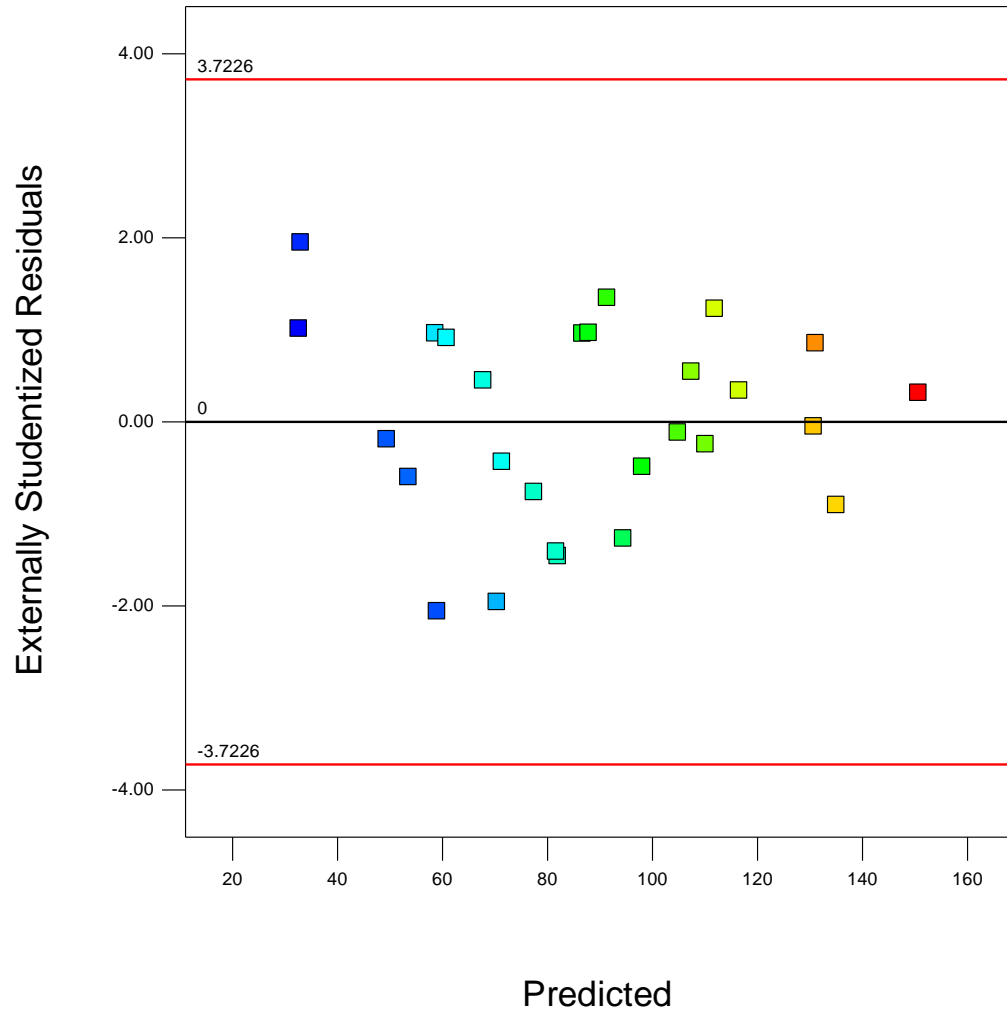
Appendix C. Full Model Adequacy Checking

In this appendix, it can be find the verification of the assumptions of equality of variance and independence for the residuals of the full model.

To evaluate the independence of residuals, a plot of residual versus run number is performed. The assumption of equality of variance was verified by plotting the residuals versus the predicted value. Below are shown these two graphs:



Residuals vs. Predicted



Appendix D. NIR calibration model for Validation Experiments

1. Calibration Model: Cohesion parameter 0.924 kPa

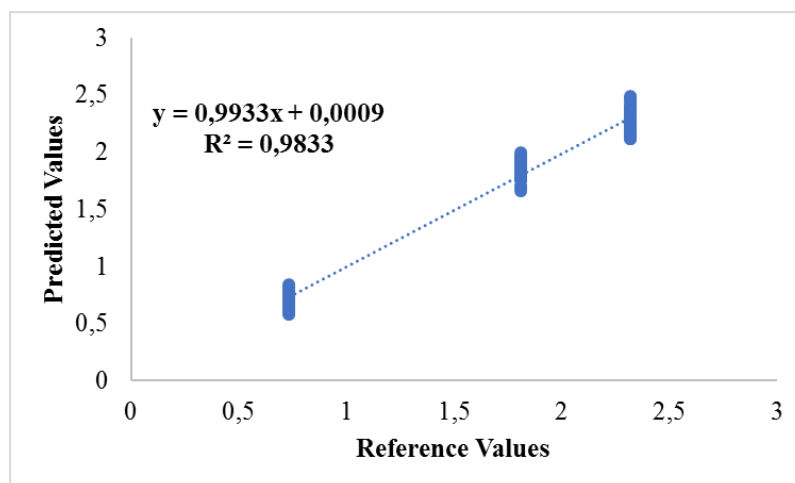
Relation of the five best calibration models developed to evaluate the validation experiments:

Data Pretreatment	Spectral Range (cm ⁻¹)	PLS Factors	RMSEP	RSEP (%)	Bias
SNV	11500-7000	1	1.190	68.039	-0.326
		2	0.554	31.661	-0.239
		3	0.360	20.558	-0.183
		4	0.199	11.365	-0.124
SNV+2nd Derivative (15 points)	11540.8-7004.73	1	1.125	64.304	-0.327
		2	0.278	15.869	-0.135
		3	0.169	9.636	-0.052
		4	0.086	4.927	-0.010
SNV+2nd Derivative (15 points)	11263.1-7220.73	1	1.099	62.838	-0.330
		2	0.257	14.671	-0.128
		3	0.129	7.359	-0.040
		4	0.088	5.019	-0.023
1er Derivative (15 point) +SNV	11448.3-7066.44	1	1.221	69.816	-0.357
		2	0.408	23.313	-0.218
		3	0.180	10.309	-0.106
		4	0.126	7.202	-0.066
SNV+1er Derivative (15 points)	11479.1 - 7004.73	1	1.196	68.375	-0.344
		2	0.341	19.513	-0.174
		3	0.343	19.639	-0.165
		4	0.170	9.708	-0.073

The calibration models with 4 PLS factor, in the spectral region from 11540.8 – 7004.73 cm^{-1} and pretreatment SNV and second derivate with 15 point was selected, because present the lower error.

This model was validated in terms of linearity, accuracy and precision in terms of repeatability and intermediate precision, following the established procedure for the three initial models:

Linearity:



Parameter	Model 1
<i>n</i>	60
Concentration range (% m/m)	0.734 – 2.317
Intercept	-0.0009 ± 0.0335
Slope	0.993 ± 0.0192
R	0.992

Accuracy

Model	RMSEP (%w/w)	RSEP (%)	Bias (w/w)
4	0.086	4.927	-0.010

Reference value	RMSEP (%w/w)	RSEP (%)	Bias (%w/w)
0.734	0.065	8.898	-0.0201
1.808	0.082	4.556	0.0499
2.137	0.106	4.573	-0.0561

Precision: Repeatability

NIR Spectra number	Validation Blend	
	2	3
1	2.052	2.391
2	2.021	2.380
3	2.018	2.371
4	2.008	2.351
5	2.047	2.370
6	2.045	2.330
Average (%w/w)	2.032	2.365
SD	0.018	0.022
RSDs (%)	0.904	0.917

Intermedia Precision:

Experimental Data:

Day	Analyst	[Caffeine]
1	1	0.692
1	2	0.789
2	1	0.769
2	2	0.801

ANOVA

ANOVA for selected factorial model

Analysis of variance table [Partial sum of squares - Type III]

Source	Sum of Squares	df	Mean Square	F Value	p-value Prob > F	
Model	0.006141	2	0.003070	2.91	0.3831	not significant
<i>A-Day</i>	<i>0.001980</i>	<i>1</i>	<i>0.001980</i>	<i>1.87</i>	<i>0.4016</i>	
<i>B-Analyst</i>	<i>0.004160</i>	<i>1</i>	<i>0.004160</i>	<i>3.94</i>	<i>0.2971</i>	
Residual	0.001056	1	0.001056			
Cor Total	0.007197	3				

2. Calibration Model: Cohesion parameter, 1.21 kPa

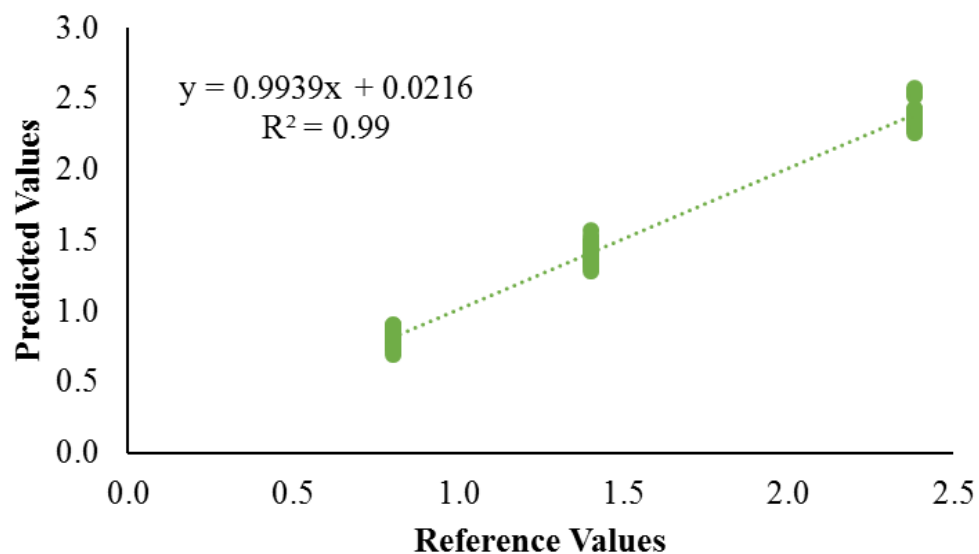
Relation of the five best calibration models developed to evaluate the validation experiments:

Data Pretreatment	Spectral Range (cm ⁻¹)	PLS Factors	RMSEP	RSEP (%)	Bias
SNV	11664.3 - 6295	1	0.706	42.206	0.407
		2	0.263	15.702	0.147
		3	0.110	6.575	0.012
		4	0.129	7.698	-0.006
SNV+2nd Derivative (15 points)	10769.4 – 7714.46	1	0.722	43.152	0.425
		2	0.290	17.321	0.173
		3	0.115	6.882	0.000
		4	0.094	5.623	-0.004
1er Derivative (15 point) +SNV	10954.5 – 6140.71	1	0.825	49.354	0.427
		2	0.138	8.281	0.065
		3	0.100	5.963	0.004
		4	0.123	7.327	-0.033
1er Derivative (9 point) +SNV	10646 – 7868.75	1	0.816	48.806	0.416
		2	0.103	6.157	-0.014
		3	0.139	8.286	-0.009
		4	0.153	9.177	0.047
1er Derivative (15 point) +SNV	10646 – 7868.75	1	0.841	50.668	0.456
		2	0.084	5.055	-0.004
		3	0.123	7.396	-0.037
		4	0.124	7.481	-0.002

The calibration models with 2 PLS factor, in the spectral region from 10646 – 7868.75 cm⁻¹ and pretreatment first derivate with 15 points and SNV was selected, because present the lower error.

This model was validated in terms of linearity, accuracy and precision in terms of repeatability and intermediate precision, following the established procedure for the three initial models:

Linearity:



Parameter	Model 1
<i>n</i>	60
Concentration range (% w/w)	0.8001 – 2.3805
Intercept	0.02164 ± 0.02418
Slope	0.994 ± 0.0159
R	0.995

Accuracy

Model	RMSEP (%w/w)	RSEP (%)	Bias (w/w)
5	0.0839	5.055	-0.0035

Reference value	RMSEP (%w/w)	RSEP (%)	Bias (%w/w)
0.8001	0.00939	9.090	0.0381
1.4016	0.0723	5.161	-0.00869
2.3805	0.103	4.328	-0.0401

Precision: Repeatability

NIR Spectra number	Validation Blend	
	2	3
1	1.503	2.737
2	1.503	2.765
3	1.493	2.715
4	1.523	2.738
5	1.523	2.751
6	1.496	2.701
Average (%w/w)	1.507	2.735
SD	0.013	0.023
RSDs (%)	0.867	0.858

Intermedia Precision:

Experimental Data:

Day	Analyst	[Caffeine]
1	1	1.404
1	2	1.411
2	1	1.417
2	2	1.427

ANOVA

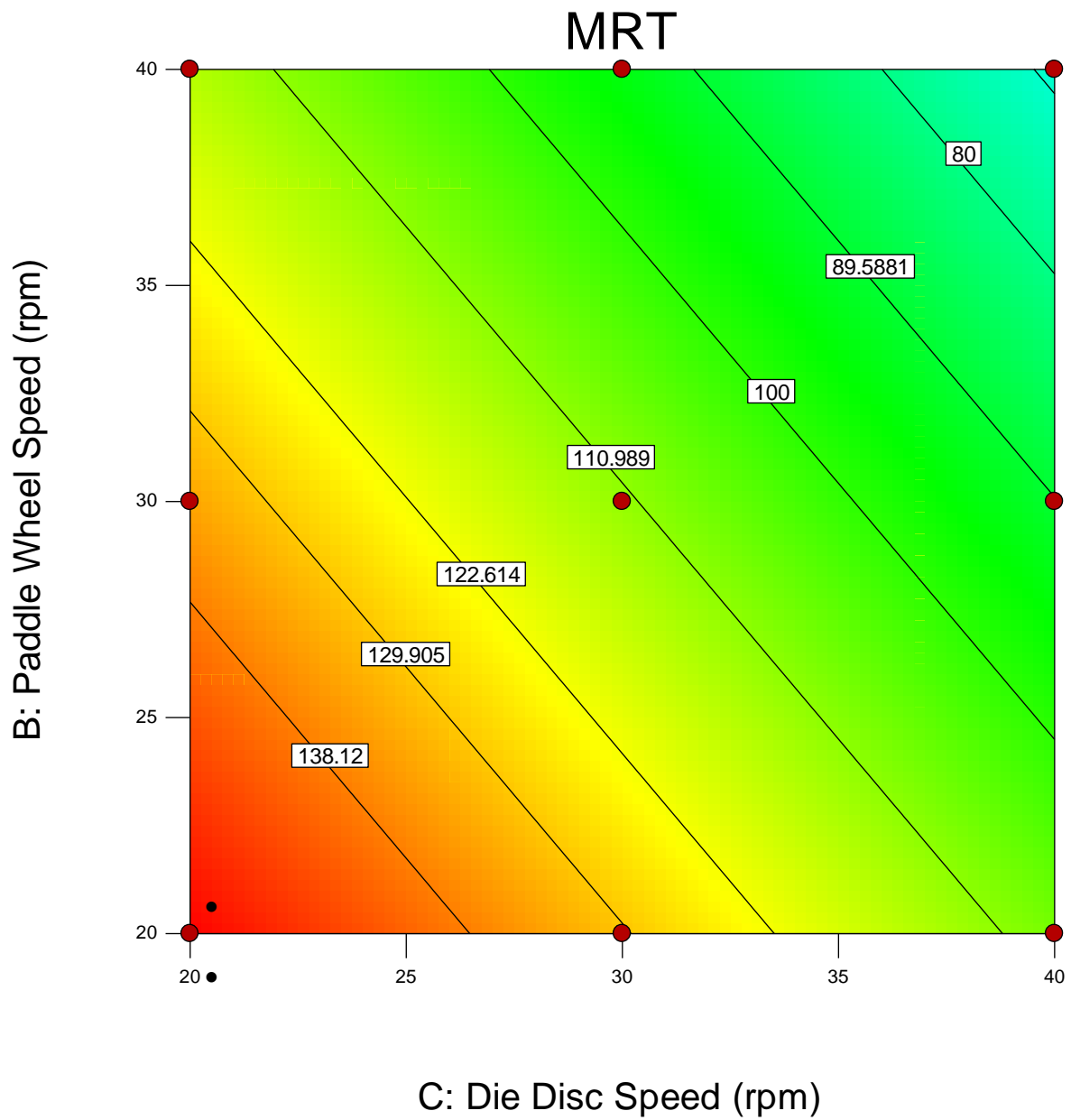
ANOVA for selected factorial model

Analysis of variance table [Partial sum of squares - Type III]

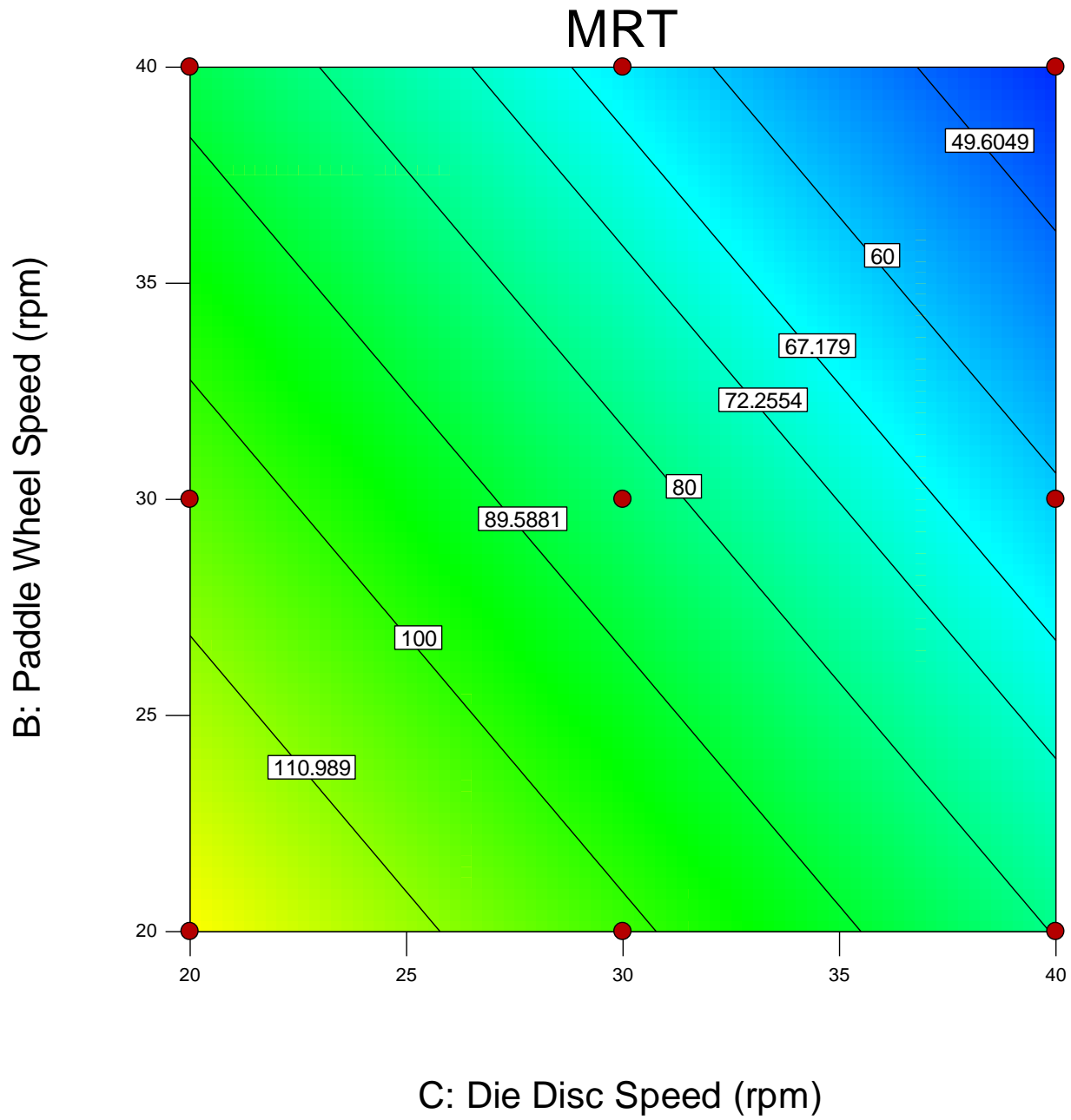
Source	Sum of Squares	df	Mean Square	F Value	p-value Prob > F	
Model	0.000282500	2	0.00014125	62.78	0.0889	not significant
<i>A-Day</i>	0.000210250	1	0.00021025	93.44	0.0656	
<i>B-Analyst</i>	0.000072250	1	0.00007225	32.11	0.1112	
Residual	0.000002250	1	0.00000225			
Cor Total	0.000284750	3				

Appendix E. Contour plots

- Contour plots at cohesion parameter: 1.055 kPa



- Contour plots at cohesion parameter: 1.433 kPa



Appendix F. Development of the optional empirical model

To develop the empirical model base on compressibility percentage the same steps were followed as in the cohesion models. The effects of the main factors (α : compressibility percentage, β : paddle wheel speed, rpm; γ : die disc speed, rpm) and their interactions were determined, based on the significance to the mean residence time, an analysis of variance (ANOVA) was performed to analyze the data.

Initially, the statistical model used is:

$$y_{ijk} = \mu + \alpha_i + \alpha_i^2 + \beta_j + \beta_j^2 + \gamma_k + \gamma_k^2 + \alpha\beta_{ij} + \alpha\gamma_{ik} + \beta\gamma_{jk} + \varepsilon_{ijk}$$

The experimental data was analyzed under the typical assumptions of normality, independence and equality of variance. The analysis of variance for this model was performed as shown in the followed table.

ANOVA for the Mean Residence Time experiments: Full model					
Source	Sum of Squares	df	Mean Square	F Value	p-value Prob > F
Model	24920.814	9	2768.979	45.279	< 0.0001
<i>A-Compressibility</i>	1227.020	1	1227.020	20.064	0.0003
<i>B-Paddle wheel speed</i>	6136.065	1	6136.065	100.337	< 0.0001
<i>C-Die disc speed</i>	8660.305	1	8660.305	141.614	< 0.0001
<i>AB</i>	280.181	1	280.181	4.582	0.0471
<i>AC</i>	150.462	1	150.462	2.460	<i>0.1352</i>
<i>BC</i>	13.860	1	13.860	0.227	<i>0.6401</i>
<i>A²</i>	7955.275	1	7955.275	130.085	< 0.0001
<i>B²</i>	84.624	1	84.624	1.384	<i>0.2557</i>
<i>C²</i>	65.909	1	65.909	1.078	<i>0.3137</i>
Residual	1039.623	17	61.154		
Cor Total	25960.437	26			

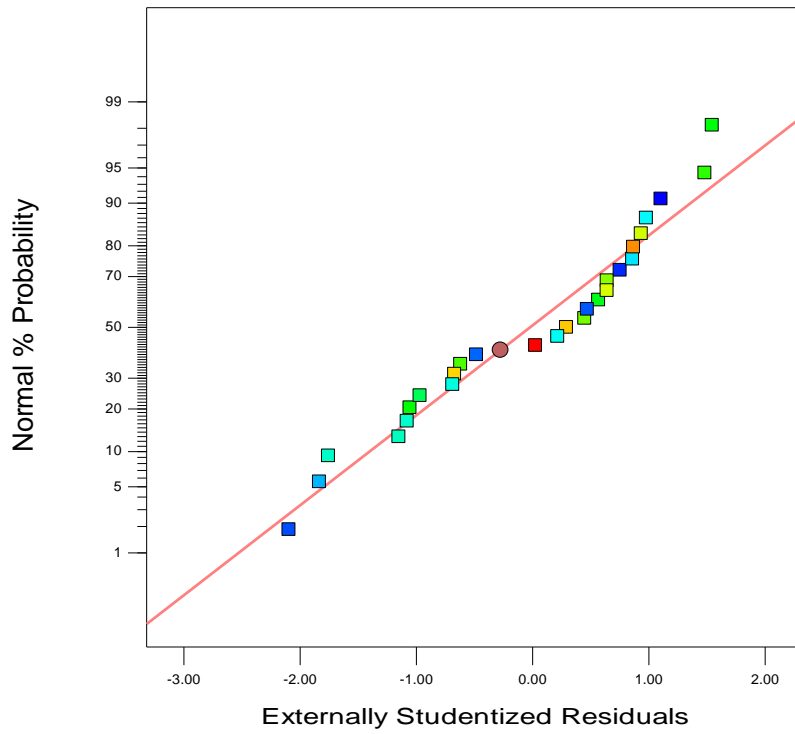
The model is significant with a p-value lower than 0.0001. Also, it can be concluded that the main factors: compressibility percentage, paddle wheel speed and die disc speed are significant, likewise the interaction between compressibility and paddle wheel speed and the quadratic term of the compressibility percentage, with a confidence level of 95%. The other interactions are enough insignificant with p-values greater than 0.1.

The nonsignificant interaction terms were removal of the full quadratic model. The equation for this model is:

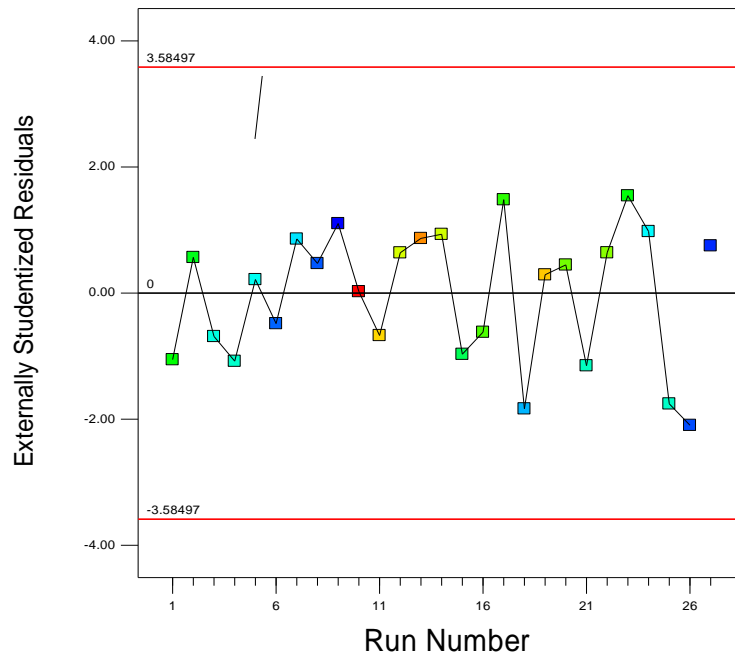
$$y_{ijk} = \mu + \alpha_i + \alpha_i^2 + \beta_j + \gamma_k + \alpha\beta_{ij} + \varepsilon_{ijk}$$

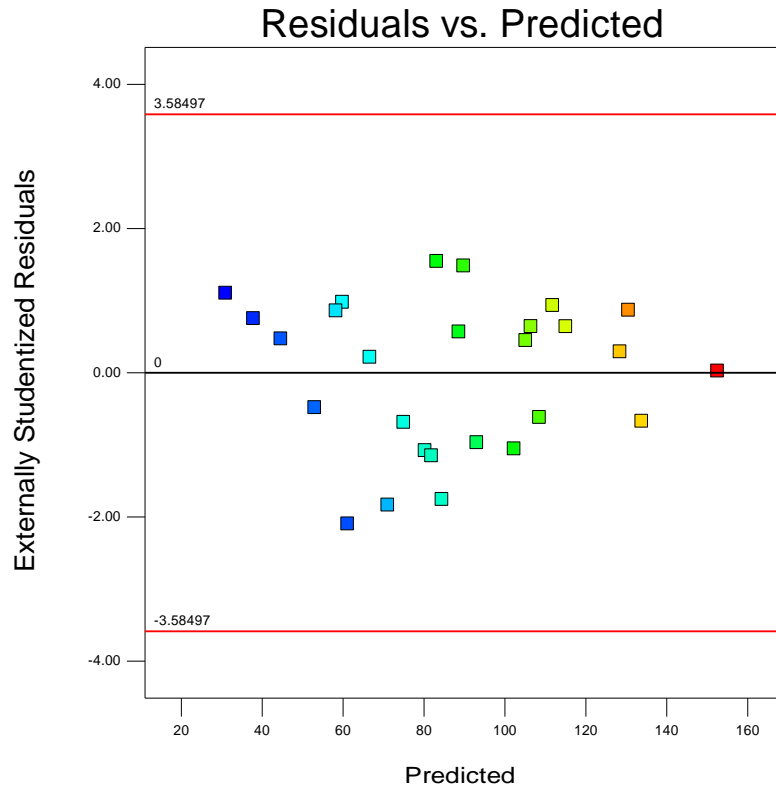
The assumptions of normality, independence, and uniformity of variance of the residuals for the fitted model are verified. Considering the following graphs, there is no reason to suspect any violation of the normality, independence or constant variance assumptions, namely, the assumptions are satisfied.

Normal Plot of Residuals



Residuals vs. Run





The following table shows the analysis of variance (ANOVA) for this model. Clearly, the *model* and all terms included are significant, presenting very small values of *p*:

ANOVA for the Mean Residence Time experiments: Fitted model

Source	Sum of Squares	Df	Mean Square	F Value	p-value Prob > F
Model	24605.96	5	4921.19	76.3	< 0.0001
<i>A-Compressibility</i>	1227.02	1	1227.02	19.02	0.0003
<i>B-Paddle wheel speed</i>	6136.06	1	6136.06	95.13	< 0.0001
<i>C-Die disc speed</i>	8719.78	1	8719.78	135.19	< 0.0001
<i>AB</i>	280.18	1	280.18	4.34	0.0495
<i>A²</i>	7955.27	1	7955.27	123.34	< 0.0001
Residual	1354.48	21	64.5		
Cor Total	25960.44	26			

R² statistics for this model are presented below:

R ² statistics for fitted model	
Statistic	Value
R ²	0.9478
Adjusted R ²	0.9354
Prediction R ²	0.9137
Adeq Precision	32.114

Finally, the *equation* in terms of natural variables to predict the mean residence time based on the compressibility percentage, feed frame paddle wheel speed, and die disc speed, is:

$$\text{MRT (s)} = -10.55 + 40.39\text{CP} - 0.74\text{FF} - 2.20\text{DD} - 0.10 \text{CP*FF} - 1.65\text{CP}^2$$

Validation of the Model

The model was validated using the same experiments used to validate the cohesion parameter model.

Validation	Compressibility percentage (%)	FF (rpm)	DD (rpm)	τ_{total} (s) Experimental	MCV	τ_{total} (s) Estimated	% Error
1	6.060	34.1	25.8	66.253	256.067	70.268	6.06
2	15.470	20	35	90.295	569.451	95.422	5.68
3	11.040	23.8	40	104.242	623.801	101.404	2.72
4	12.52	30	30	102.383	592.421	109.424	6.88
5	12.52	22.9	37.5	96.804	507.88	107.308	10.85

Appendix G. NIR Calibration Model Adequacy Checking: Model 1

In this appendix, it can be find the verification of the assumptions of normality, equality of variance and independence for the residuals of the NIR calibration model 1.

To evaluate the normality was used Anderson-Darling analytical test. Independence of residuals with a plot of residual versus run number is performed. The assumption of equality of variance was verified by plotting the residuals versus the predicted value.

Blend	Reference	Prediction	Residual
1	0.000	0.034	0.034
2	0.252	0.252	0.000
3	0.529	0.564	0.036
4	1.065	1.017	-0.048
5	1.509	1.500	-0.009
6	2.024	2.014	-0.010
7	2.518	2.498	-0.020
8	3.070	3.087	0.017

